DOKUZ EYLÜL UNIVERSITY

GRADUATE SCHOOL OF NATUREL AND APPLIED SCIENCES

EFFECT OF HOLE NUMBER TO BEARING STRENGTH IN PIN LOADED LAMINATED COMPOSITE PLATES

by

Numan TAYLAK

February, 2006

İZMİR

EFFECT OF HOLE NUMBER TO BEARING STRENGTH IN PIN LOADED LAMINATED COMPOSITE PLATES

A Thesis Submitted to the

Graduate School and Applied Sciences of Dokuz Eylül University

In Partial Fulfillment of the Requirements for the Degree of Master of Science

in Mechanical Engineering, Mechanics Program

by

Numan TAYLAK

February, 2006

İZMİR

Ms. Sc. THESIS EXAMINATION RESULT FORM

We have read the thesis, entitled **"EFFECT OF HOLE NUMBER TO BEARING STRENGTH IN PIN LOADED LAMINATED COMPOSITE PLATES"** completed by **NUMAN TAYLAK** under supervision of **Prof. Dr. RAMAZAN KARAKUZU** and we certify that in our opinion it is fully adequate, in scope and in quality, as a thesis for the degree of Master of Science.

Prof. Dr. Ramazan Karakuzu

Supervisor

(Committee Member) (Committee Member)

Prof. Dr. Cahit Helvacı
Director
Graduate School of Natural and Applied Sciences

ACKNOWLEDGEMENTS

I would like to express to my deep sense of appreciation and gratitude to Prof. Dr. Ramazan KARAKUZU, for his supervision, valuable guidance and continuous encouragement throughout this study.

I also would like to thank Prof. Dr. Onur Sayman for their academic support and encouragement through my M.Sc program.

I also extend my sincere thanks to Özgür Ahıshalı, Cihan Rıza Çalışkan and Tuncer Yıldız for their great help during my study. I want to express my thanks to the research assistants of Department of Mechanic at Dokuz Eylül University for their helps during experimental phase of this study.

I want to thank to Ahmet Yiğit, technician in the Machine Tool Laboratory of the Mechanical Engineering Department.

Thanks go out to Izoreel Firm that helped me for the production of glass-vinylester composite plates.

Finally, I am deeply indebted to my family for their support, patience and understanding throughout my life.

Numan TAYLAK

EFFECT OF HOLE NUMBER TO BEARING STRENGTH IN PIN LOADED LAMINATED COMPOSITE PLATES

ABSTRACT

The aim of this study is to research failure mode, failure load and bearing strength in a laminated glass-vinylester composite plate with two parallel circular holes, which are subjected to traction forces by two parallel rigid pins. The behaviour of pin loaded composite plates has been observed experimentally and numerically with different dimensions.

These are performed at three different modes; the distance from the free edge of the plate to diameter of holes (E/D) ratio (1,2,3,4,5), the distance between upper part of plate and centre of holes to diameter of holes K/D ratio (2,3,4) and the distance between two holes to diameter of holes M/D ratio (2,3,4,5). The failure analysis is performed numerically and experimentally and the orientation of fiber $\theta = 0°$ is constant during study.

Failure types and failure loads on the specimens have been determined from experimental study. In numerical study, three dimensional finite element method was used by assistance of LUSAS 13.6 finite element analysis program. In this program, maximum failure load is found with nonlinear analysis. Hashin failure criteria is used in this failure analysis. In the case of failure, appropriate properties of the nodes failed of the composite plate are reduced.

The experimental results are compared with the numerical results and it has been seen that a good agreement between experimental and numerical results.

Keywords: Composite Plate, Bearing Strength, Pin Loading

PİM YÜKLEMELİ KOMPOZİT PLAKLARDA YATAK MUKAVEMETİNE DELİK SAYISININ ETKİSİ

ÖZ

Bu çalışmanın amacı iki paralel rijit pim tarafından değişken yayılı yüke maruz kalmış iki paralel delikli tabakalı glass-vinylester kompozit plaktaki, hasar modunu, hasar yükünü ve yatak mukavemetini araştırmaktır. Pim yüklü tabakalı kompozit plakanın davranışı, deneysel ve nümerik olarak farklı ölçülerde gözlemlenmiştir.

Bu çalışmalar, üç farklı şekilde gerçekleştirilmiştir. Plakanın uç kısmının deliğin çapına oranı (E/D); birden beşe kadar, plakanın üst kısmı ile deliğin merkezi arasındaki uzaklığın, deliğin çapına oranı (K/D); ikiden dörde kadar ve iki delik arasının, delik çapına oranı (M/D); ikiden beşe kadar. Hasar analizi, deneysel ve nümerik olarak gerçekleştirilmiştir ve fiber yönlendirme açısı θ= 0 sabittir.

Numunelerdeki hasar tipleri ve hasar yükleri deneysel çalışmalardan bulunmuştur. Nümerik çalışmada üç boyutlu sonlu eleman metodu, Lusas 13.6 sonlu eleman programı yardımıyla yapılmıştır. Bu program maksimum hasar yükünü nonlieer analizle bulur. Hasar analizinde Hashin hasar kriteri kullanılmıştır. Hasar durumunda kompozit plağın hasarlı düğümlerindeki malzeme özellikleri indirgenir.

Deneysel sonuçlar, nümerik sonuçlarla karşılaştırılmış ve aralarında iyi bir uyum olduğu gözlenmiştir.

Anahtar sözcükler : Kompozit Plak, Yatak Gerilmesi, Pimle Yükleme

CONTENTS

NOMENCLATURE

Abbreviation	**Term**
D	Hole diameter
E	End distance from the hole center
W	Width of the plate
K	Distance between two holes
t	Thickness of the plate
L	Distance from hole center to fixed end
a, b, c, t_i	Dimensions of Iosipescu testing specimen
P	Tensile load
P_{ult}	Maximum failure load
θ	Fiber orientation angle
E_{ij}	Elastic moduli in material directions
G_{ij}	Shear moduli
ν_{12}	Poisson's ratio
V_f	Fiber volume friction
σ_b	Bearing strength
X_t	Tensile strength in the fibre direction
X_c	Compressive strength in the fibre direction
Y_t	Tensile strength in the transverse direction
Y_c	Compressive strength in the transverse direction
S	Shearing strength
ε_{ij}	Strains
σ_{ij}	Stress
$[\overline{C}_{ij}]$	Reduced-stiffness matrix
$[C_{ij}]$	Inverse of compliance matrix
$[S_{ij}]$	Compliance matrix
u, v, w	Displacement component

CHAPTER ONE
INTRODUCTION

Composite materials are highly used in structures when high strength to weight and stiffness to weight ratios are required. Because of this, application areas of composite materials have increased in recent years. There are a lot of different techniques for joining composite members. Some of them are bonding and bolted. The use of bolted joints is promising technique since it is easier and more economical than others. It is often used due to this materials are easy for disassembly. However, mechanical fastened joints require holes to be drilled and therefore large stress zones tend to develop. Because of anisotropic and heterogeneous nature, the joint problem in composites is more difficult to analyze than the case with isotropic materials. For this reason, finding and improving to new design methods is very important to avoid cost penalties and weaknesses.

A large part of the literature published so far on mechanically fastened joints present experimental results on the effect of the dimensions, clearance between the hole and the pin, and the stacking sequence. Several numerical methods have also been investigated to predict failure of pinned joints. Most of them are reviewed in detail by Camanho & Matthews (1997). Kretsis & Matthews (1985) showed, using E glass fiber-reinforced plastic and carbon fiber reinforced plastic, that as the width of the specimen decreases, there is a point where the made of failure changes from one of bearing to one of tension. A similar behaviour between the end distance and the shear-out mode of failure was found. They concluded that lay-up had a great effect on both joint strength and failure mechanism. A computer code which can be used calculated the maximum load has been developed by Chang et al. (1982). In that work Yamada failure criterion has been used. Then Chang et al. (1984a) have developed their analysis to T300/T300/1034-C laminates containing a pin loaded hole or two pin loaded holes in series or in series. Chang et al (1984b) have developed a model and corresponding computer code to determine failure strength and failure mode of composite laminates containing a pin loaded hole even when the material exhibits nonlinearly elastic behaviour. Chang (1986) has carried out a study to evaluate the effect of the assumed pin load distribution. The calculation have utilized a finite element method of stress analysis combined with the Yamata-Sun failure criterion applied along the Chang-Scott- Springer characteristic curve. A three dimensional finite element model to perform stress analysis of single and multi-bolted double shear lap connections of glass fiber reinforced plastic has been used by Hassan et al. (1996) with using ANSYS program.

Aktas & Karakuzu (1999) have investigated the strength of mechanically fastened carbon fiber reinforced epoxy composite plate at the different arbitrary orientations. They have analyzed failure load and failure mode numerically and experimentally by using Tsai-Hill and fiber tensile compressive failure criteria. Icten & Karakuzu (2002) have investigated to prediction of the behaviours of the pined joint carbon epoxy composite plates. In that work Hashin and Hoffman criteria was used to determine failure load and failure mod. Icten & Sayman (2003) have investigated failure load and failure mod in an aluminum glass epoxy sandwich composite plate which is subjected to a traction force by a pin. Parametric studies were carried out experimentally to obtain the effects of join geometry and fiber orientation on the failure strength and failure mode. Okutan, Aslan & Karakuzu (2001) have studied the effects of woven fiber, specimen with-to-hole diameter (W/D) and the ratio of edge distance to hole diameter (E/D) on the bearing strength of woven laminated composites. They have tested single-hole pin loaded specimens for their tensile response. They have observed failure propagation and failure type on the specimens. Gülem, Içten & Karakuzu (2004) have investigated the bearing strength and failure analysis of woven laminated glass-vinylester. In this study, effect of holes has been investigated for the different geometries.

Kim et al (1998) have performed a progressive failure analysis to predict the failure loads of pin loaded composites. Camanho & Matthews (1999) have improved a 3D finite element model to predict damage progression and strength of mechanically fastened joints in carbon fiber reinforced plastics. In that work Hashin failure criteria has been used to predict the failure mode.

Lessard & Shokrieh (1995) have numerically investigated the damage modeling of pin loaded composite. In that work fiber tensile compressive shearing, matrix tensile compressive and fiber matrix shearing criterias have been used.

Hung et al (1996) have investigated failure analysis of T800/3900-2 graphite-epoxy materials by using Hashin failure criteria.

Pierron & Cerisier (2000) have performed a numerical and experimental study to determine the bearing strength of bolted woven composite joints. Hamada & Maekawa (1996) have investigated failure analysis of quasi isotropic carbon epoxy T300/#2500 laminates numerically and experimentally.

Dano et al. (2000) have examined progressive failure analysis of pin loaded composite plate to predict the bearing stress pin displacement curve until joint failure occurs. In that analysis, contact between the pin and hole, progressive damage, large deformation theory and a non linear shear stress strain relationship have been investigated.

This study is concerned with the bearing strength, failure mode and failure load in pin loaded which is subjected to traction force by rigid pins glass-vinylester laminated composite plate. The failure mode and bearing strength have been examined numerically and experimentally. To determine the failure mode and failure load, a three dimensional finite element method has been used. The effects of changing the geometric parameters are observed.

CHAPTER TWO
MACROMECHANICAL BEHAVIOUR OF A LAMINA

2.1 Laminated Composite Materials

Laminated composite materials consist of layers of at least two different materials that are bonded together. Lamination is used to combine the best aspects of the constituent layers and bonding material in order to achieve a more useful constituent layers and bonding material. The properties that can be emphasized by lamination are strength, stiffness, low weight, corrosion resistance, wear resistance, beauty or attractiveness, thermal insulation, acoustical insulation, etc. (Johns, 1999)

2.1.1 Lamina

A lamina is a single ply in laminate, which is made up of a series of layers. The basic building block of a lamina is a lamina which is a flat arrangement of unidirectional fibers or woven in a matrix. Laminated composite materials typically have exceptional properties in the direction of the reinforcing fibers, but poor to mediocre properties to the fibers. The problem is how to obtain maximum advantage from the exceptional fiber directional properties while minimizing the effects of the low transverse properties.

A laminate consists of multiple layers of lamina with unique orientation. A typical laminate is shown in Figure 2.1. Mostly the fiber orientation of the layers is not symmetric as shown in Figure 2.1. As a result of this, the laminate may not have definable only principal directions.

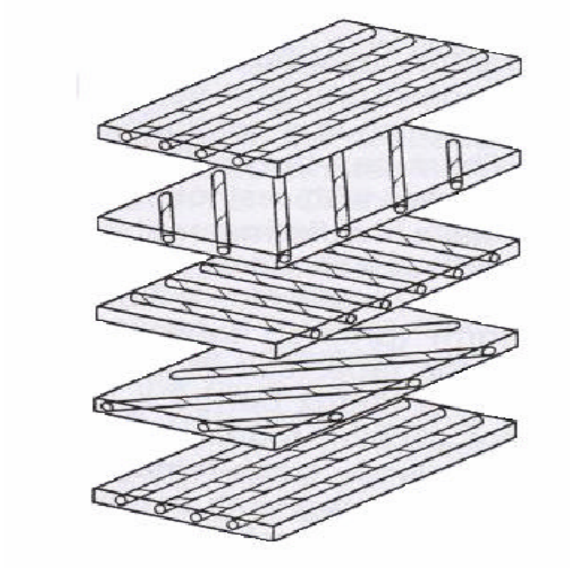

Figure 2.1Construction of a laminate

2.2 Stress Analysis

In most cases an accurate understanding of the loads and stress levels in component operations is one of the critical involved in defining source of failure. Even though other methods of analysis may identify the origin and mode of crack propagation, stress analysis most often provides a quantitative explanation for the cause of failure. Through this analysis step, engineers involved in future or corrective redesigns are provided direct feedback regarding the actual loads experienced by the part, poor design practices and configurations, and the effectiveness of the analysis methods used in design.

Stress analysis procedures for composite materials can be relatively complex, due to the several factors. Because composite materials are fabricated by the lamination of highly anisotropic plies, a nearly infinite variety of directional module and strength can be achieved. Because of this flexibility, a different set of material properties must be considered for each failure case being examined.

2.2.1 Stress –Strain Relations for a Lamina

A unidirectional ply is shown in Figure 2.2, along with a coordinate system used to establish notation. Here directions 1 and 2 indicate to the fiber directions and transverse to the fibers in the plane of the ply, and direction 3 refers to the through the thickness direction.

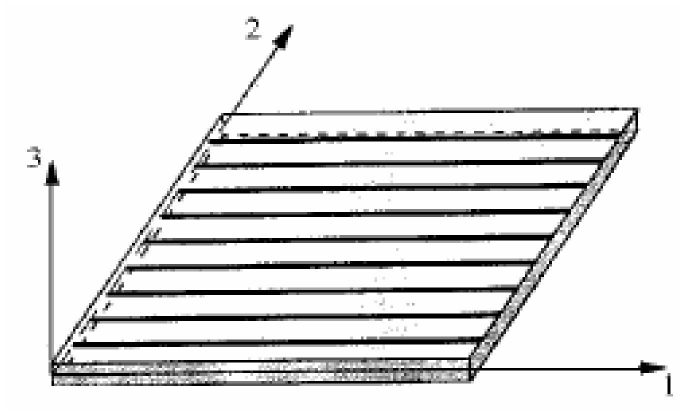

Figure 2.2 Unidirectional fiber reinforced ply

Stress-strain relations can be expressed in matrix form as,

$$\begin{Bmatrix} \varepsilon_1 \\ \varepsilon_2 \\ \varepsilon_3 \\ \gamma_{23} \\ \gamma_{31} \\ \gamma_{12} \end{Bmatrix} = \begin{bmatrix} \frac{1}{E_1} & \frac{-\nu_{21}}{E_2} & \frac{-\nu_{31}}{E_3} & 0 & 0 & 0 \\ \frac{-\nu_{12}}{E_1} & \frac{1}{E_2} & \frac{-\nu_{32}}{E_3} & 0 & 0 & 0 \\ \frac{-\nu_{13}}{E_1} & \frac{-\nu_{23}}{E_2} & \frac{1}{E_3} & 0 & 0 & 0 \\ 0 & 0 & 0 & \frac{1}{G_{23}} & 0 & 0 \\ 0 & 0 & 0 & 0 & \frac{1}{G_{31}} & 0 \\ 0 & 0 & 0 & 0 & 0 & \frac{1}{G_{12}} \end{bmatrix} \begin{Bmatrix} \sigma_1 \\ \sigma_2 \\ \sigma_3 \\ \tau_{23} \\ \tau_{31} \\ \tau_{12} \end{Bmatrix} \tag{2.1}$$

or

$$\{\varepsilon\} = [S]\{\sigma\} \tag{2.2}$$

The S matrix is often called to as the compliance matrix for the lamina, or the strain-stress form of material properties with the strains as the dependent variables. It can be shown that the matrices describing the stress-strain as the dependent variables. It can be shown that the matrices describing the stress-strain relationship of an elastic material must be symmetric, so that relationships such as,

$$E_1\nu_{21} = E_2\nu_{12} \text{ or } \frac{\nu_{12}}{E_1} = \frac{\nu_{21}}{E_2} \tag{2.3}$$

Hold for the off-diagonal terms, so that only nine material properties are required to fully characterize the linear behaviour of a lamina in 3-D stress and strain states. The zeros in the compliance matrix reflect the fact that it is describing the stress-strain behaviour of an orthotropic material and that the description is made with respect to the principal material axes.

The stress-strain matrix can be inverted to obtain stress-strain relations:

$$\begin{Bmatrix} \sigma_1 \\ \sigma_2 \\ \sigma_3 \\ \tau_{23} \\ \tau_{31} \\ \tau_{12} \end{Bmatrix} = \begin{bmatrix} C_{11} & C_{12} & C_{13} & 0 & 0 & 0 \\ C_{12} & C_{22} & C_{23} & 0 & 0 & 0 \\ C_{13} & C_{23} & C_{33} & 0 & 0 & 0 \\ 0 & 0 & 0 & C_{44} & 0 & 0 \\ 0 & 0 & 0 & 0 & C_{55} & 0 \\ 0 & 0 & 0 & 0 & 0 & C_{66} \end{bmatrix} \begin{Bmatrix} \varepsilon_1 \\ \varepsilon_2 \\ \varepsilon_3 \\ \gamma_{23} \\ \gamma_{31} \\ \gamma_{12} \end{Bmatrix} \tag{2.4}$$

The stiffness matrix, C_{ij}, for an orthotropic materials in terms of the engineering constants, is obtained by inversion of the compliance matrix, S_{ij}. The stiffnesses in Eq. (2.3) are,

$$C_{11} = \frac{1-\nu_{23}\nu_{32}}{E_2E_3\Delta}, \qquad C_{22} = \frac{1-\nu_{13}\nu_{31}}{E_1E_3\Delta}, \qquad C_{12} = \frac{\nu_{21}+\nu_{31}\nu_{23}}{E_2E_3\Delta} = \frac{\nu_{12}+\nu_{32}\nu_{13}}{E_1E_3\Delta},$$

$$C_{23} = \frac{\nu_{32}+\nu_{12}\nu_{31}}{E_1E_3\Delta} = \frac{\nu_{23}+\nu_{21}\nu_{13}}{E_1E_2\Delta}, \qquad C_{13} = \frac{\nu_{31}+\nu_{21}\nu_{32}}{E_2E_3\Delta} = \frac{\nu_{13}+\nu_{12}\nu_{23}}{E_1E_2\Delta},$$

$$C_{33} = \frac{1-\nu_{12}\nu_{21}}{E_1 E_2 \Delta}, \qquad C_{44} = G_{23}, \qquad C_{55} = G_{31}, \qquad C_{66} = G_{12} \tag{2.5}$$

where

$$\Delta = \frac{1-\nu_{12}\nu_{21}-\nu_{23}\nu_{32}-\nu_{31}\nu_{13}-2\nu_{21}\nu_{32}\nu_{13}}{E_1 E_2 E_3} \tag{2.6}$$

2.2.2 Stress-Strain Relations for a Lamina of Arbitrary Orientation

The stress-strain relation has been explained in the principal material coordinates on previous section. However, the principal directions of orthotrophy often do not coincide with coordinate directions that are geometrically natural to the solution of the problem. Due to this cause a method of transforming stress-strain relations from one coordinate to another system is required.

The transformation of stress matrix is,

$$\begin{Bmatrix} \sigma_x \\ \sigma_y \\ \sigma_z \\ \tau_{yz} \\ \tau_{xz} \\ \tau_{xy} \end{Bmatrix} = \begin{bmatrix} \cos^2\theta & \sin^2\theta & 0 & 0 & 0 & -\sin 2\theta \\ \sin^2\theta & \cos^2\theta & 0 & 0 & 0 & \sin 2\theta \\ 0 & 0 & 1 & 0 & 0 & 0 \\ 0 & 0 & 0 & \cos\theta & \sin\theta & 0 \\ 0 & 0 & 0 & -\sin\theta & \cos\theta & 0 \\ \sin\theta\cos\theta & -\sin\theta\cos\theta & 0 & 0 & 0 & \cos^2\theta-\sin^2\theta \end{bmatrix} \begin{Bmatrix} \sigma_1 \\ \sigma_2 \\ \sigma_3 \\ \tau_{23} \\ \tau_{31} \\ \tau_{12} \end{Bmatrix} \tag{2.7}$$

θ is the angle between principal directions (1-2-3) and coordinate directions (x-y-z).

The stress-strain relation in x-y-z coordinates are,

$$\begin{Bmatrix} \sigma_x \\ \sigma_y \\ \sigma_z \\ \tau_{yz} \\ \tau_{xz} \\ \tau_{xy} \end{Bmatrix} = \begin{bmatrix} \overline{C}_{11} & \overline{C}_{12} & \overline{C}_{13} & 0 & 0 & \overline{C}_{16} \\ \overline{C}_{21} & \overline{C}_{22} & \overline{C}_{23} & 0 & 0 & \overline{C}_{26} \\ \overline{C}_{31} & \overline{C}_{32} & \overline{C}_{33} & 0 & 0 & \overline{C}_{36} \\ 0 & 0 & 0 & \overline{C}_{44} & \overline{C}_{45} & 0 \\ 0 & 0 & 0 & \overline{C}_{45} & \overline{C}_{55} & 0 \\ \overline{C}_{16} & \overline{C}_{26} & \overline{C}_{36} & 0 & 0 & \overline{C}_{66} \end{bmatrix} \begin{Bmatrix} \varepsilon_x \\ \varepsilon_y \\ \varepsilon_z \\ \gamma_{yz} \\ \gamma_{xz} \\ \gamma_{xy} \end{Bmatrix} \tag{2.8}$$

The transformed compliance coefficients $\overline{C}_{ij}$, indicated to the (x, y, z) system,

$$\overline{C}_{11} = C_{11}\cos^4\theta - 4C_{16}\cos^3\theta\sin\theta + 2(C_{12} + C_{66})\cos^2\theta\sin^2\theta - 4C_{26}\cos\theta\sin^3\theta + C_{22}\sin^4\theta$$

$$\overline{C}_{12} = C_{12}\cos^4\theta + 2(C_{16} - C_{26})\cos^3\theta\sin\theta + (C_{11} + C_{12} - 4C_{66})\cos^2\theta\sin^2\theta + 2(C_{26} - C_{16})\cos\theta\sin^3\theta + C_{12}\sin^4\theta$$

$$\overline{C}_{13} = C_{13}\cos^2\theta - 2C_{36}\cos\theta\sin\theta + C_{23}\sin^2\theta$$

$$\overline{C}_{16} = C_{16}\cos^4\theta + (C_{11} - C_{12} - 2C_{66})\cos^3\theta\sin\theta + 3(C_{26} - C_{16})\cos^2\theta\sin^2\theta + (2C_{66} + C_{12} - C_{22})\cos\theta\sin^3\theta - C_{26}\sin^4\theta$$

$$\overline{C}_{22} = C_{22}\cos^4\theta + 4C_{26}\cos^3\theta\sin\theta + 2(C_{12} + 2C_{66})\cos^2\theta\sin^2\theta + 4C_{16}\cos\theta\sin^3\theta + C_{11}\sin^4\theta$$

$$\overline{C}_{23} = C_{23}\cos^2\theta + 2C_{36}\cos\theta\sin\theta + C_{13}\sin^2\theta$$

$$\overline{C}_{26} = C_{26}\cos^4\theta + (C_{12} - C_{22} + 2C_{66})\cos^3\theta\sin\theta + 3(C_{16} - C_{26})\cos^2\theta\sin^2\theta + (C_{11} - C_{12} - 2C_{66})\cos\theta\sin^3\theta - C_{16}\sin^4\theta$$

$$\overline{C}_{33} = C_{33}$$

$$\overline{C}_{36} = (C_{13} - C_{23})\cos\theta\sin\theta + C_{36}(\cos^2\theta - \sin^2\theta)$$

$$\overline{C}_{44} = C_{44}\cos^2\theta + C_{55}\sin^2\theta + 2C_{45}\cos\theta\sin\theta$$

$$\overline{C}_{45} = C_{45}(\cos^2\theta - \sin^2\theta) + (C_{55} - C_{44})\cos\theta\sin\theta$$

$$\overline{C}_{55} = C_{55}\cos^2\theta + C_{44}\sin^2\theta - 2C_{45}\cos\theta\sin\theta$$

$$\begin{aligned}\overline{C}_{66} &= 2(C_{16} - C_{26})\cos^3\theta\sin\theta + (C_{11} + C_{22} - 2C_{12} - 2C_{66})\cos^2\theta\sin^2\theta \\ &\quad + 2(C_{26} - C_{16})\cos\theta\sin^3\theta + C_{66}(\cos^4\theta + \sin^4\theta)\end{aligned} \tag{2.9}$$

Note that C_{14}, C_{15}, C_{16}, C_{24}, C_{25}, C_{26}, C_{34}, C_{35}, C_{36}, C_{45}, C_{46}, and C_{56} are zero for an orthotropic material.

The relation of stress-strain for the x-y-z coordinates are,

$$\begin{Bmatrix} \varepsilon_x \\ \varepsilon_y \\ \varepsilon_z \\ \gamma_{yz} \\ \gamma_{xz} \\ \gamma_{xy} \end{Bmatrix} = \begin{bmatrix} \overline{S}_{11} & \overline{S}_{12} & \overline{S}_{13} & 0 & 0 & \overline{S}_{16} \\ \overline{S}_{21} & \overline{S}_{22} & \overline{S}_{13} & 0 & 0 & \overline{S}_{26} \\ \overline{S}_{31} & \overline{S}_{32} & \overline{S}_{33} & 0 & 0 & \overline{S}_{36} \\ 0 & 0 & 0 & \overline{S}_{44} & \overline{S}_{45} & 0 \\ 0 & 0 & 0 & \overline{S}_{45} & \overline{S}_{55} & 0 \\ \overline{S}_{16} & \overline{S}_{26} & \overline{S}_{36} & 0 & 0 & \overline{S}_{66} \end{bmatrix} \begin{Bmatrix} \sigma_x \\ \sigma_y \\ \sigma_z \\ \tau_{yz} \\ \tau_{xz} \\ \tau_{xy} \end{Bmatrix} \tag{2.10}$$

The transformed compliance coefficients $\overline{S}_{ij}$, indicated to the (x, y, z) system,

$$\begin{aligned}\overline{S}_{11} &= S_{11}\cos^4\theta - 2S_{16}\cos^3\theta\sin\theta + (2S_{12} + S_{66})\cos^2\theta\sin^2\theta - 2S_{26}\cos\theta\sin^3\theta \\ &\quad + S_{22}\sin^4\theta\end{aligned}$$

$$\begin{aligned}\overline{S}_{12} &= S_{12}\cos^4\theta + (S_{16} - S_{26})\cos^3\theta\sin\theta + (S_{11} + S_{22} - S_{66})\cos^2\theta\sin^2\theta \\ &\quad + (S_{26} - S_{16})\cos\theta\sin^3\theta + S_{12}\sin^4\theta\end{aligned}$$

$$\bar{S}_{13} = S_{13}\cos^2\theta - S_{36}\cos\theta\sin\theta + S_{23}\sin^2\theta$$

$$\bar{S}_{16} = S_{16}\cos^4\theta + \left(2S_{11} - 2S_{12} - S_{66}\right)\cos^3\theta\sin\theta + 3(S_{26} - S_{16})\cos^2\theta\sin^2\theta$$
$$+ (S_{66} + 2S_{12} - 2S_{22})\cos\theta\sin^3\theta - S_{26}\sin^4\theta$$

$$\bar{S}_{22} = S_{22}\cos^4\theta + 2S_{26}\cos^3\theta\sin\theta + \left(2S_{12} + S_{66}\right)\cos^2\theta\sin^2\theta + 2S_{16}\cos\theta\sin^3\theta$$
$$+ S_{11}\sin^4\theta$$

$$\bar{S}_{23} = S_{23}\cos^2\theta + S_{36}\cos\theta\sin\theta + S_{13}\sin^2\theta$$

$$\bar{S}_{26} = S_{26}\cos^4\theta + (2S_{12} - 2S_{22} + S_{66})\cos^3\theta\sin\theta + 3(S_{16} - S_{26})\cos^2\theta\sin^2\theta$$
$$+ (2S_{11} - 2S_{12} - S_{66})\cos\theta\sin^3\theta - S_{16}\sin^4\theta$$

$$\bar{S}_{33} = S_{33}$$

$$\bar{S}_{36} = 2\left(S_{13} - S_{23}\right)\cos\theta\sin\theta + S_{36}\left(\cos^2\theta - \sin^2\theta\right)$$

$$\bar{S}_{44} = S_{44}\cos^2\theta + 2S_{45}\cos\theta\sin\theta + S_{55}\sin^2\theta$$

$$\bar{S}_{45} = S_{45}(\cos^2\theta - \sin^2\theta) + (S_{55} - S_{44})\cos\theta\sin\theta$$

$$\bar{S}_{55} = S_{55}\cos^2\theta + S_{44}\sin^2\theta - 2S_{45}\cos\theta\sin\theta$$

$$\bar{S}_{66} = S_{66}\left(\cos^2\theta - \sin^2\theta\right)^2 + 4(S_{16} - S_{26})(\cos^2\theta - \sin^2\theta)\cos\theta\sin\theta$$
$$+ 4\left(S_{11} + S_{22} - 2S_{12}\right)\cos^2\theta\sin^2\theta \qquad (2.11)$$

2.3 Failure Analysis

The rapid advancement of composite materials over the past two decades has outstripped the development of appropriate failure analysis techniques. This is particularly true of the fiber composite material systems used in primary structural applications in any industries. Although some of the knowledge gained over the years in performing failure analysis on metals is applicable to composites, the fundamentally different nature of the two materials prohibits the widespread transfer of information.

Numerous failure theories have been proposed and are available to the composite structural designer. They are classified into three groups, limit or noninteractive theories (maximum stress, maximum strain); interactive theories (Tsai-Hill, Tsai-Wu); and partially interactive or failure mode based theories (Hashin).

The validity and applicability of a given theory depend on the convenience of application and agreement with experimental results. The plethora of theories is accompanied by a dearth of suitable and reliable experimental data, which makes the selection of one theory over another rather difficult. Considerable effort has been devoted recently to alleviate this difficulty.

2.3.1 Hashin Failure Criterion

In this study, Hashin failure criteria (1980) has been used due to this criterion is a preference for use in finite element models.

Two proposals of failure criterion for fibrous composite materials that are associated with Hashin may be found in the literature. The first reference 1 of the review is known as the Hashin- Rotem criterion. This criterion predicts failure when one of the following equations is satisfied.

2.3.1.1 Hashin & Rotem Criterion (1973)

Fiber Failure in Tension

$$\sigma_{11} = X_t \qquad (\sigma_{11}, X_t > 0) \tag{2.12}$$

Fiber Failure in Compression

$$-\sigma_{11} = X_t \qquad (\sigma_{11} < 0; X_c > 0) \tag{2.13}$$

Matrix Failure in Tension

$$\left(\frac{\sigma_{22}}{Y_t}\right)^2 + \left(\frac{\tau_{12}}{S}\right)^2 = 1 \tag{2.14}$$

Matrix Failure in Compression

$$\left(\frac{\sigma_{22}}{Yc}\right)^2 + \left(\frac{\tau_{12}}{S}\right)^2 = 1 \tag{2.15}$$

where

σ_{11} is the nominal stress in the lamina in the direction of the fibers.

σ_{22} is the nominal stress in the lamina in the transverse direction to the fibers.

τ_{12} is the nominal shear stress in the plane of the lamina.

X_t is the tensile strength of the fibers.

Y_t is the tensile strength in the transverse direction of the fibers.

X_c is the compressive strength of the fibers.

Y_c is the compression strength in the transverse direction of the fibers.

S is the shear strength.

Based on observations of specimen failure in tension with different orientations of the fibers, the author of this proposal concludes that there are only two mechanisms of failure; fiber or matrix failure. With reference to the second, they do not distinguish whether the failure is exactly at the interface or inside the matrix and thus propose that both σ_2 and σ_{12} contribute to the appearance of the failure (the proposal is in quadratic form).

The historical importance of this proposal is that initiates a different way of approaching the generation of composites failure criteria. The authors first set out to recognize modes of failure, then to understand the variables with these nodes and propose and interaction between them.

The idea seems adequate for the type of materials under consideration; although it may be argued that not all failure modes that can appear in fibrous composites are covered in the proposal. It is also not clear that the variables they propose for each case are the most appropriate or in what they combine them.

In 1980, Hashin re-examined the proposal and established some modifications. There are also four expressions involved in the proposal that Hashin developed for the 3D case.

Hashin Criterion 3D (1980)

Tensile Fiber Mode

$$\left(\frac{\sigma_1}{X_t}\right)^2 + \frac{1}{S^2}\left(\tau_{12}^2 + \tau_{13}^2\right) = 1 \tag{2.16}$$

or

$$\sigma_{11} = X_t \tag{2.17}$$

Compressive Fiber Mode

$$\left|\sigma_{11}\right| = X_c \tag{2.18}$$

Tensile Matrix Mode $(\sigma_{22} + \sigma_{33} > 0)$

$$\frac{1}{Y_T^2}\left(\sigma_{22} + \sigma_{33}\right)^2 + \frac{1}{S_T^2}\left(\tau_{23}^2 - \sigma_{22}\sigma_{33}\right) + \frac{1}{S^2}\left(\tau_{12}^2 + \tau_{13}^2\right) = 1 \tag{2.19}$$

Compressive Matrix Mode $(\sigma_{22} + \sigma_{33})$ *<0*

$$\frac{1}{Y_C}\left[\left(\frac{Y_C}{2S_T}\right)^2 - 1\right]\left(\sigma_2 + \sigma_3\right) + \frac{1}{4S_T{}^2}\left(\sigma_2 + \sigma_3\right)^2 + \frac{1}{S_T^2}\left(\tau_{23}^2 - \sigma_2\sigma_3\right)$$
$$+ \frac{1}{S^2}\left(\tau_{12}^2 + \tau_{13}^2\right) = 1 \tag{2.20}$$

where in addition to the previous definitions, S_T represents the transverse shear strength, the allowable value of shear stress τ_{23} (the allowable value of τ_{13} is, as for τ_{12}, S).

CHAPTER THREE
NUMERICAL STUDY

3.1 Introduction

Numerical analysis techniques, such as finite element analysis (FEA) are used extensively in the design and stress analysis of adhesively bonded and bolted structures. These techniques offer solutions to complex problems that are too difficult or impossible to resolve using analytical, closed-form solutions. Numerous FEA programs are available. These programs provide in-built constitutive models for simulating the behavior of most adhesive, allowing for non-uniform stress-strain distributions, geometric non-linearity, hydrothermal effects, elastic-plastic behavior, static and dynamic analysis, and strain rate dependence. Orthotropic element types include two dimensional solid plane stress or plain strain elements, axisymetric shell or solid elements, three dimensional solid or “brick” elements and crack tip elements. A number of automatic mesh (element) generators are available with post processing capabilities.

3.2 Three Dimensional Finite Element Method

In the three-dimensional finite element formulation, the displacements, traction components, and distributed body force values are the functions of the position indicated by *(x, y, z).* The displacement vector **u** is given as (Chandrupatla, 1991)

$$\mathbf{u} = [u, v, w]^T \tag{3.1}$$

where u, v and w are the x, y and z components of **u**, respectively. The stress and strains are given by

$$\sigma = [\sigma_{xx}, \sigma_{yy}, \sigma_{zz}, \sigma_{yz}, \sigma_{xz}, \sigma_{xy}]^T$$
$$\varepsilon = [\varepsilon_{xx}, \varepsilon_{yy}, \varepsilon_{zz}, \gamma_{yz}, \gamma_{xz}, \gamma_{xy}]^T \tag{3.2}$$

From Figure 3.1, representing the three- dimensional problem in a general setting, the body force and traction vector are given by

$$\mathbf{f} = [f_x, f_y, f_z]^T \quad , \mathbf{T} = [T_x, T_y, T_z]^T \tag{3.3}$$

The body force **f** has dimensions of force per unit volume, while the traction force **T** has dimensions of force per unit area.

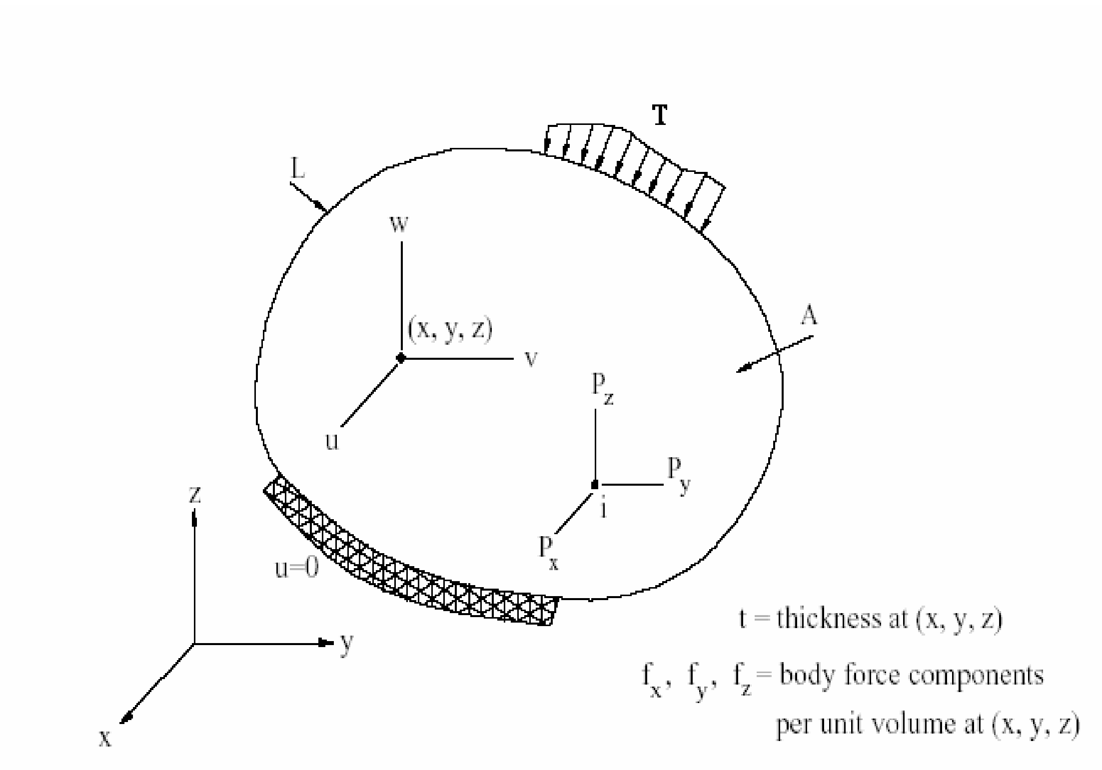

Figure 3.1 Three-dimensional problem

3.3 The sixteen-Node Brick Element

In this study, the sixteen-node brick element was used. A typical sixteen-node brick element is shown in figure 3.1. A 3D isoparametric solid continuum element capable of modeling curved boundaries. The element is numbered according to right hand screw rule in the local z direction. Freedoms of the element are u, v, w at each node and node coordinates are x, y, z at each node. (Gülem, 2004)

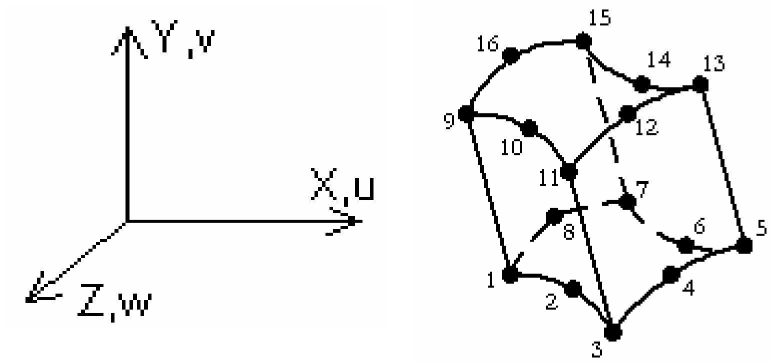

Figure 3.2 Sixteen-node brick element

3.4 Modeling of the Problem in Finite Element Program

The maximum failure load values have been found by nonlinear analysis in Lusas 13.6 finite element program. First of all composite plate was modeled as a half model and symmetry boundary conditions were used to reduce to size of the model. Then mesh has been graded manually by specifying the number of elements on each of the boundary lines. After that, the surface was swept through the depth of the plate to create a volume. One element only is required through the depth of the plate the default number of mesh divisions must be set to one.

Then translation value of the surface was defined. The translation direction is Z and its value is 2.8mm. Next we assigned the volume with mesh dataset Composite Brick (HX16L), this element descriptions are generic element type (Structural Composite), element shape (Hexahedral), interpolation order (Quadratic). After that, the element axis of the model oriented to lie along the global X axis. The meshing half model was shown in figure 3.3.

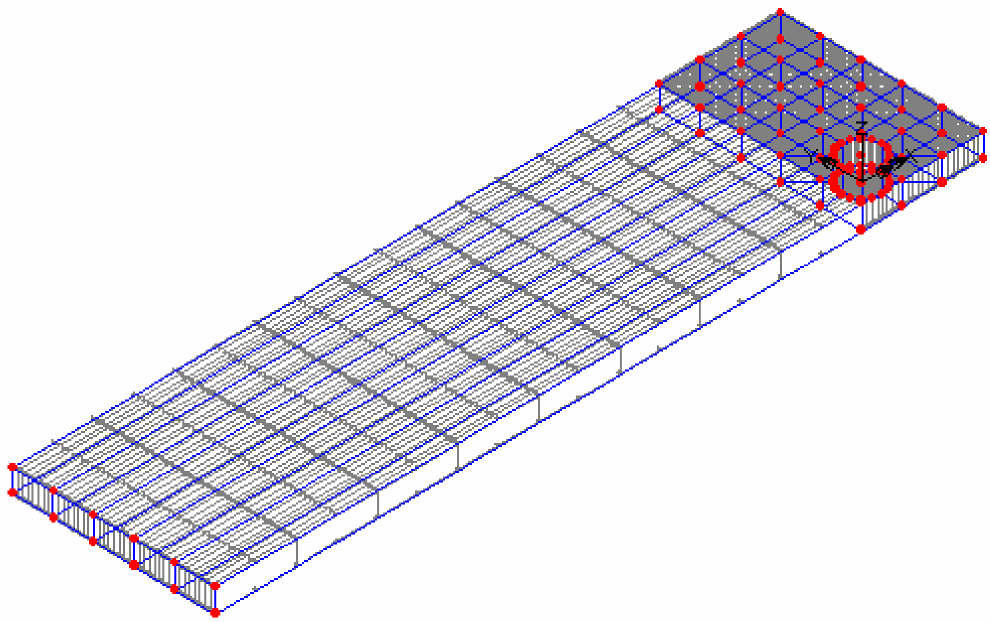

Figure 3.3 Meshing of the half model

After completed above parts, model properties were defined. In this section of program, orthotropic material was defined, the mechanical properties of glass-vinylester composite material was added to composite library, leave the units N, mm, t, C, s. 3D solid is chosen and the option to output parameters were selected for the Hashin Damage model. Mechanical properties of glass-vinylester are shown in Table 4.2.

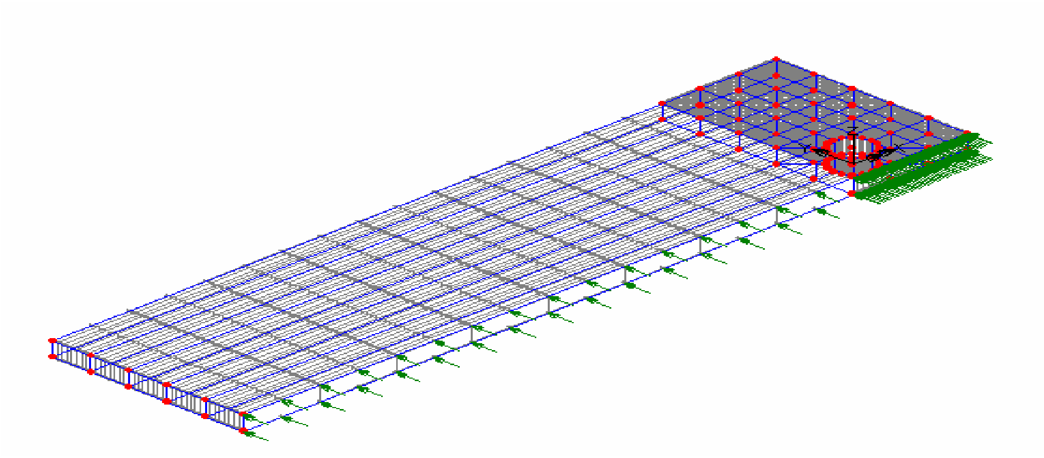

Figure 3.4 Supported surfaces on symmetry XZ plane

After that, support conditions of the model were defined. Firstly, the bottom surfaces of the half model have been supported on symmetry XZ plane as shown in Figure in 3.4. Secondly, cylindrical axis is performed surfaces on semi cylinder. These surfaces of the plate were supported in X direction as shown in figure 3.5

Finally, tensile load was performed one by one to per unit on surface as shown in figure 3.6 and CTRL and A keys were used together whole model was selected and assigned, the element axis was selected and click OK to finish this part of the study.

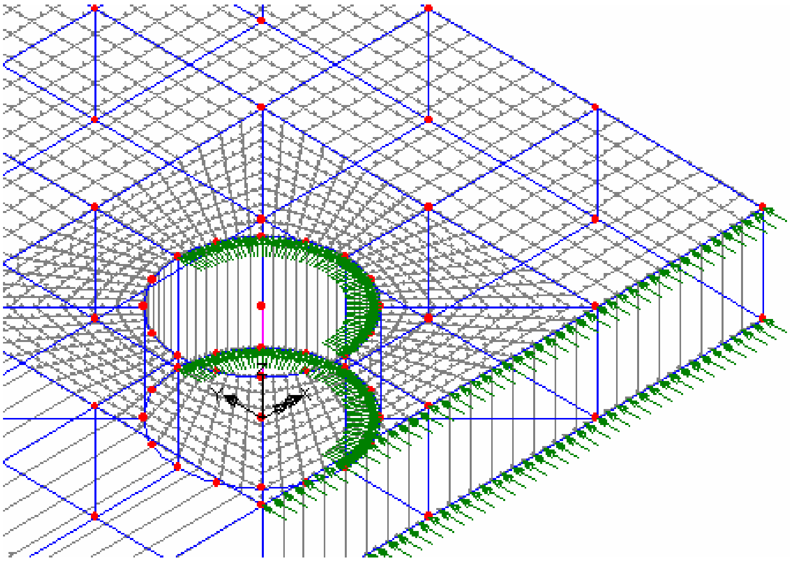

Figure 3.5 Supported surfaces in X direction with respect to cylindrical

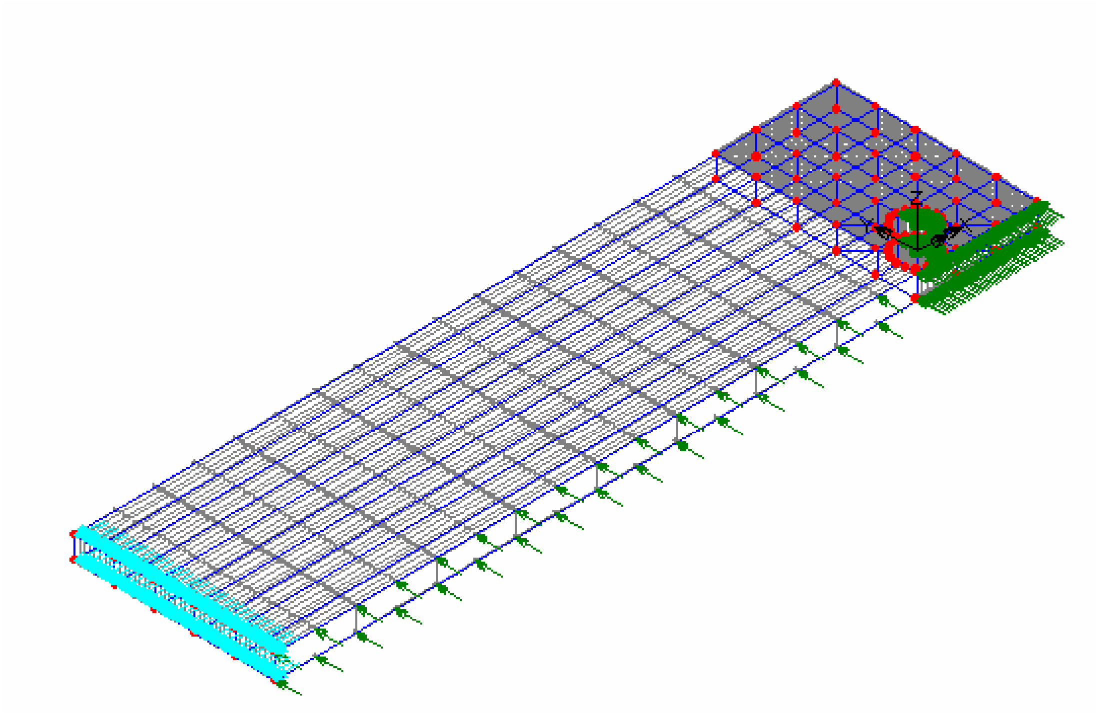

Figure 3.6 Tensile load direction

CHAPTER FOUR
EXPERIMENTAL STUDY

4.1 Problem Statement

Consider a composite rectangular plate of length L+E, L is fixed at a constant value 85mm, width W with two hole of diameter D, the hole diameters were fixed at a constant 5mm, the distance between holes is M, the distance from upper part of plate to centre of hole is K, as depicted in Figure 4.1. The holes are at a distance E from the free edge of the plate. Rigid pins are located at the centre of the holes. A tensile load is applied at one edge of the plate and is resisted the pins.

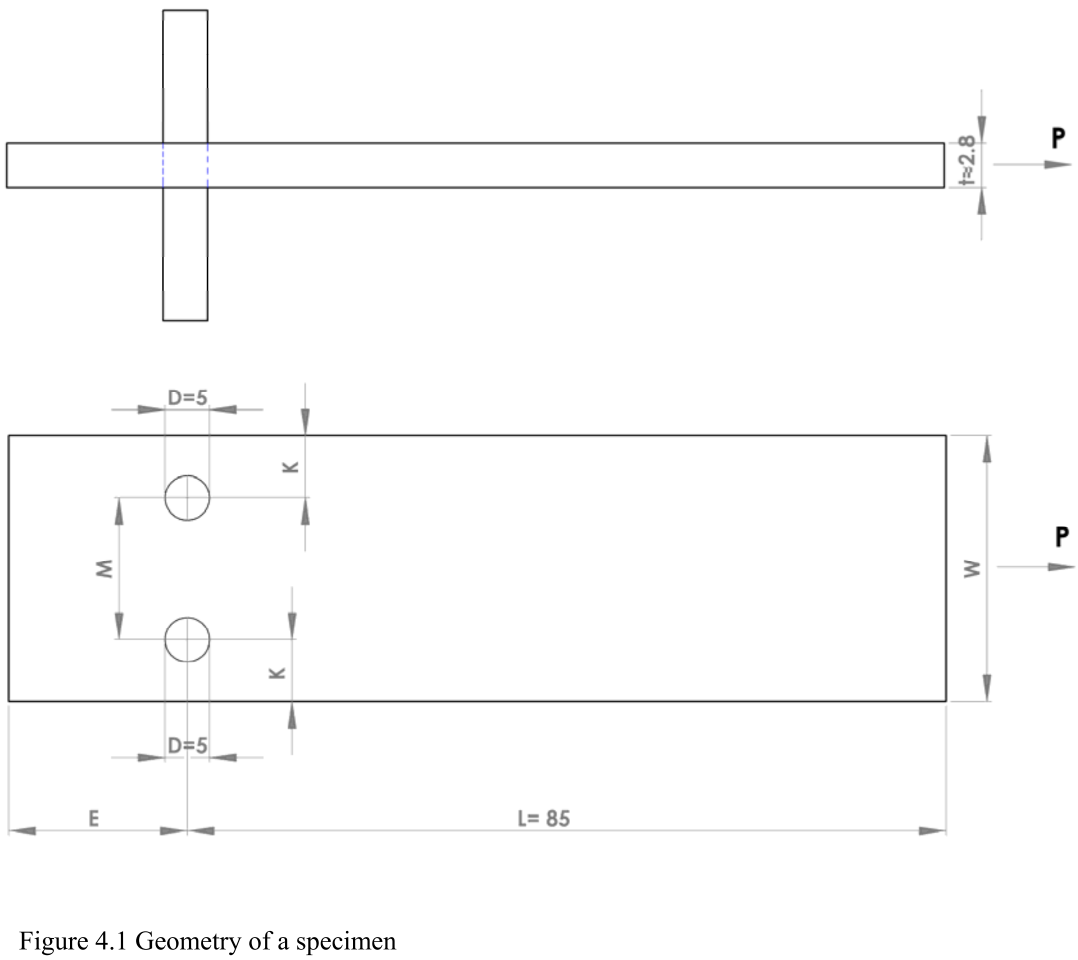

Figure 4.1 Geometry of a specimen

Depending on the geometry, the specimens may fail in tension, shear-out, or bearing. These three modes are shown in Figure 4.2. In real life applications, bearing failure is usually preferred because it is not catastrophic and provides the highest joint strength.

The ratio of K/D, E/D and M/D are changed from 2 to 4, 1 to5, 2 to 5 respectively. In order to find the strength of two parallel pin loaded specimens, the static bearing strength is defined as:

$$\sigma_b = \frac{P}{2Dt} \tag{4.1}$$

Table 4.1 Typical failure modes for bolted joints

Failure mode		Comment
Shear out	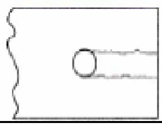	Caused by shear stresses and occurs along shear out planes on hole edge, typical failure mode when end distance is short.
Tension (net-section)	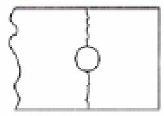	Caused by tangential tensile or compressive stresses at the edge of the hole. For uniaxial loading conditions, failure occurs when bypass/bearing stress ratio is high (or **d/w** is high).
Bearing	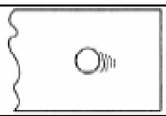	Occurs in area adjacent to contact area due to compressive stresses, likely when bypass/bearing stress ratio is low (or **d/w** is low), strongly effected by through-thickness clamping force.
Bearing/shear out	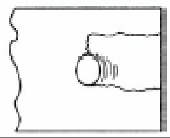	Mixed-mode
Bearing/tension/shear out	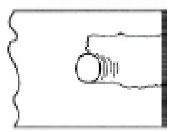	
Tension/shear out	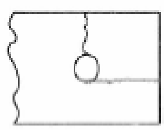	

4.2 Manufacturing of the Specimens

Izoreel Company produced composite materials which were used in this study. Composite plate was consisted of twelve laminas. Thickness of each lamina was 0.3 mm. The woven of glass-vinylester prepress are cured about 30 minutes at 100 C°

under 10 MPa pressure. At the end of the producing, composite plate thickness was measured as 2.8 mm. Volume fraction of the glass fiber was approximately 63%.

4.3 Determination of Mechanical Properties

The modulus in direction of the fibers E_1 and the Poisson's ratio ν_{12} can be characterized by means of tension tests on unidirectional coupons that instrumented with electric resistance strain gages, as depicted in Figure 4.2. One of them is placed to the fiber direction, the other in the matrix direction. The Poisson's ratio is just $\nu_{12} = -\varepsilon_2/\varepsilon_1$, it may be noted that some nonlinearity may be observed in these tests. E_2 is equal to E_1 due to the woven structure.

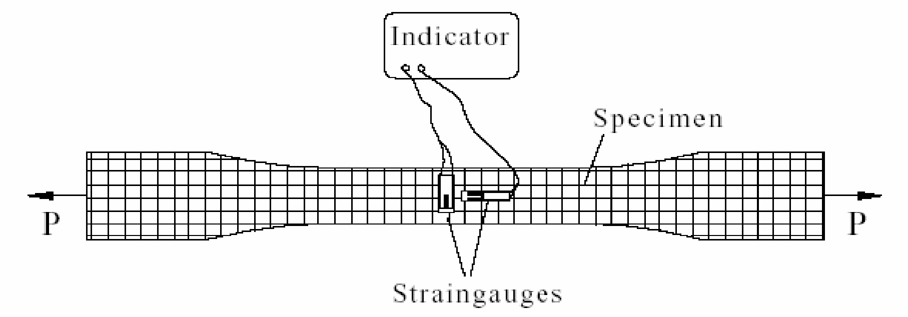

Figure 4.2 Longitudinal tension test specimen for determination of E_1 and ν_{12}

$$\sigma_1 = \frac{P}{A}, \qquad E_1 = \frac{\sigma_1}{\varepsilon_1}, \qquad E_2 = E_1 \tag{4.2}$$

X_t is calculated by dividing the ultimate force by the cross-sectional area of the specimen.

$$X_t = \frac{P_{ult}}{A} \tag{4.3}$$

To find X_c, a rectangular specimen with small length whose fiber direction coincides with the loading direction is taken and it is subjected to compressive loading Figure 4.3. X_c is also calculated by dividing the ultimate force by the cross-sectional area of the specimen.

$$X_c = \frac{P_{ult}}{A} \tag{4.4}$$

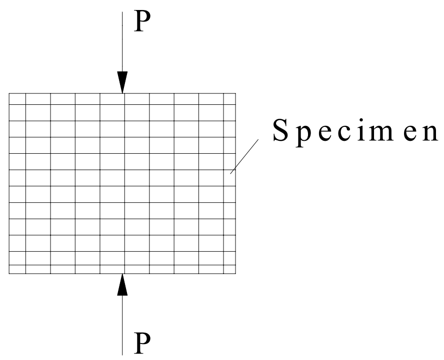

Figure 4.3 Longitudinal compression test

The in-plane shear modulus can be obtained in a number of ways (Jones, 1999). One of them is to use angel ply coupons, made up of alternating layers of plies at an angle to the axis of the specimen. It will be simply stated that the stress and strain response in the axial direction of at 45° laminate can be interpreted to give G_{12} according to the following expression:

$$E_x = \frac{P/A}{\varepsilon_x}$$

$$G_{12} = \frac{1}{\dfrac{4}{E_x} - \dfrac{1}{E_1} - \dfrac{1}{E_2} + \dfrac{2\nu_{12}}{E_1}} \tag{4.5}$$

Iosipescu testing method is used to define the shear strength S Figure 4.4. The dimensions of the specimen are chosen as; a=80 mm, b=20 mm, c=12 mm and t_i=2.8 mm. A compression test is applied to the specimen. In failure, S is calculated from

$$S = \frac{P_{max}}{t_i.c} \tag{3.6}$$

where P_{max} is the failure force. (Gibson, 1994)

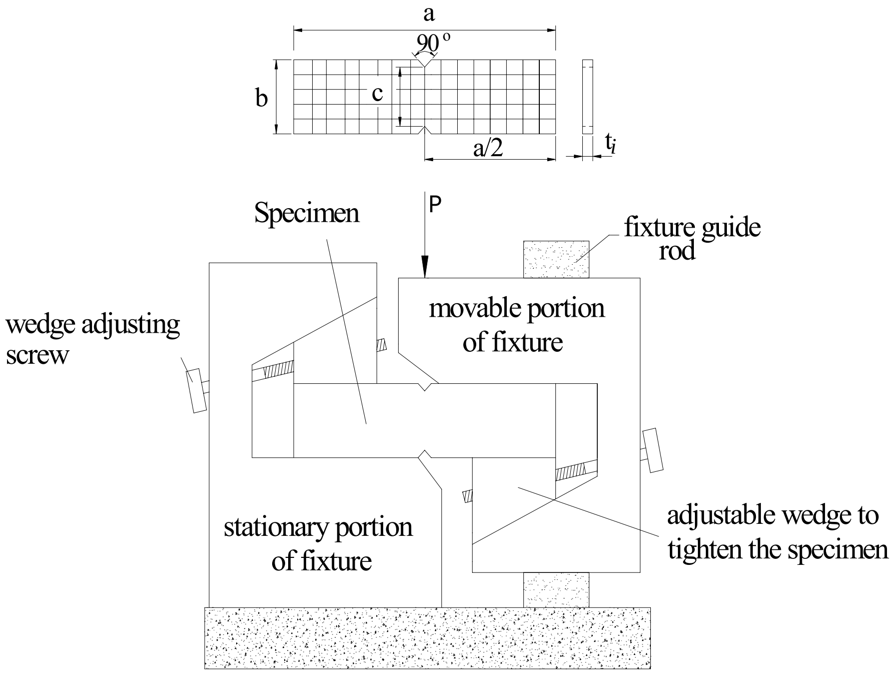

Figure 4.4 Iosipescu testing fixture

Y_t and Y_c are equal to, X_t and X_c, respectively because of the woven structure. The mechanical properties of glass-vinylester composite plate which are obtained from the experimental study have been given in Table 3.1. (Gülem, 2004)

Table 4.2 Mechanical properties of glass-vinlyester composite materials

$E_1=E_2$ (GPa)	G_{12} (GPa)	ν_{12}	$X_t=Y_t$ (MPa)	$X_c=Y_c$ (MPa)	S (MPa)	V_f (%)
20.769	4.133	0.09	395	260	75	63

To find the failure load and the failure mode, a series of experiments were carried out. The specimens were trimmed as depicted in Figure 4.1. The effects of the pin location were studied by varying the distance from upper part of plate and centre of holes (K/D) ratio from 2 to 4, edge distance to diameter (E/D) ratio from 1 to 5 and between two holes distance to diameter (M/D) ratio from 2 to 5, for the 0° fiber orientation angle while keeping D, t and L constant. 60 different geometries were used. All specimens were tested two times each.

The experiments were carried out in tension mode on the Tensile Machine. The lower edge of the specimen clamped and loaded from the steel pins by stretching the specimens at a ratio 0.5 mm/min Figure 4.5. The load-pin displacement diagrams for all composite configurations were plotted.

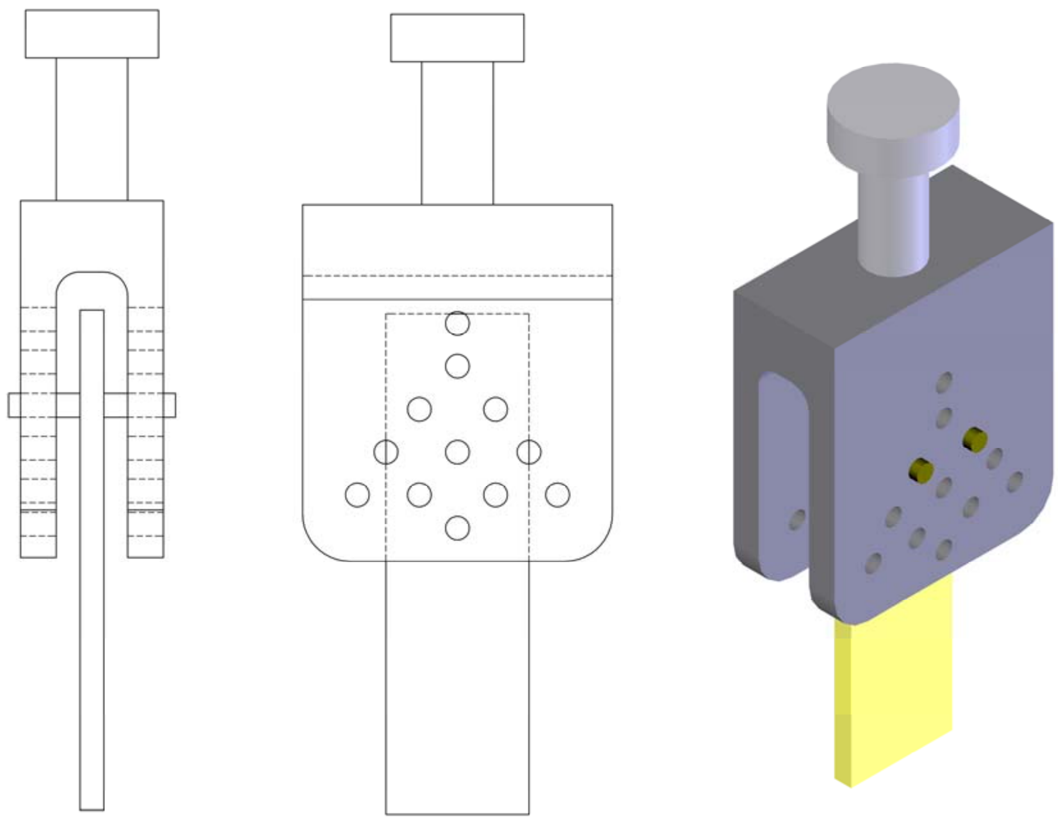

Figure 4.5 Experimental setup for pin-joint testing

CHAPTER FIVE
RESULTS AND DISCUSSION

In this investigation, progressive failure analysis of pin loaded composite plates is performed to predict failures and bearing stresses and also it is compared with different geometries. The analysis takes into account contact between the pins and holes and a non-linear shear stress-strain relationship. To predict the failure, the Hashin Criteria was used for numerical analysis. After that these results have been compared with the experimentally conclusions.

In the experimental study, it is seen that load–displacement curves are linear before the initial failure. But then load decreases while deformation increases for most of the specimens. Some of them continued to keep loading on. Sometimes the highest load becomes after this event.

It is seen that when edge distance to diameter ratio (E/D), distance between holes to diameter (M/D) and distance between center of holes and upper part of plates to diameter ratio (K/D) are increased, failure load reaches higher values.

Especially when E/D ratio is 1 for M/D=2, 3 and K/D=2, failure load occurs lower values. In this case, plate is the weakest. E/D ratio begins to increase when M/D and K/D are constant; failure load reaches the higher values. For example E/D is 4-5 for M/D=4-5 and K/D is 4, failure load occurs 7500-8000 N.

In the same way, failure occurs quickly while M/D ratio is 2-3 for E/D=1 and K/D=2. When the M/D ratio is increased such as 4and 5, failure load values reaches higher values.

Load-displacements curves of the experimental study are shown in Appendix A.

Bearing strength rises with increasing M/D ratio, while E/D and K/D ratio are constant. It reaches higher values when M/D 4, 5 for E/D=1 K/D=2-3.

When E/D ratio reaches 4 or 5 value, failure mode generally either bearing or bearing and shear out. It is shown in Figure 5.1 and 5.2

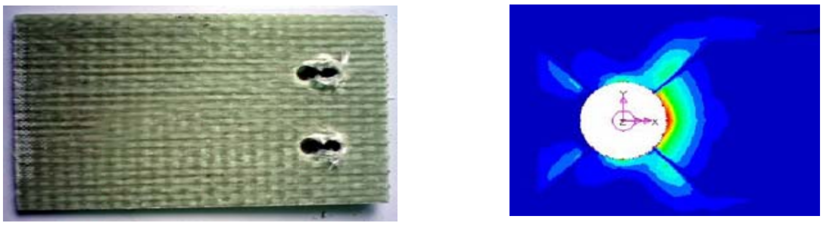

Figure5.1 The bearing mode for E/D=5, M/D=5, K/D=4

Figure5.2 The bearing and shear out mode for E/D=2, M/D=3, K/D=3

At low values of E/D, the failure types are shear out which are weak type of failure. This mode can be shown in Figure 5.3

Figure5.3 The shear out mode for E/D=1, M/D=5, K/D=2

The other modes of failure of comparison with experimental and Hashin results are shown in Appendix B.40

Figures from 5.4 to 5.15 are concerned with the bearing strength. It is clearly seen from the graphics that bearing strength is depend on E/D ratio. Bearing strength reaches lowest values while E/D=1 for M/D=2-3, K/D=2-3. As the E/D and M/D ratio are increases, the failure load reaches higher values.

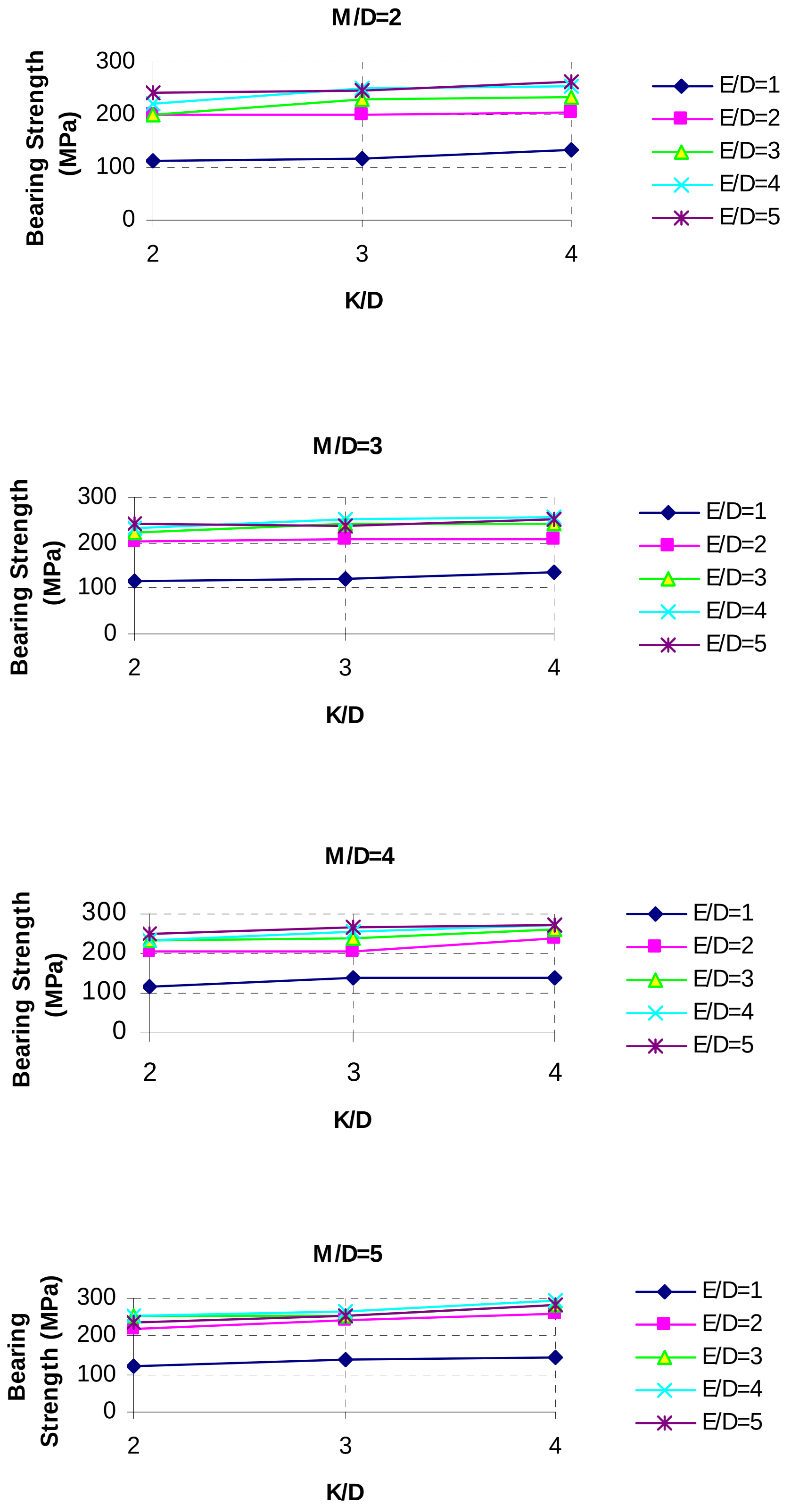

Figure 5.4 The effect of K/D ratio according to E/D=1, 2, 3, 4, 5, M/D=2, 3, 4, 5

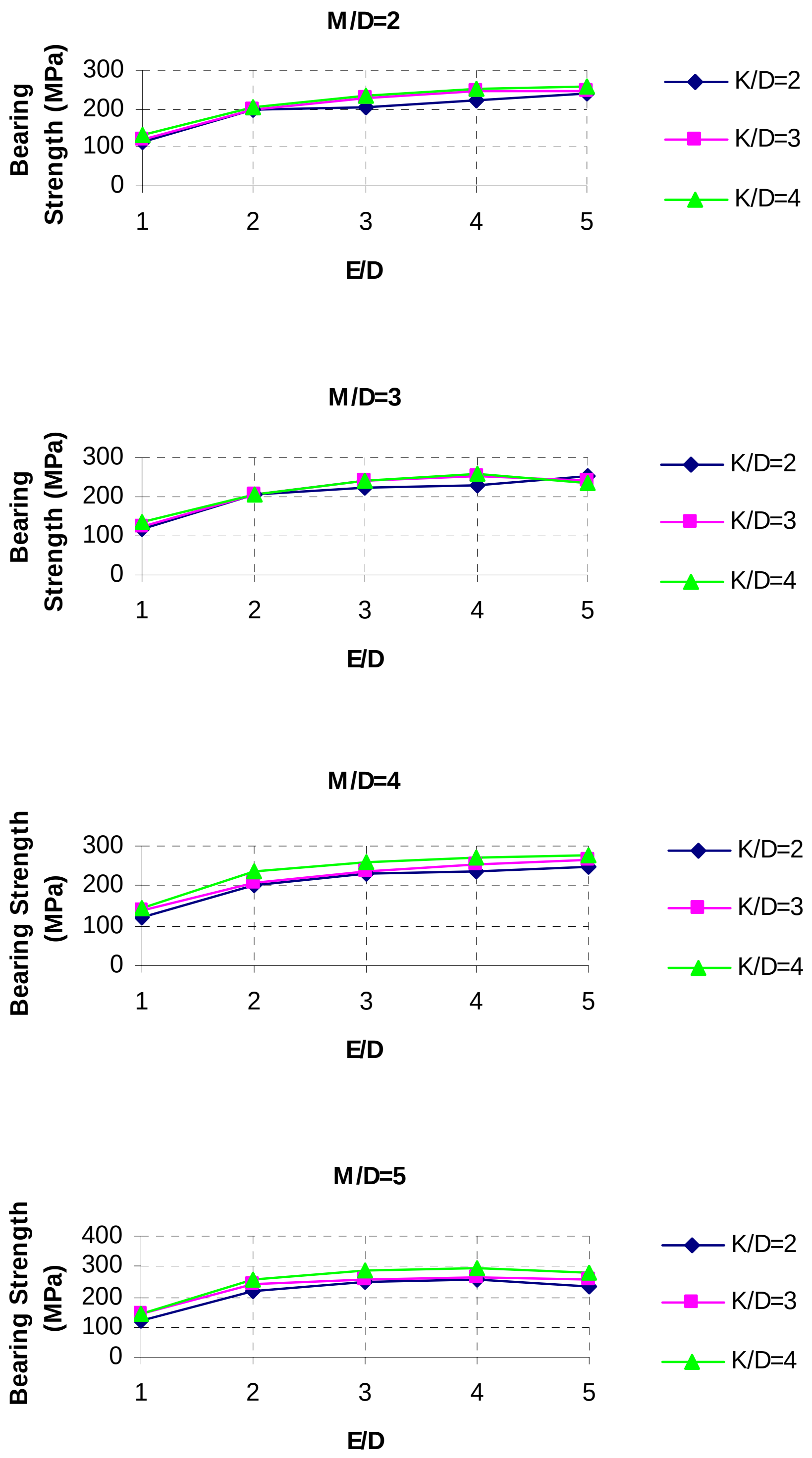

Figure 5.5 The effect of E/D ratio according to K/D= 2, 3, 4, M/D=2, 3, 4, 5

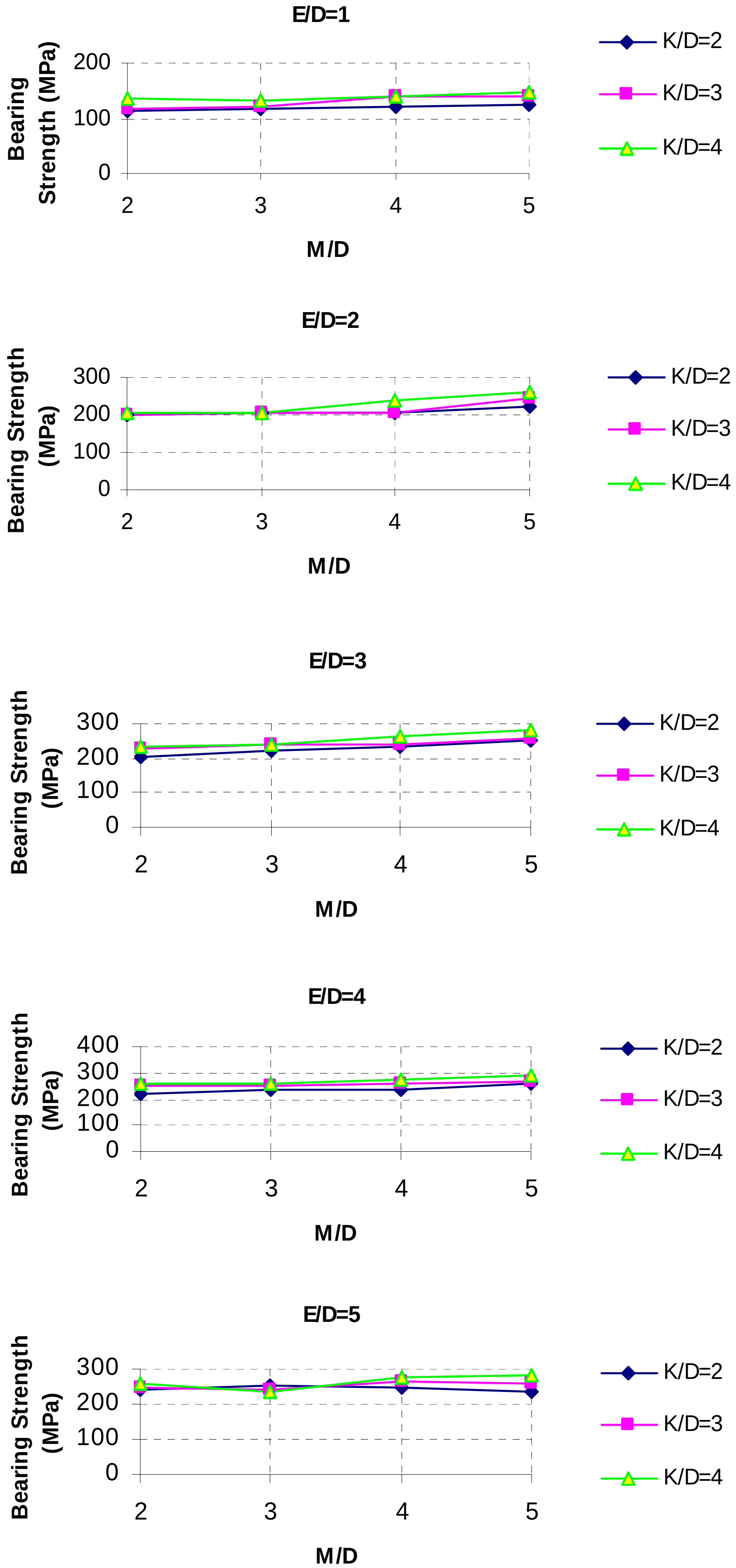

Figure 5.6 The effect of M/D ratio according to K/D= 2, 3, 4, E/D=1, 2, 3, 4, 5

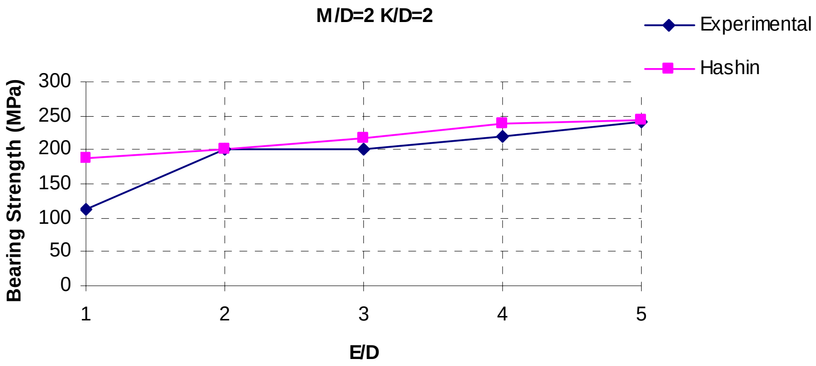

(a)

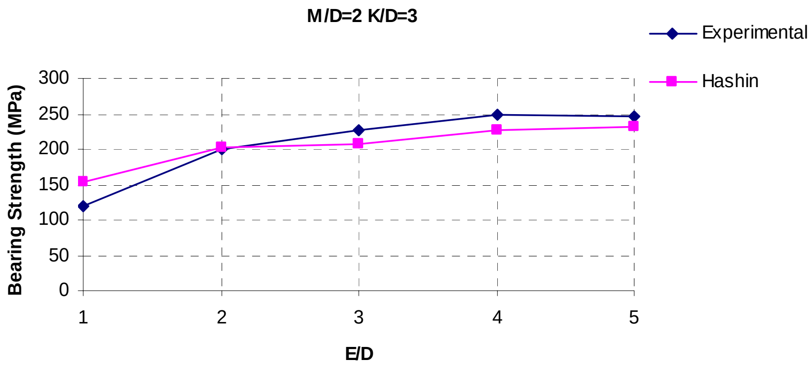

(b)

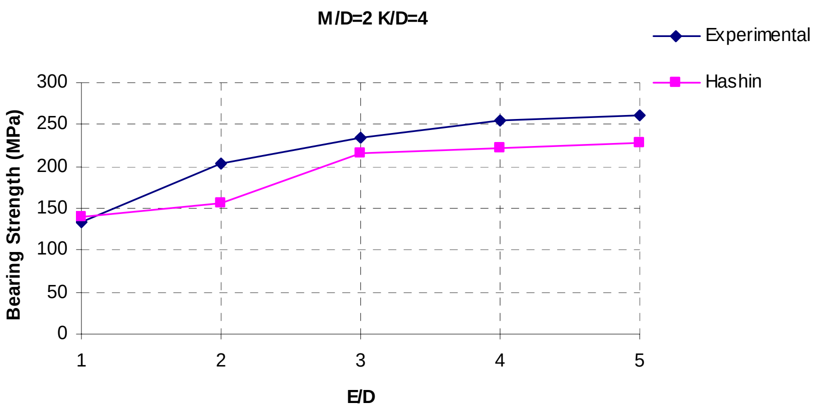

(c)

Figure 5.7 The effect of E/D ratio on the bearing strength for M/D=2 a) K/D=2, b) K/D=3 c) K/D=4

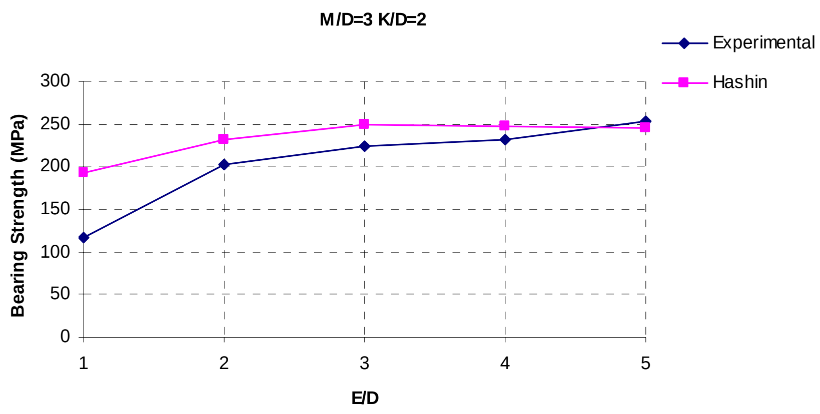

(a)

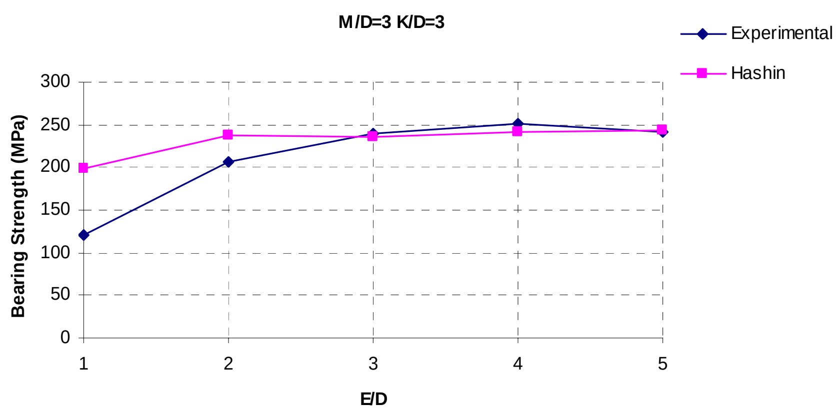

(b)

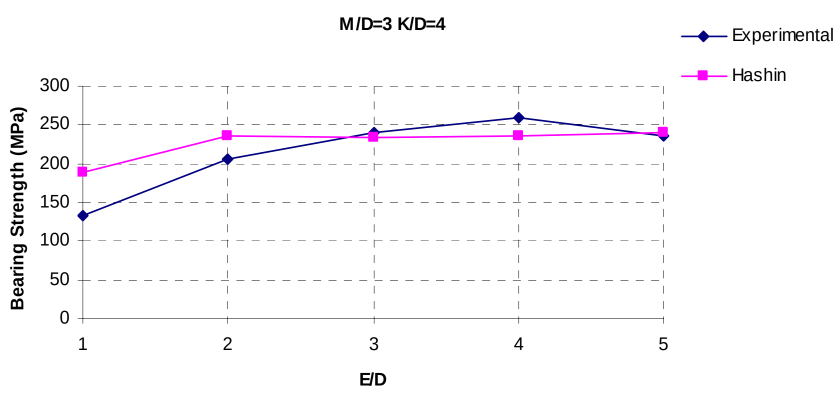

(c)

Figure 5.8 The effect of E/D ratio on the bearing strength for M/D=3 a) K/D=2, b) K/D=3 c) K/D=4

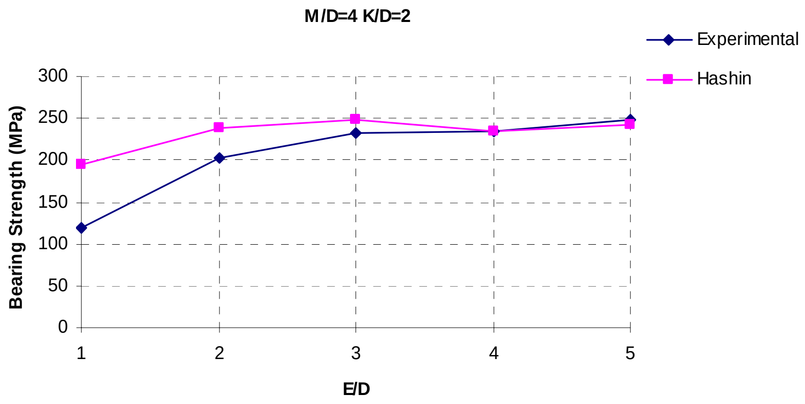

(a)

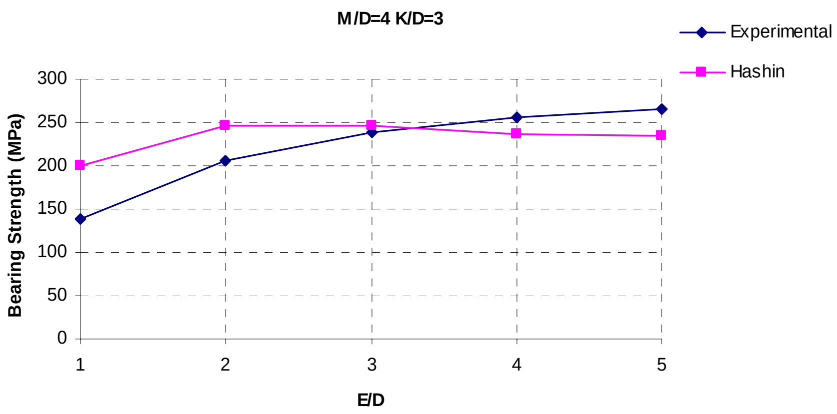

(b)

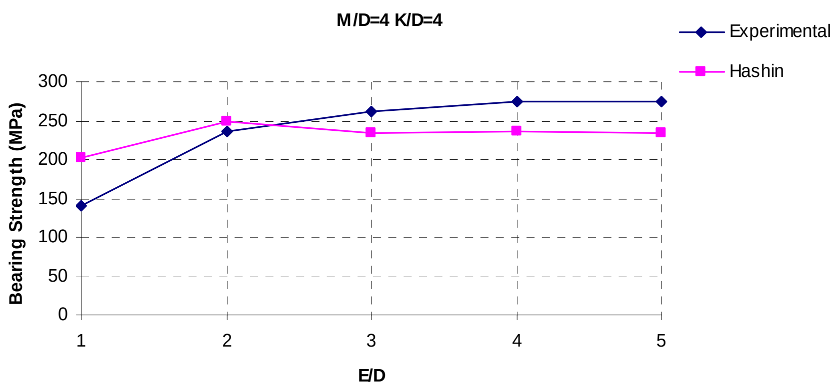

(c)

Figure 5.9 The effect of E/D ratio on the bearing strength for M/D=4 a) K/D=2, b) K/D=3 c) K/D=4

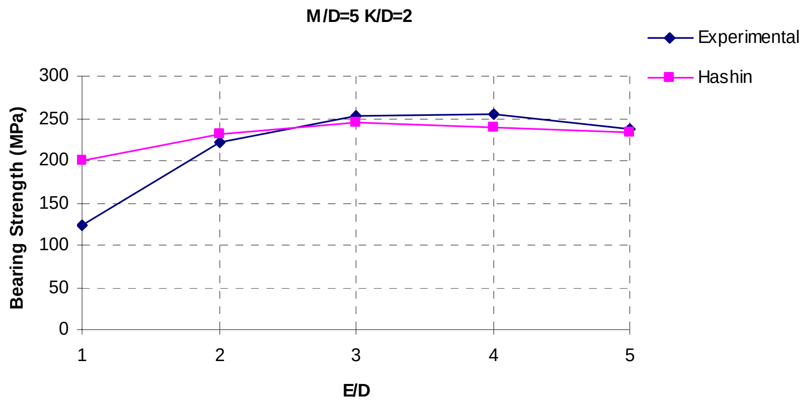

(a)

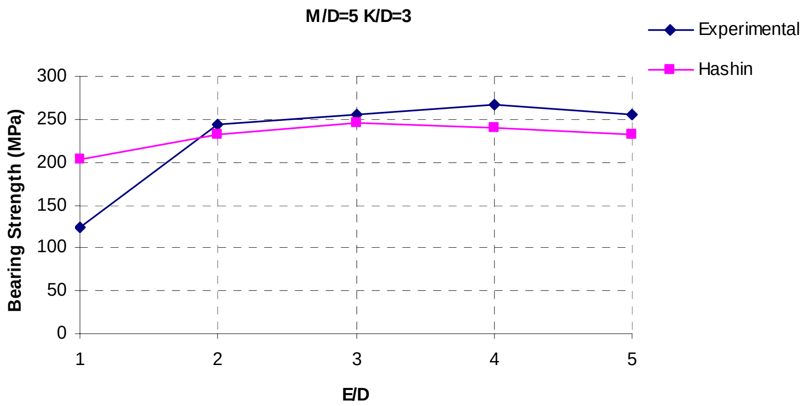

(b)

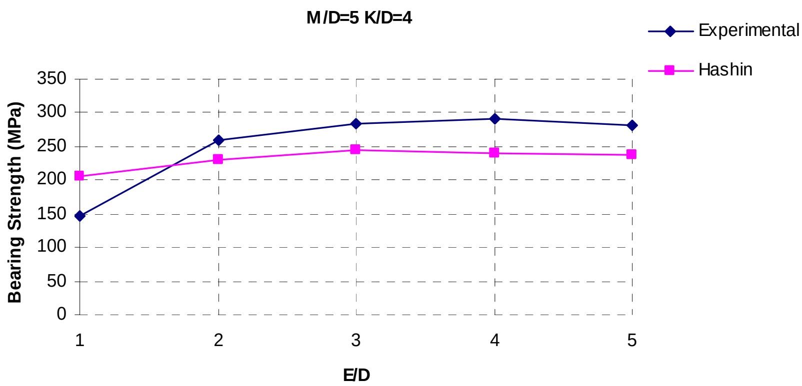

(c)

Figure 5.10 The effect of E/D ratio on the bearing strength for M/D=5 a) K/D=2, b) K/D=3 c) K/D=4

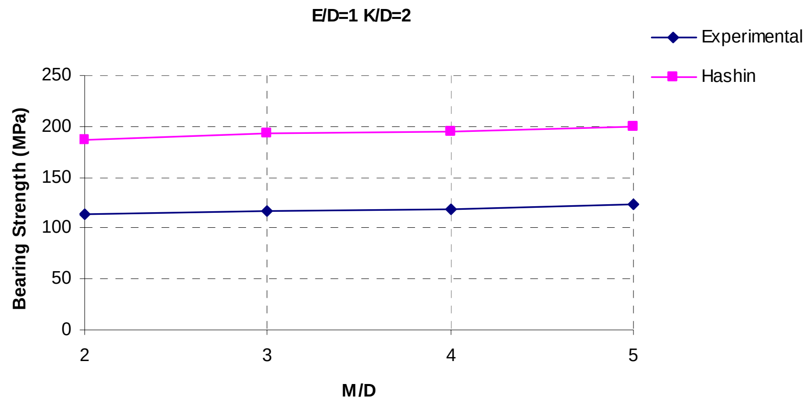

(a)

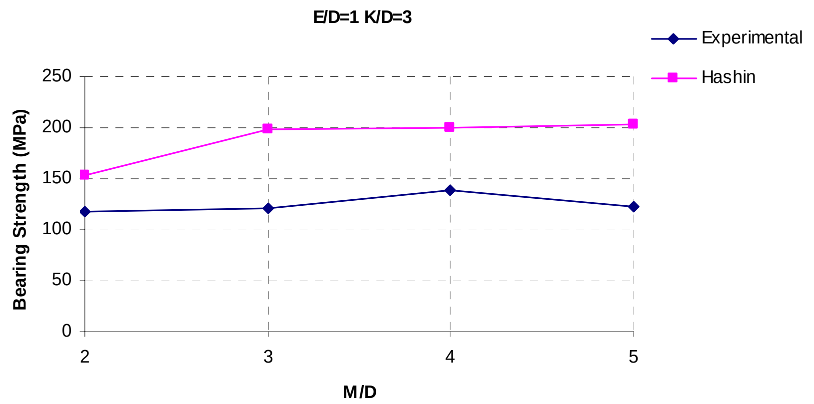

(b)

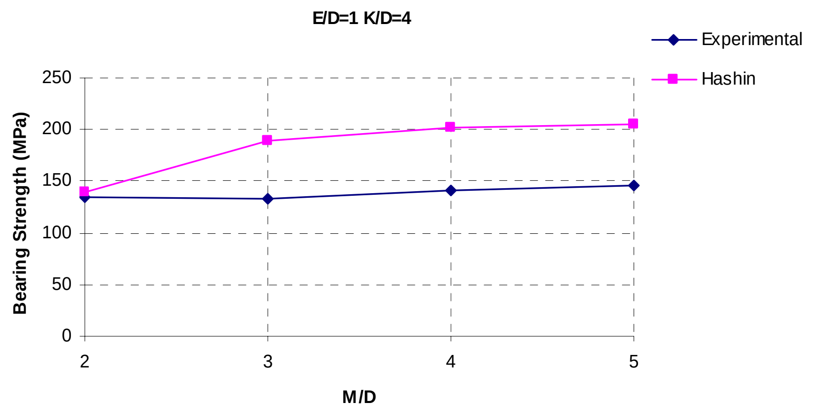

(c)

Figure 5.11 The effect of M/D ratio on the bearing strength for E/D=1 a) K/D=2, b) K/D=3 c) K/D=4

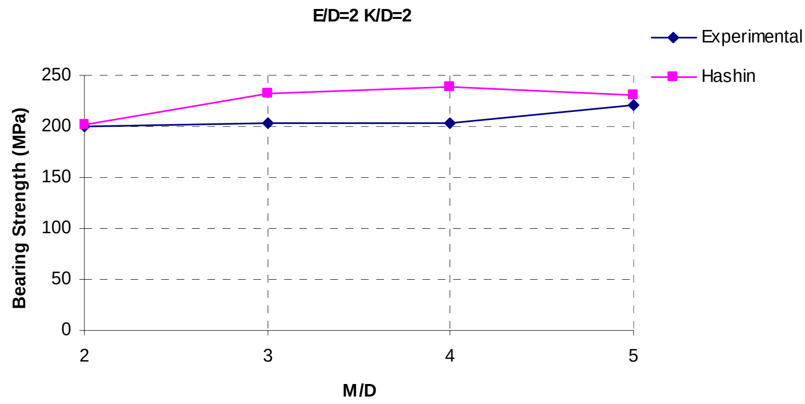

(a)

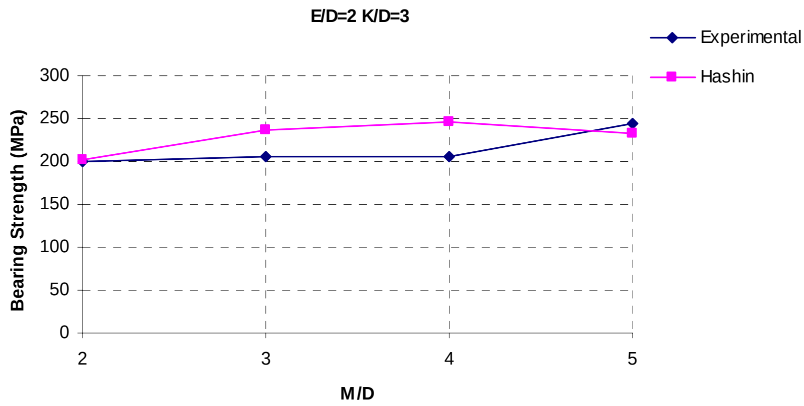

(b)

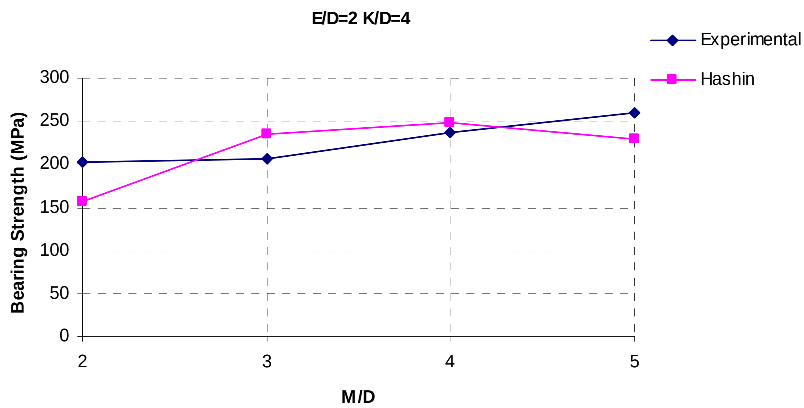

(c)

Figure 5.12 The effect of M/D ratio on the bearing strength for E/D=2 a) K/D=2, b) K/D=3 c) K/D=4

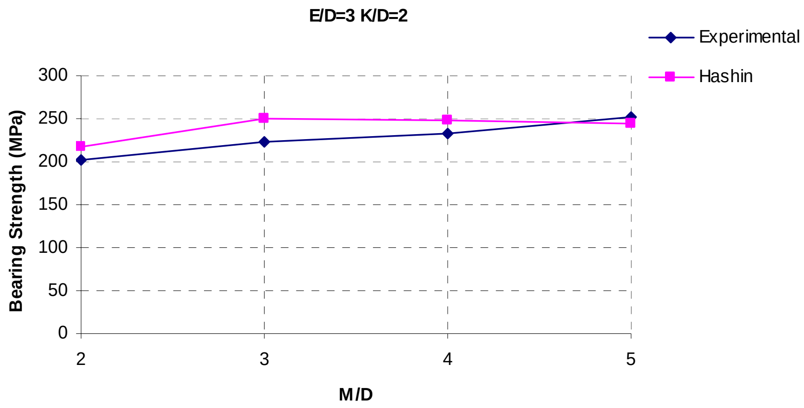

(a)

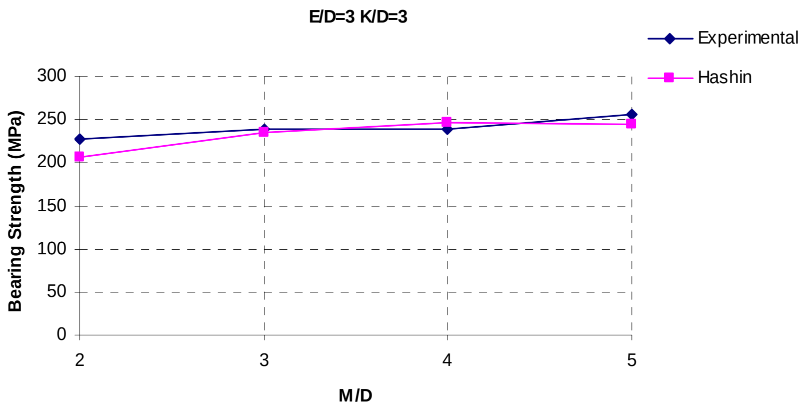

(b)

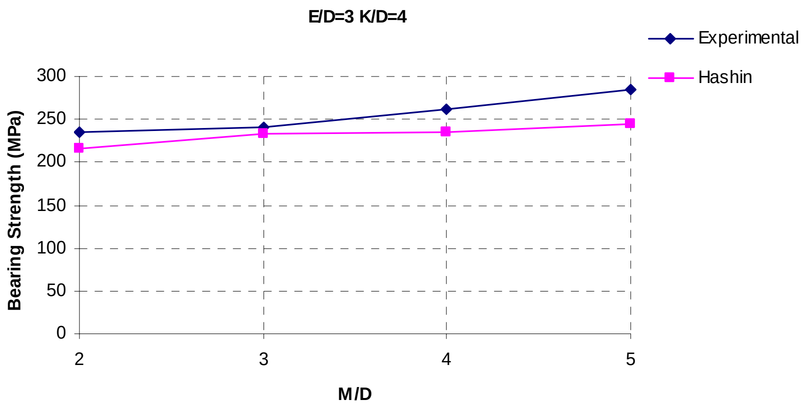

(c)

Figure 5.13 The effect of M/D ratio on the bearing strength for E/D=3 a) K/D=2, b) K/D=3 c) K/D=4

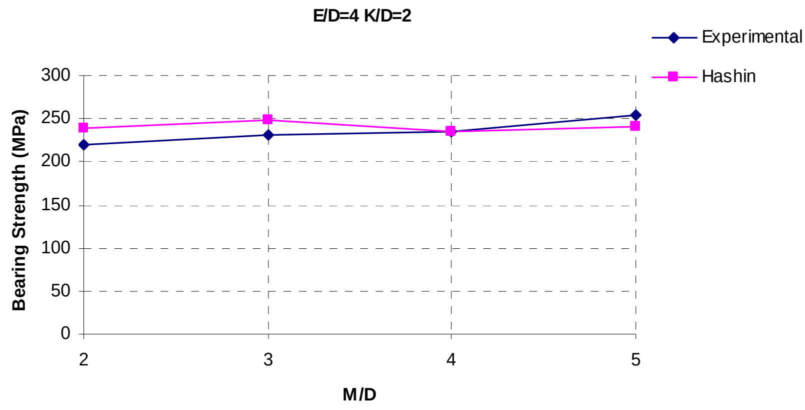

(a)

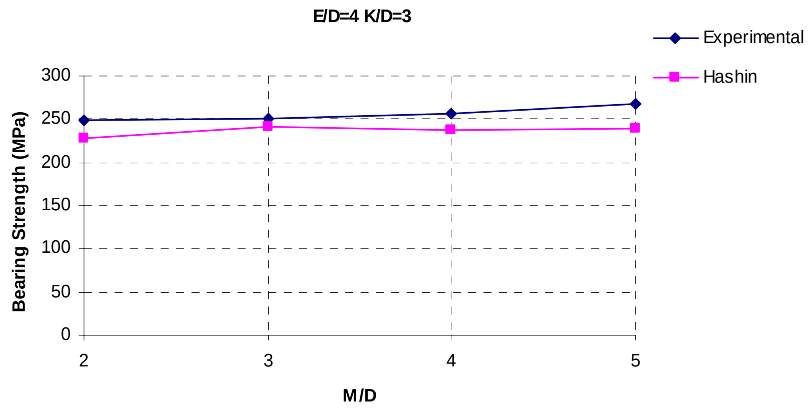

(b)

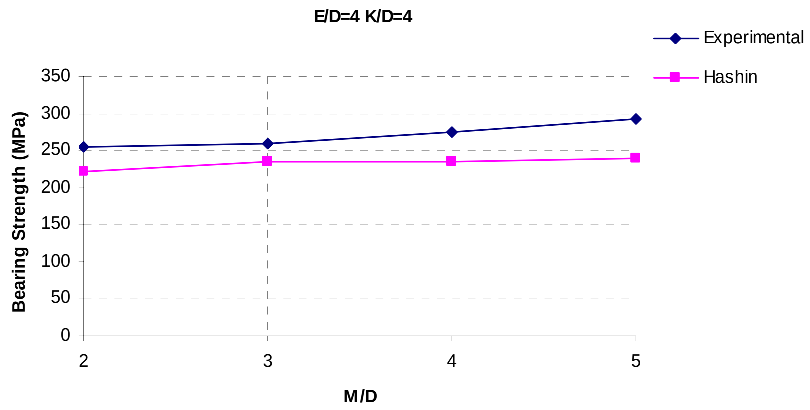

(c)

Figure 5.14 The effect of M/D ratio on the bearing strength for E/D=4 a) K/D=2, b) K/D=3 c) K/D=4

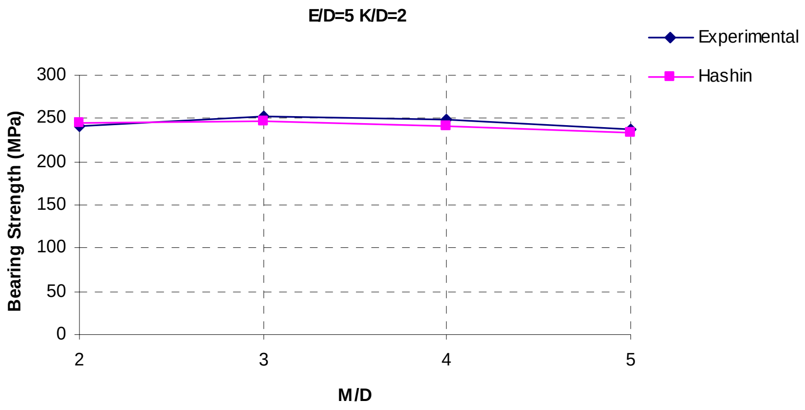

(a)

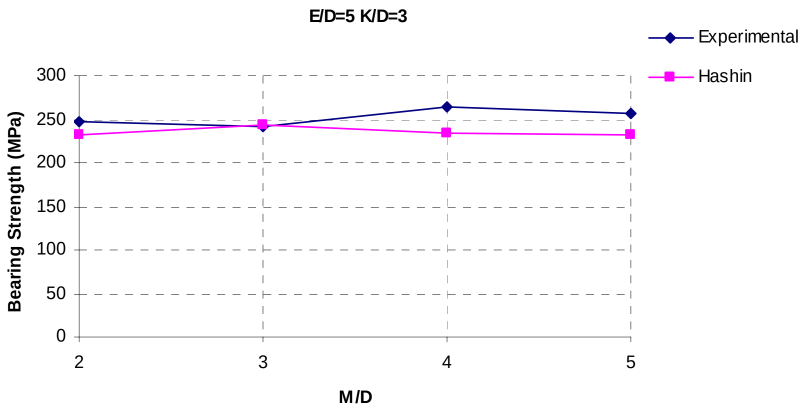

(b)

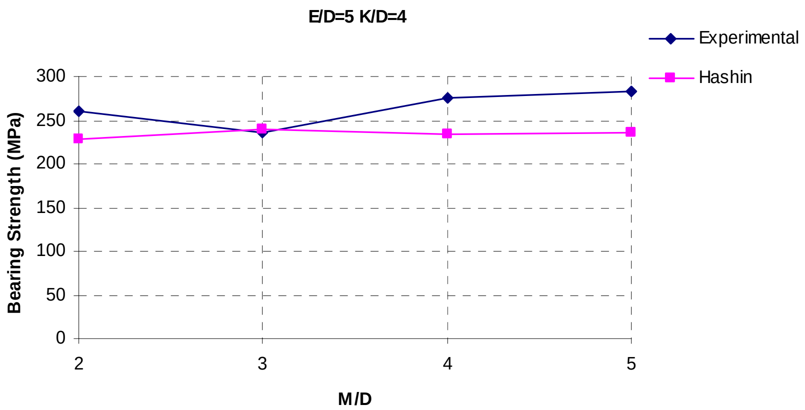

(c)

Figure 5.15 The effect of M/D ratio on the bearing strength for E/D=5 a) K/D=2, b) K/D=3 c) K/D=4

Table 5.1 Comparisons of experimental and numerical failure loads and bearings for E/D=1

E/D=1		Failure Load (N)		Bearing Strength (MPa)	
		Experimental	Hashin	Experimental	Hashin
K/D=2	M/D=2	3163	5235	113	187
	M/D=3	3278	5400	117	193
	M/D=4	3332	5452	119	195
	M/D=5	3457	5578	123	199
K/D=3	M/D=2	3314	4288	118	153
	M/D=3	3404	5560	122	199
	M/D=4	3874	5601	138	200
	M/D=5	3454	5706	123	204
K/D=4	M/D=2	3762	3912	134	140
	M/D=3	3737	5304	133	189
	M/D=4	3961	5652	141	202
	M/D=5	4083	5750	146	205

Table 5.2 Comparisons of experimental and numerical failure loads and bearings for E/D=2

E/D=2		Failure Load (N)		Bearing Strength (MPa)	
		Experimental	Hashin	Experimental	Hashin
K/D=2	M/D=2	5604	5640	200	201
	M/D=3	5695	5684	203	203
	M/D=4	5696	6663	203	238
	M/D=5	6177	6463	221	231
K/D=3	M/D=2	5625	5635	201	201
	M/D=3	5775	6640	206	237
	M/D=4	5750	6912	205	247
	M/D=5	6851	6501	245	232
K/D=4	M/D=2	5689	4368	203	156
	M/D=3	5781	5676	206	203
	M/D=4	6628	6944	237	248
	M/D=5	7284	6441	260	230

Table 5.3 Comparisons of experimental and numerical failure loads and bearings for E/D=3

E/D=3		Failure Load (N)		Bearing Strenth (MPa)	
		Experimental	Hashin	Experimental	Hashin
K/D=2	M/D=2	5635	6105	201	218
	M/D=3	6273	7000	224	250
	M/D=4	6515	6936	233	248
	M/D=5	7073	6850	253	245
K/D=3	M/D=2	6378	5788	228	207
	M/D=3	6711	6600	240	236
	M/D=4	6683	6912	239	247
	M/D=5	7159	6864	256	245
K/D=4	M/D=2	6585	6025	235	215
	M/D=3	6744	6540	241	234
	M/D=4	7344	6566	262	235
	M/D=5	7952	6840	284	244

Table 5.4 Comparisons of experimental and numerical failure loads and bearings for E/D=4

E/D=4		Failure Load (N)		Bearing Strenth (MPa)	
		Experimental	Hashin	Experimental	Hashin
K/D=2	M/D=2	6152	6690	220	239
	M/D=3	6482	6940	232	248
	M/D=4	6585	6576	235	235
	M/D=5	7140	6720	255	240
K/D=3	M/D=2	6970	6376	249	228
	M/D=3	7026	6750	251	241
	M/D=4	7185	6624	257	237
	M/D=5	7475	6723	267	240
K/D=4	M/D=2	7137	6220	255	222
	M/D=3	7247	6600	259	236
	M/D=4	7670	8165	274	292
	M/D=5	8165	6690	292	239

Table 5.5 Comparisons of experimental and numerical failure loads and bearings for E/D=5

E/D=5		Failure Load (N)		Bearing Strenth (MPa)	
		Experimental	Hashin	Experimental	Hashin
K/D=2	M/D=2	6779	6840	242	244
	M/D=3	7065	6900	252	246
	M/D=4	6954	6768	248	242
	M/D=5	6630	6531	237	233
K/D=3	M/D=2	6931	6520	248	233
	M/D=3	6754	6800	241	243
	M/D=4	7407	6570	265	235
	M/D=5	7176	6508	256	232
K/D=4	M/D=2	7302	6400	261	229
	M/D=3	6589	6720	235	240
	M/D=4	7688	6529	275	233
	M/D=5	7909	6630	282	237

CHAPTER SIX
CONCLUSION

In this investigation, failure mode, maximum failure load and bearing strength in a glass vinylester composite plate with two circular and parallel holes, which is subjected to traction force by two parallel rigid pins, are performed experimentally and numerically. In numerical study, Hashin failure criteria was used to predict the maximum failure load and failure types. In the experimental study, the specimens for each E/D, M/D and K/D ratio have been tested. Experimental results concerning failure types and failure loads were obtained and compared with numerical results. It is seen that these results are close to each other. In addition the effects of geometric parameters are observed. All the numerical and experimental results which is obtained have been presented in tables and figures.

Bearing strength of the composite plate increases by going up the geometric parameters. It means that, when edge distance to diameter ratio (E/D), distance between center of the holes (M/D) and distance from center of holes to upper edge of plates (K/D) are increased, the bearing strength reaches higher values.

When E/D ratio is 1, the bearing strength is small and failure mode is generally shear out. In addition, when the E/D ratio 3, 4 or 5, the failure load reaches higher values and failure modes is bearing which is the best mode of resisting load.

While the M/D and K/D ratios are increased, the bearing strengths generally reach high values as E/D ratio. Failure types are bearing.

At low values of M/D, the failure types are shear out or shear out and bearing together which are weak type of failure

REFERENCES

Aktaş, A, & Karakuzu, R. (1999). Failure Analysis of Two-Dimensional Carbon-Epoxy Composite Plate Pinned Joint. *Mechanics of Composite Materials and Structures*, *6*, 347-361.

Camanho, P.P., & Matthews, F.L. (1997). Stress analysis and strength prediction of mechanically fastened joints in FRP: a review. *Composites Part A, 28A*, 529-47.

Camanho, P.P, & Matthews, F.L. (1999). A Progressive Damage Model for Mechanically Fastened Joints in Composite Laminates. *Journal of Composite Materials*, *33*, 2248-2280

Chandrupatla, T.R., & Belengundu, A.D. (1991). *Introduction to Finite Elements in Engineering.* Prentice-Hall.

Chang, F.K., Scott, R.A., & Springer, G.S. (1984)b. Failure Strength of Nonlinearly Elastic Composite Laminates Containing a Pin Loaded Hole. *Journal of Composite Materials*, *18*, 464-477

Chang, F.K. (1986). The Effect of Pin Load Distribution on the Strength of Pin Loaded Holes in Laminated Composites. *Journal of Composite Materials*, *20*, 401-408

Dano, M.L., Gendron, G., & Piccard, A. (2000). Stress and Failure Analysis of Mechanically Fastened Joints in Composite Laminates. *Composite Structures*, *50*, 287-296.

Gülem, T., Icten, B.M., Karakuzu, R. (2004). Failure Analysis of Woven Laminated Glass-vinylester Composites with Pin-loaded Hole. *Composite Structures*, Hamada, H., & Maekawa, Z.I. (1996). Strength Prediction of Mechanically Fastened Quasi-Isotropic Carbon/Epoxy Joints. *Journal of Composite Materials*, *30*, 1596-1612.

Hassan, N.K., Mohamedien, M.A., & Rizkalla, S.H. (1996). Finite element analysis of bolted connections for PFRP composites. *Composites: Part B, 27B*, 339-349.

Hung, C.L., & Chang, F.K. (1996). Bearing Failure of Bolted Composite Joints. Part II: Model and Verification. *Journal of Composite Materials*, *30*, 1359-1400.

Icten, B.M., & Karakuzu, R. (2002). Progressive failure analysis of pin loaded carbon-epoxy woven composite plates. *Composite Science and Technology*, *62*, 1259-1271.

Icten, B.M., & Sayman, O., (2003). Failure analysis of pin-loaded aluminum-glass-epoxy sandwich composite plates. *Composite Science and Technology*, *63*, 727-737

Jones, R. M. (1999). *Mechanics of Composite Material. (2nd ed.).* Tokyo: Taylor& Francis.

Kim, S.J., Hwang, J.S., & Kim, J.H. (1998, January). Progressive failure analysis of pin-loaded laminated composites using penalty finite element method. *AIAA Journal*, *36*, No: 1, 75-80.

Kretsis, G., & Matthews, F.L. (1985, April). The strength of bolted joints in glass fibre/epoxy laminates. *Journal of Composite Materials*, 16, 92-102

Lessard, L.B., & Shokrieh, M.M. (1995). Two-Dimensional Modeling of Composite Pinned-Joint Failure. *Journal of Composite Materials*, 29, 671-697.

Okutan, B., Aslan, Z., & Karakuzu, R. (2001). A Study of The Effects of Various Geometric Parameters On The Failure Strength of Pin-Loaded Woven-Glass-Fiber Reinforced Epoxy Laminate. *Composite Science and Technology*, *61*, 1491-1497.

Pierron, F., & Cerisier, F. (2000). A Numerical and Experimental Study of Woven Composite Pin-Joints. *Journal of Composite Materials*, *34*, 1028-1054.

APPENDIX A

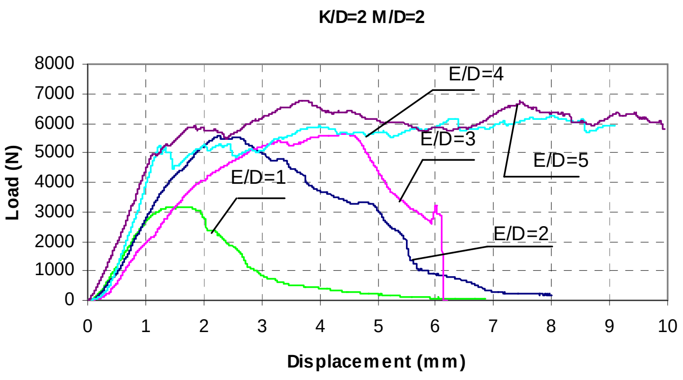

(a)

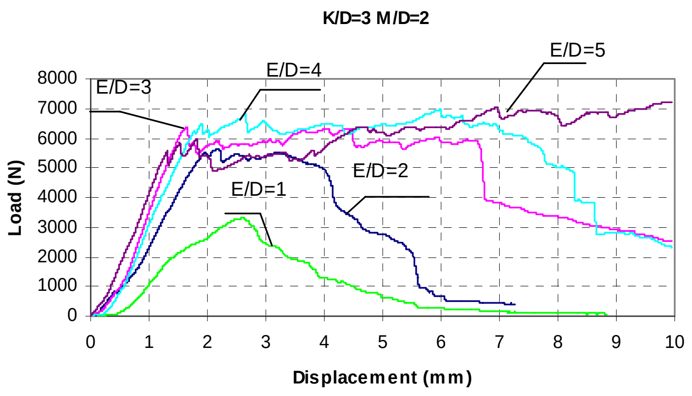

(b)

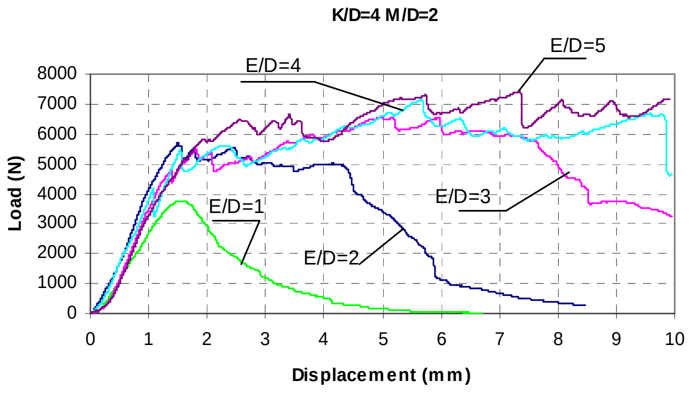

(c)

Figure A.1 Load-displacement curves for pin-loaded glass-vinylester composite plates (E/D=1,2,3,4,5 M/D=2) a) K/D=2, b) K/D=3, c) K/D=4

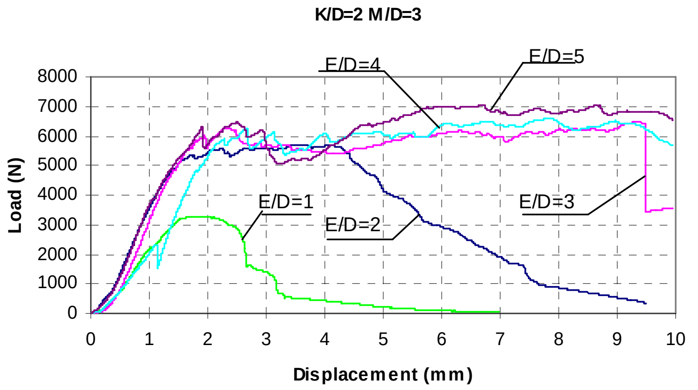

(a)

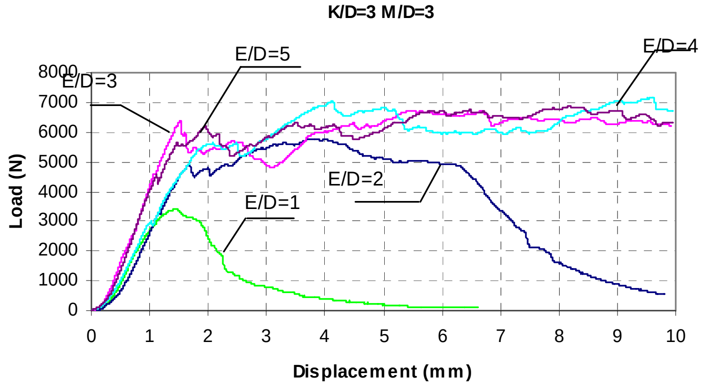

(b)

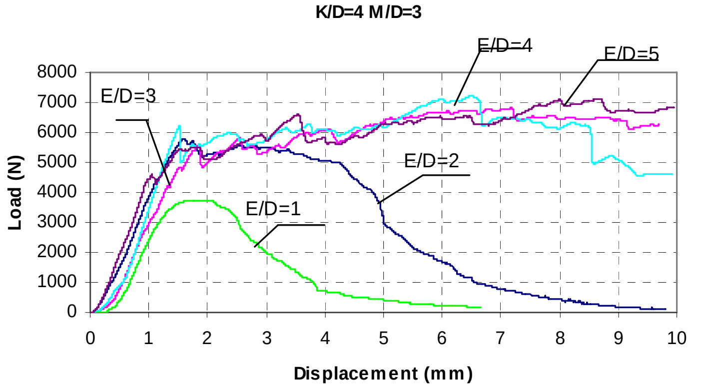

(c)

Figure A.2 Load-displacement curves for pin-loaded glass-vinylester composite plates (E/D=1,2,3,4,5 M/D=3) a) K/D=2, b) K/D=3, c) K/D=4, d) K/D=5

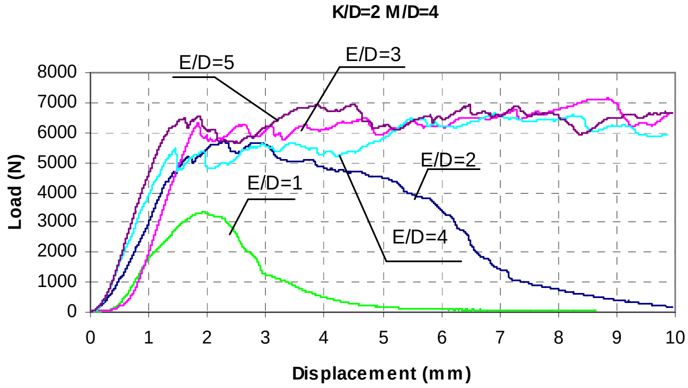

(a)

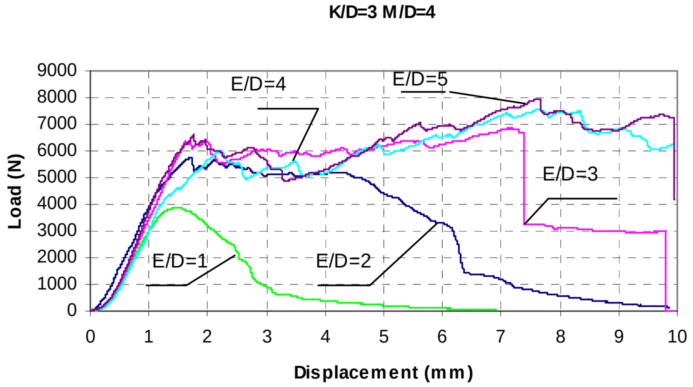

(b)

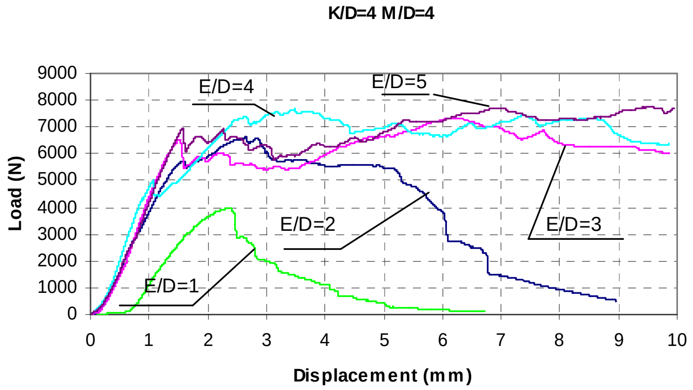

(c)

Figure A.3 Load-displacement curves for pin-loaded glass-vinylester composite plates (E/D=1,2,3,4,5 M/D=4) a) K/D=2, b) K/D=3, c) K/D=4

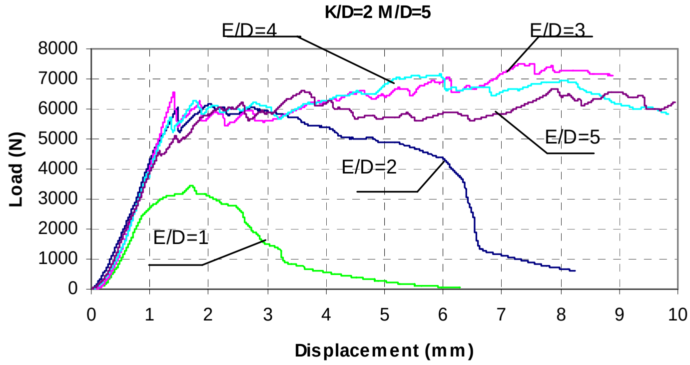

(a)

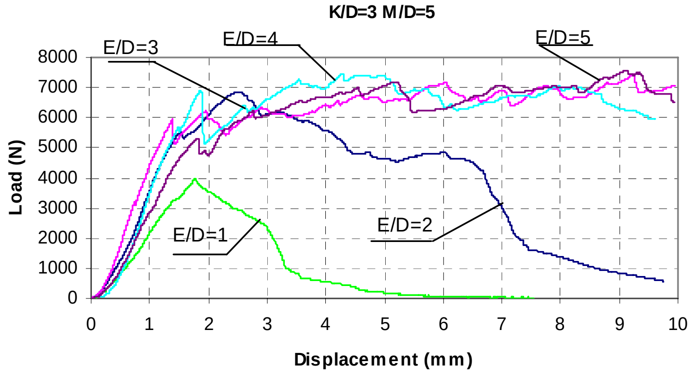

(b)

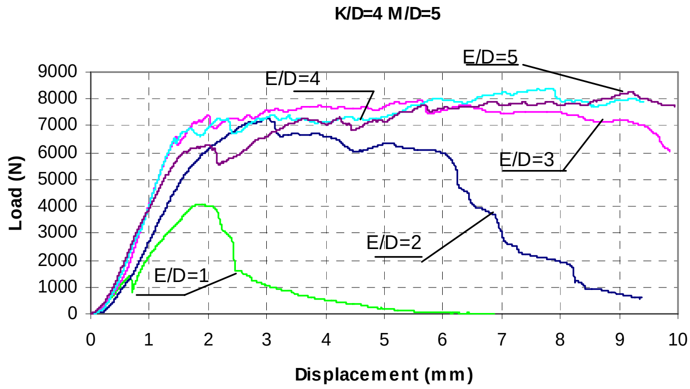

(c)

Figure A.4 Load-displacement curves for pin-loaded glass-vinylester composite plates (E/D=1,2,3,4,5 M/D=5) a) K/D=2, b) K/D=3, c) K/D=4

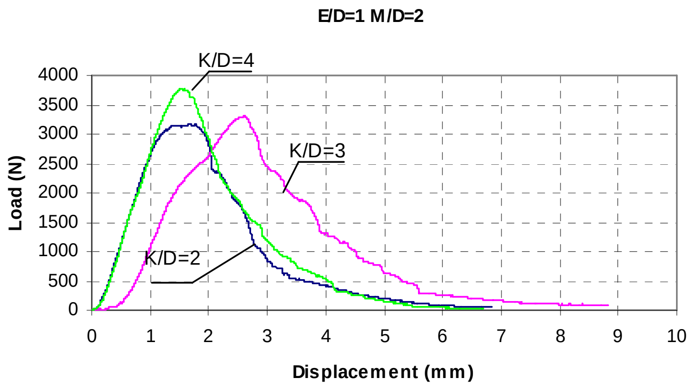
E/D=1 M/D=2
K/D=4
K/D=3
K/D=2
Load (N)
Displacement (mm)

(a)

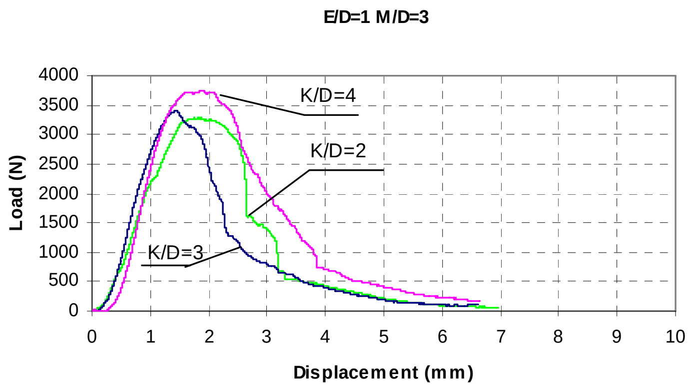
E/D=1 M/D=3
K/D=4
K/D=2
K/D=3
Load (N)
Displacement (mm)

(b)

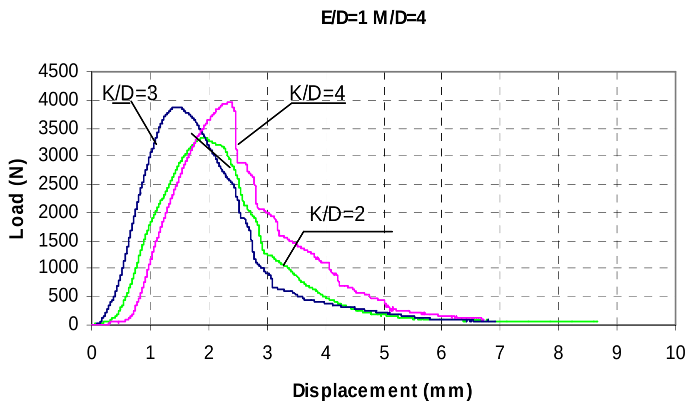
E/D=1 M/D=4
K/D=3
K/D=4
K/D=2
Load (N)
Displacement (mm)

(c)

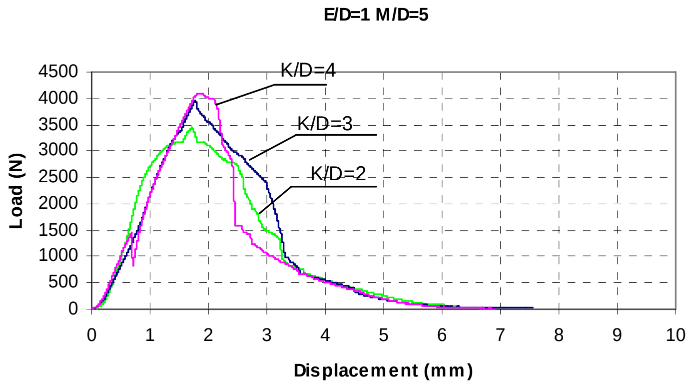

(d)

Figure A.5 Load-displacement curves for pin-loaded glass-vinylester composite plates (K/D=2, 3, 4 E/D=1) a) M/D=2, b) M/D=3, c) M/D=4, d) M/D=5

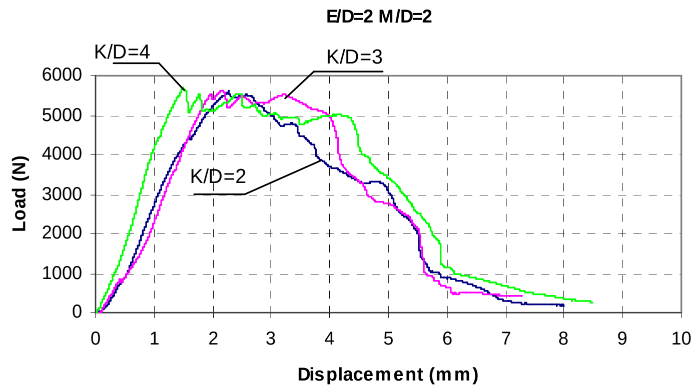

(a)

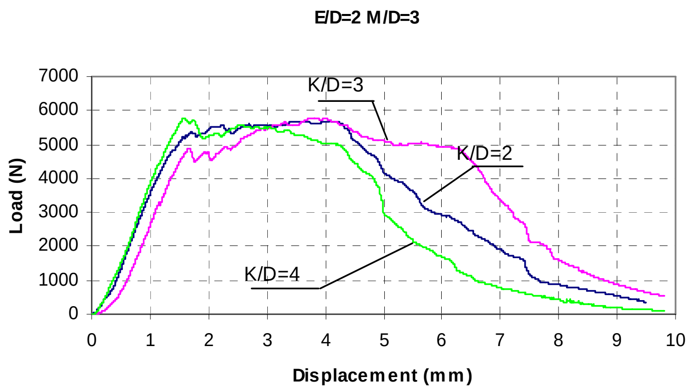

(b)

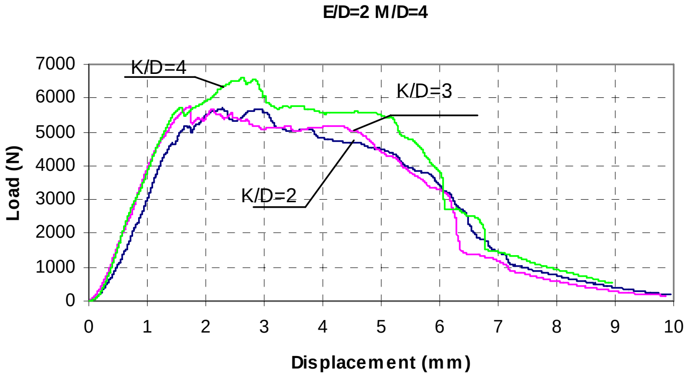

(c)

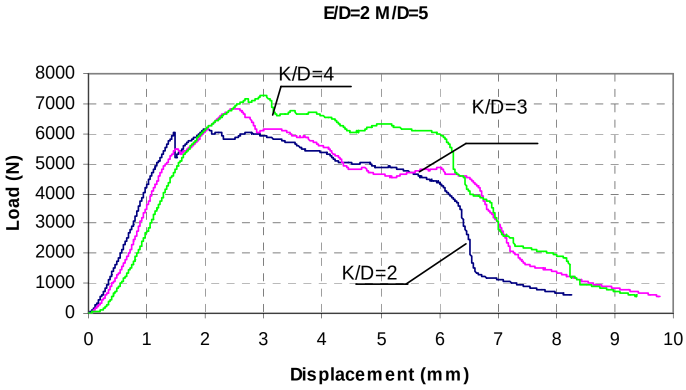

(d)

Figure A.6 Load-displacement curves for pin-loaded glass-vinylester composite plates (K/D=2, 3, 4 E/D=2) a) M/D=2, b) M/D=3, c) M/D=4, d) M/D=5

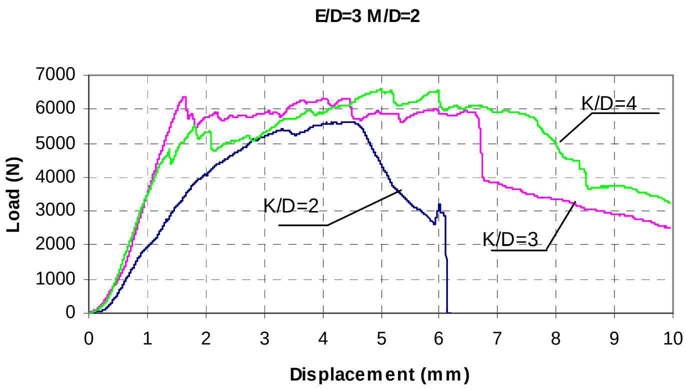

(a)

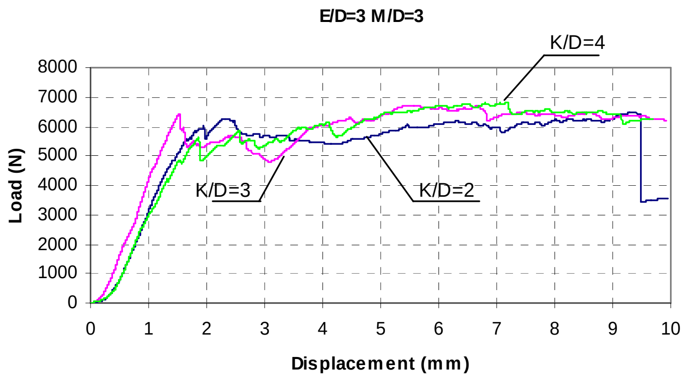

(b)

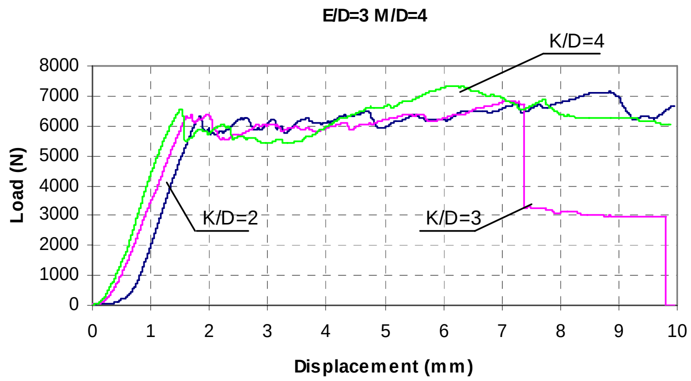

(c)

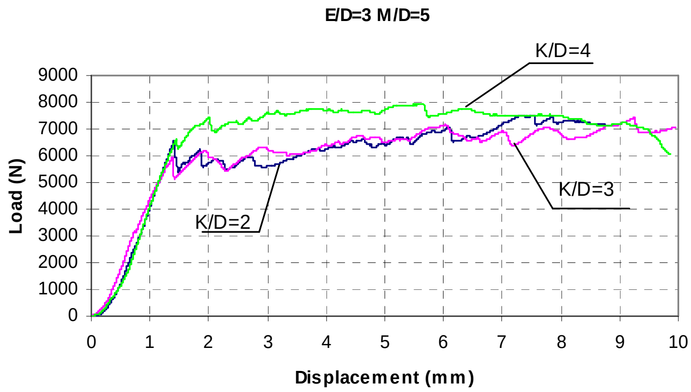

(d)

Figure A.7 Load-displacement curves for pin-loaded glass-vinylester composite plates (K/D=2, 3, 4 E/D=3) a) M/D=2, b) M/D=3, c) M/D=4 d) M/D=5

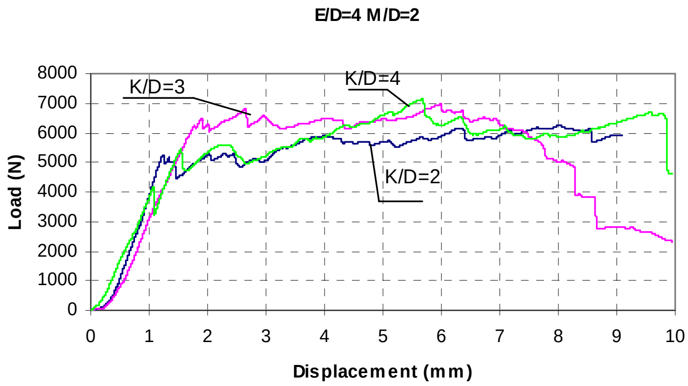
E/D=4 M/D=2
K/D=3
K/D=4
K/D=2
Load (N)
Displacement (mm)

(a)

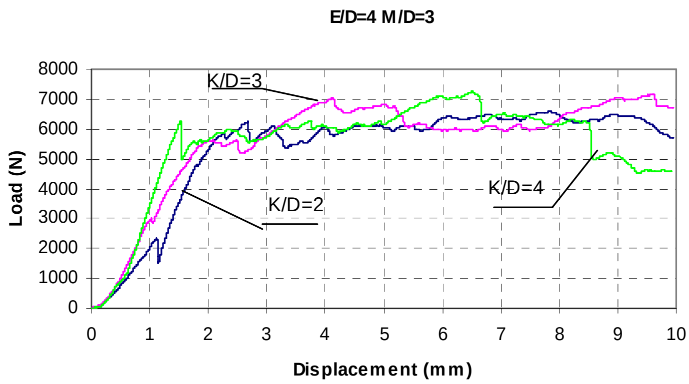
E/D=4 M/D=3
K/D=3
K/D=2
K/D=4
Load (N)
Displacement (mm)

(b)

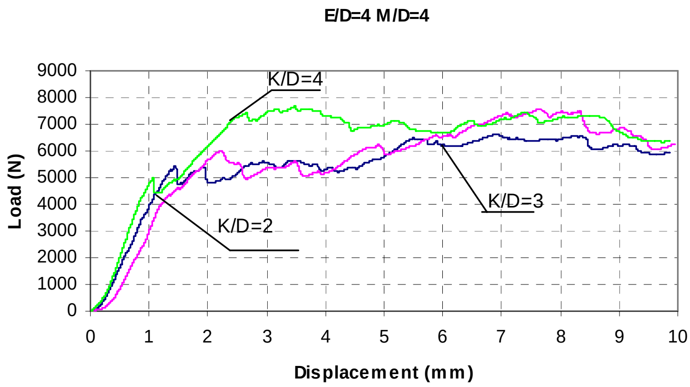
E/D=4 M/D=4
K/D=4
K/D=2
K/D=3
Load (N)
Displacement (mm)

(c)

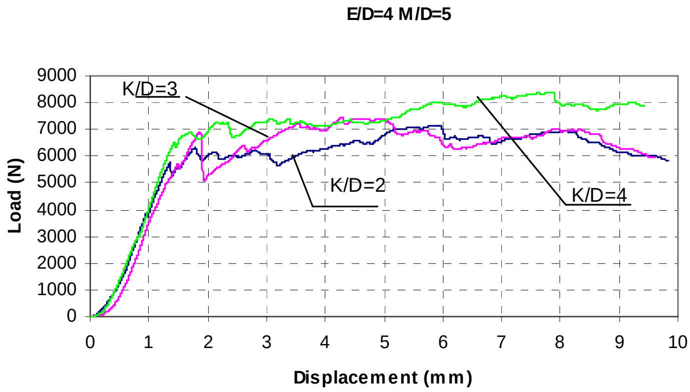

(d)

Figure A.8 Load-displacement curves for pin-loaded glass-vinylester composite plates (K/D=2, 3, 4 E/D=4) a) M/D=2, b) M/D=3, c) M/D=4 d) M/D=5

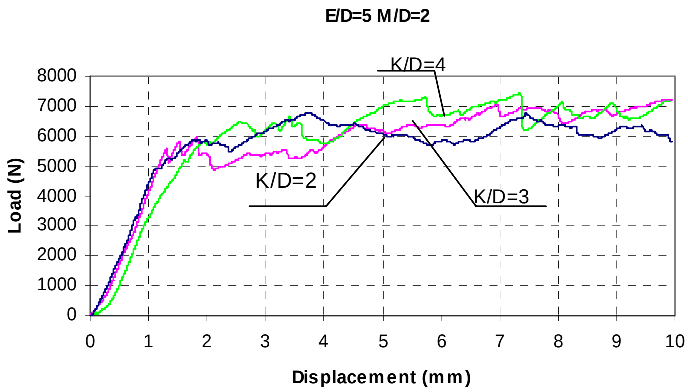

(a)

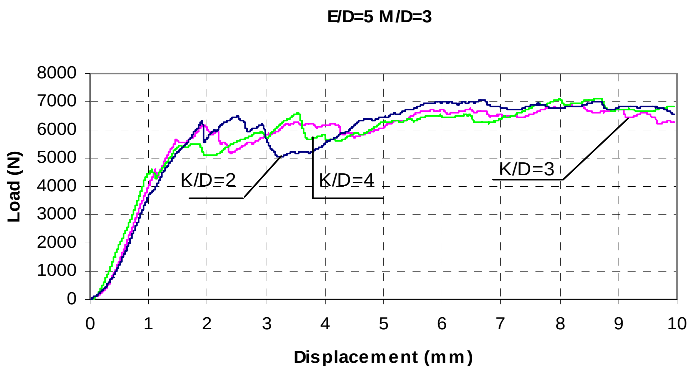

(b)

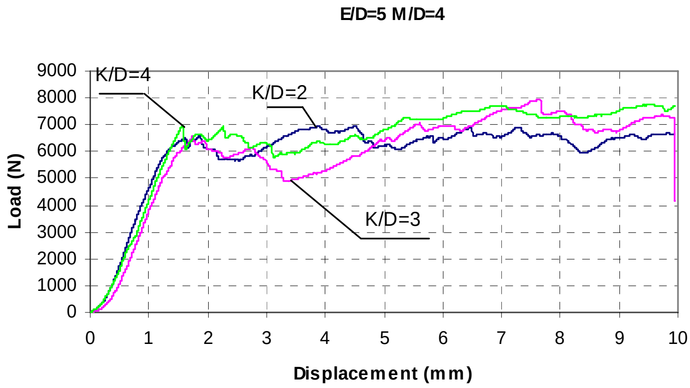

(c)

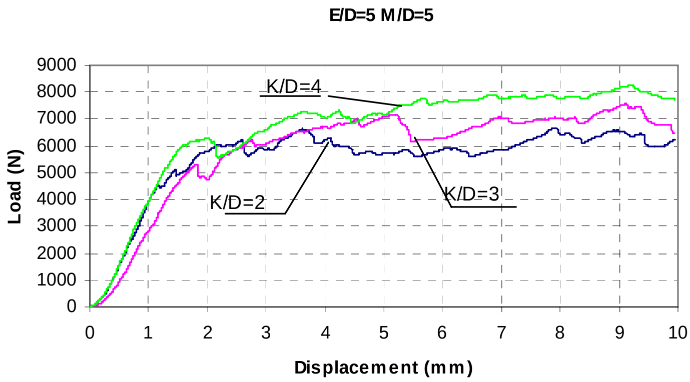

(d)

Figure A.9 Load-displacement curves for pin-loaded glass-vinylester composite plates (K/D=2, 3, 4 E/D=5) a) M/D=2, b) M/D=3, c) M/D=4 M/D=5

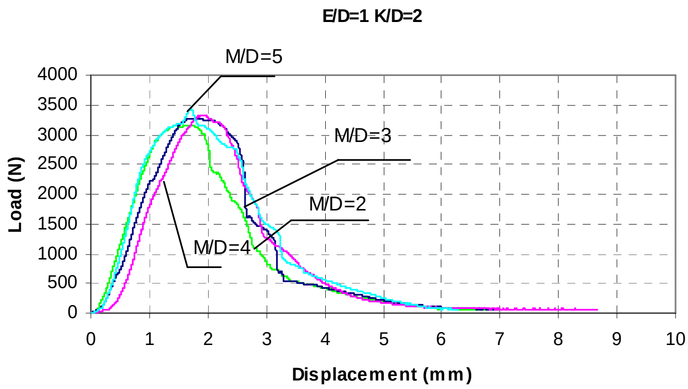

(a)

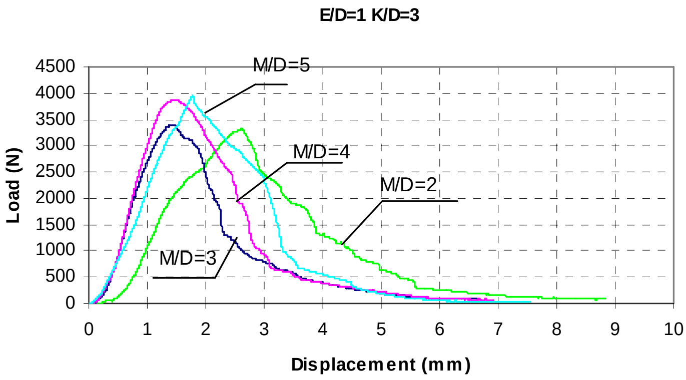

(b)

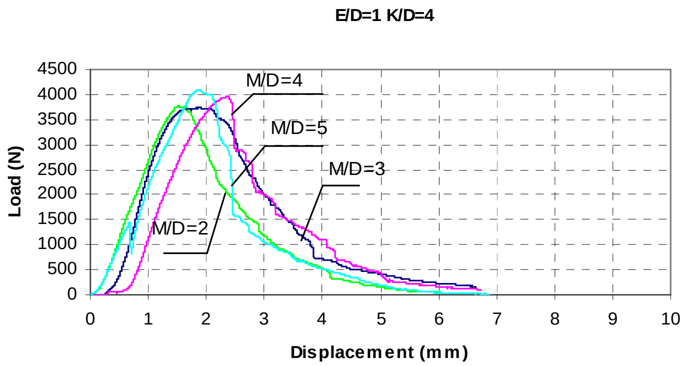

(c)

Figure A.10 Load-displacement curves for pin-loaded glass-vinylester composite plates (M/D=2, 3, 4,5 E/D=1) a) K/D=2, b) K/D=3, c) K/D=4

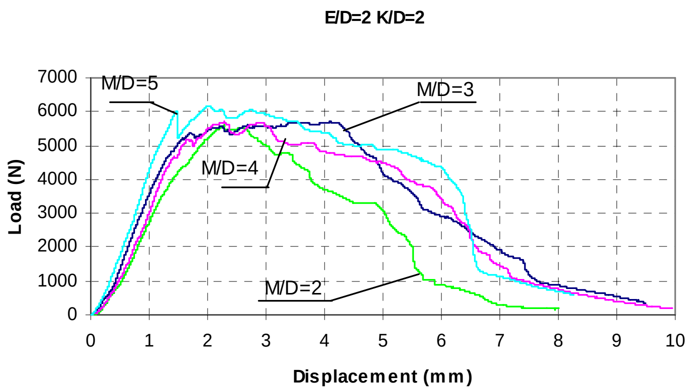

(a)

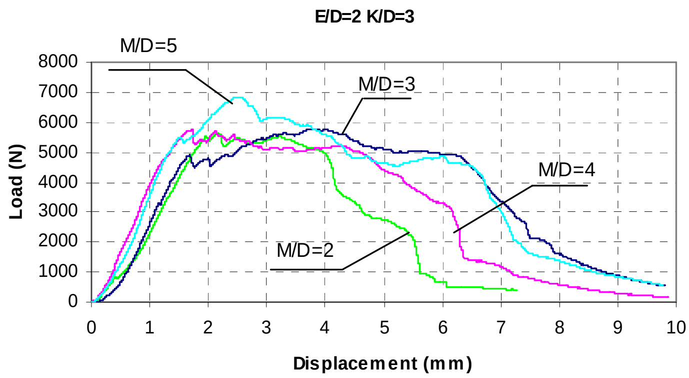

(b)

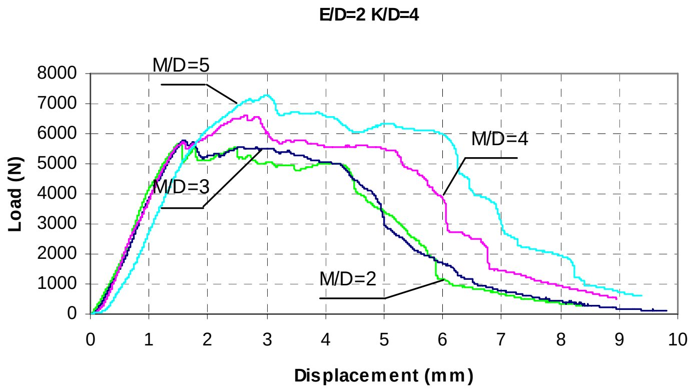

(c)

Figure A.11 Load-displacement curves for pin-loaded glass-vinylester composite plates (M/D=2, 3, 4, 5 E/D=2) a) K/D=2, b) K/D=3, c) K/D=4

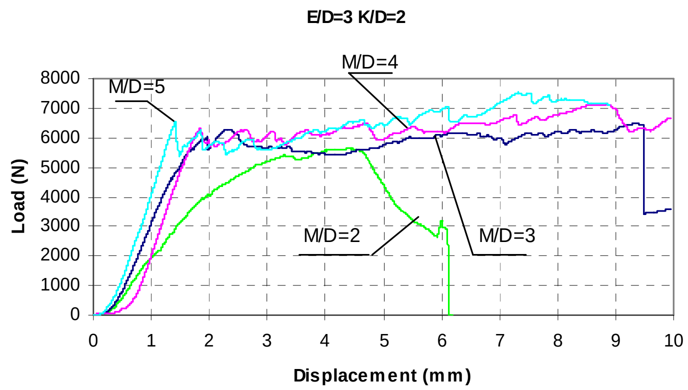

(a)

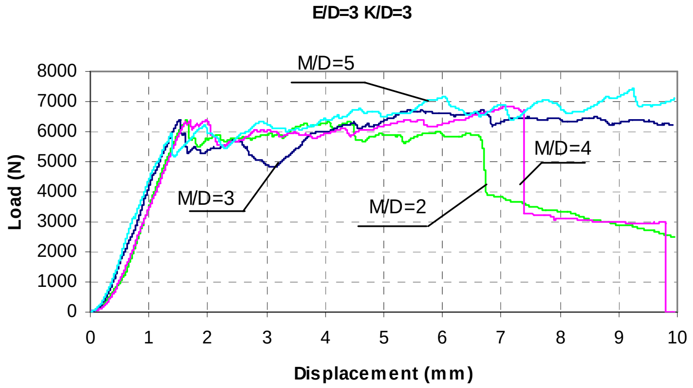

(b)

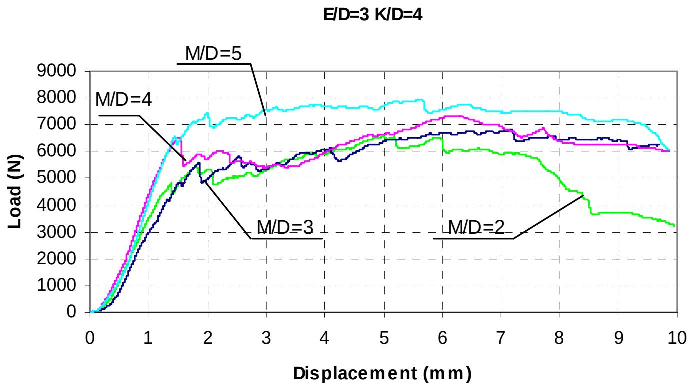

(c)

Figure 5.12 Load-displacement curves for pin-loaded glass-vinylester composite plates (M/D=2, 3, 4, 5 E/D=3) a) K/D=2, b) K/D=3, c) K/D=4

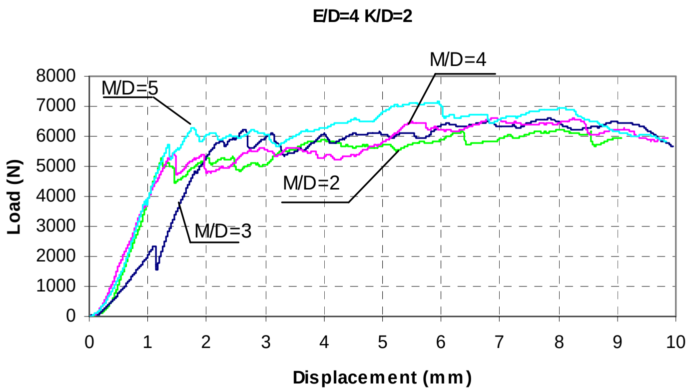

(a)

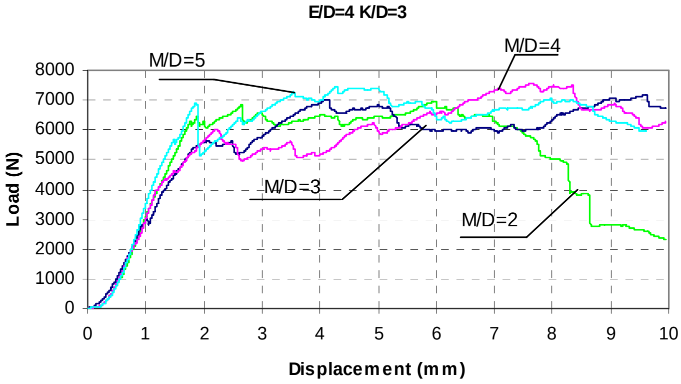

(b)

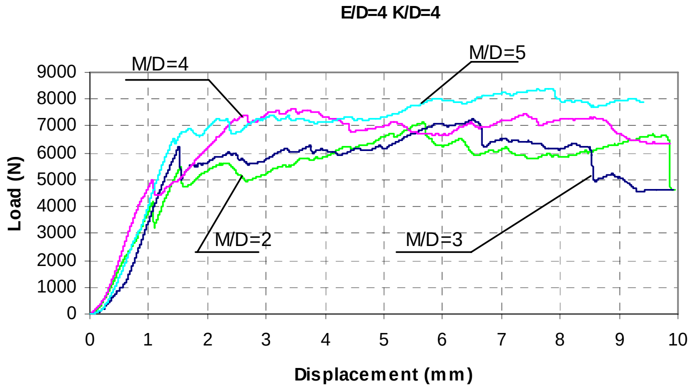

(c)

Figure A.13 Load-displacement curves for pin-loaded glass-vinylester composite plates (M/D=2, 3, 4, 5 E/D=4) a) K/D=2, b) K/D=3, c) K/D=4

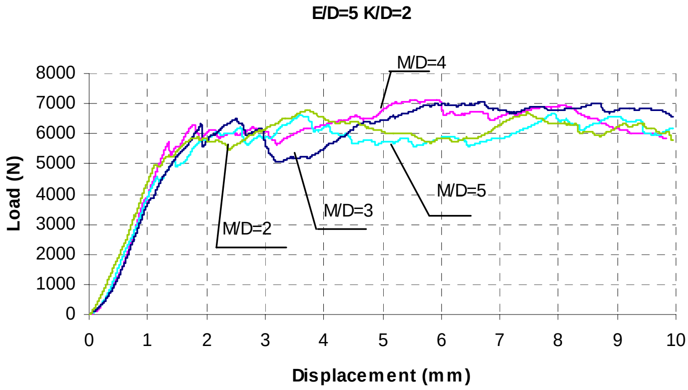

(a)

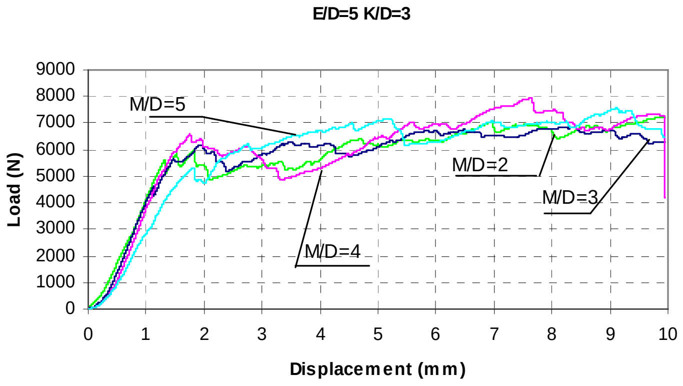

(b)

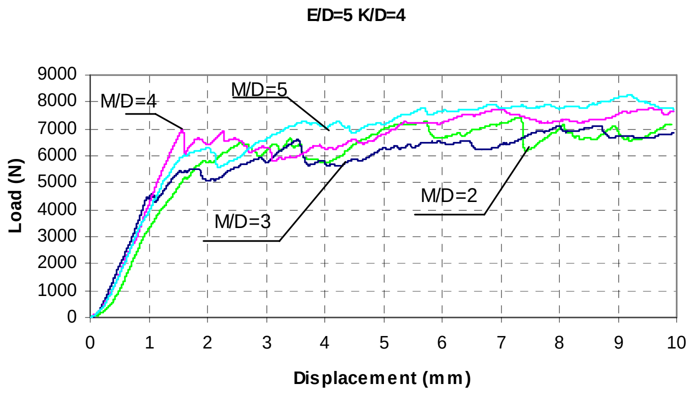

(c)

Figure A.14 Load-displacement curves for pin-loaded glass-vinylester composite plates (M/D=2, 3, 4, 5 E/D=5) a) K/D=2, b) K/D=3, c) K/D=4

APPENDIX B

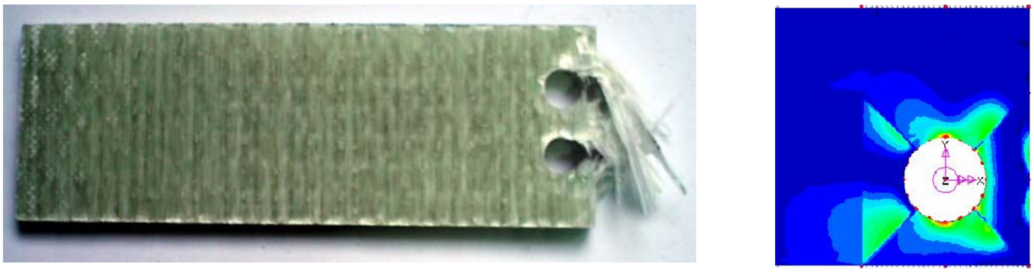

(a)

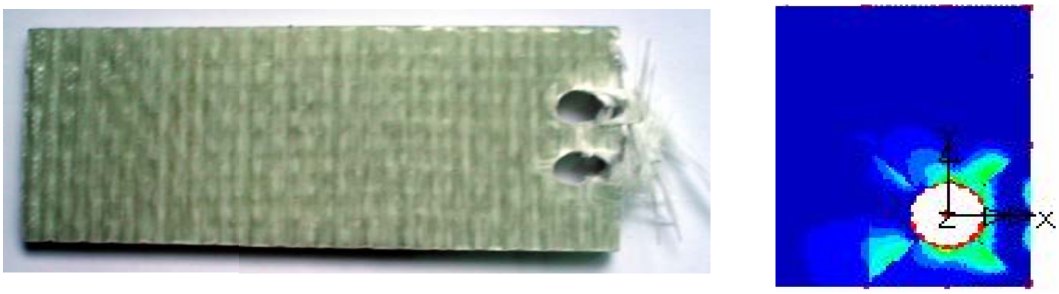

(b)

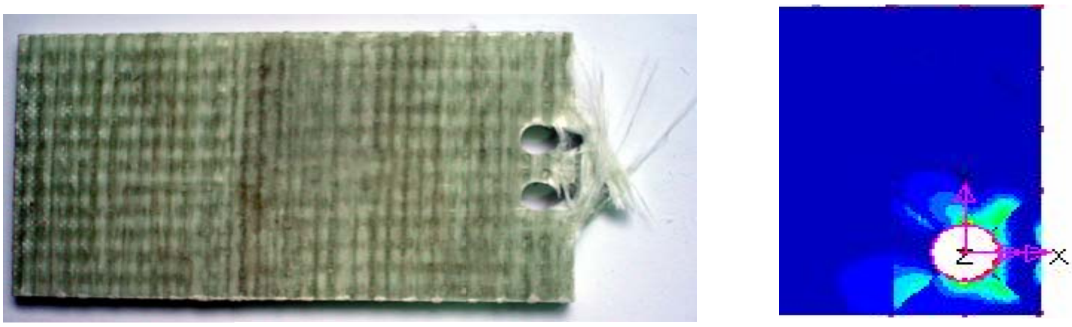

(c)

Figure B.1 Comparison with experimental and Hashin results a) E/D=1 M/D=2 K/D=2, b) E/D=1 M/D=2 K/D=3, c) E/D=1 M/D=2 K/D=3

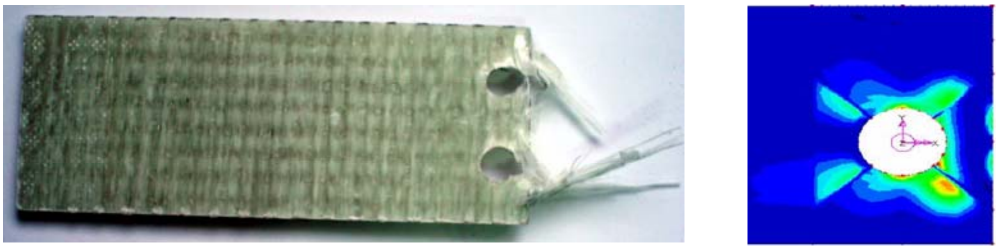

(a)

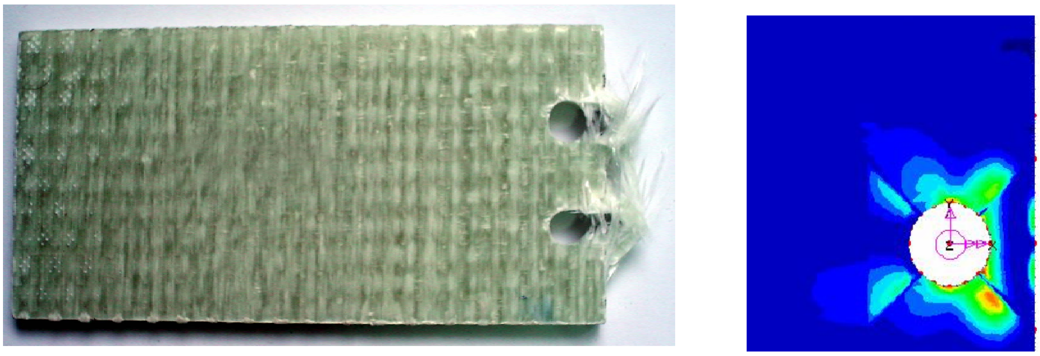

(b)

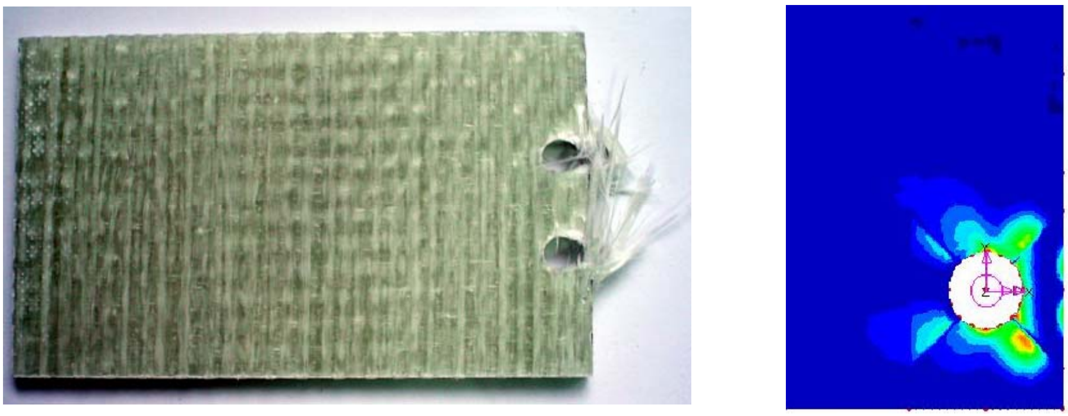

(c)

Figure B.2 Comparison with experimental and Hashin results a) E/D=1 M/D=3 K/D=2, b) E/D=1 M/D=3 K/D=3, c) E/D=1 M/D=3 K/D=3

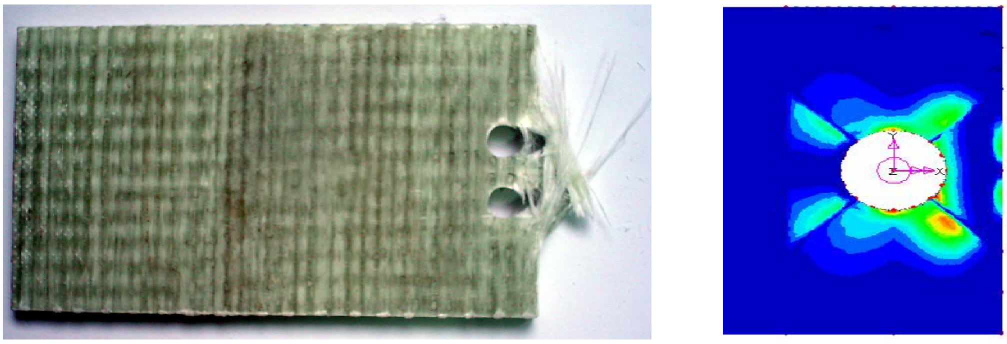

(a)

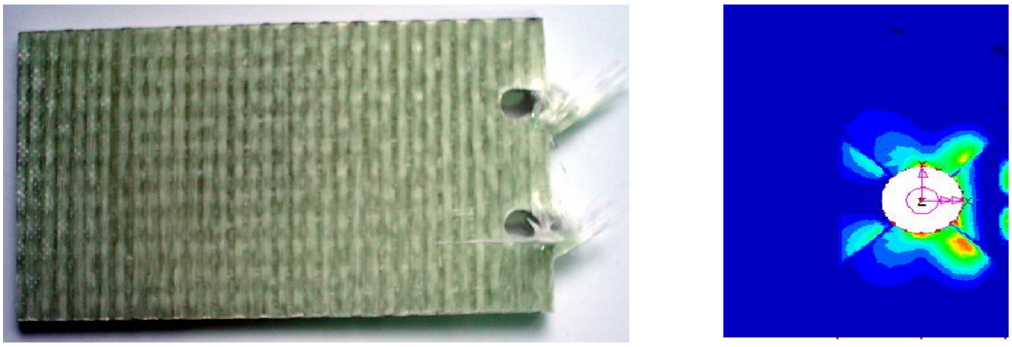

(b)

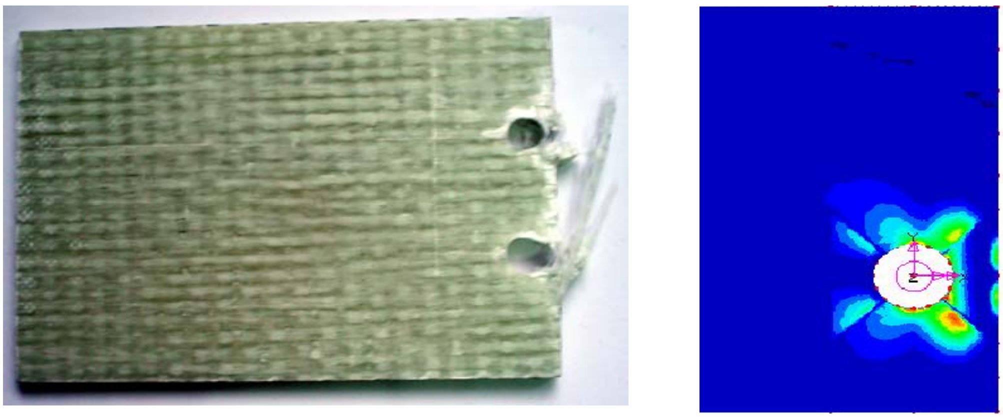

(c)

Figure B.3 Comparison with experimental and Hashin results a) E/D=1 M/D=4 K/D=2, b) E/D=1 M/D=3 K/D=4, c) E/D=1 M/D=4 K/D=3

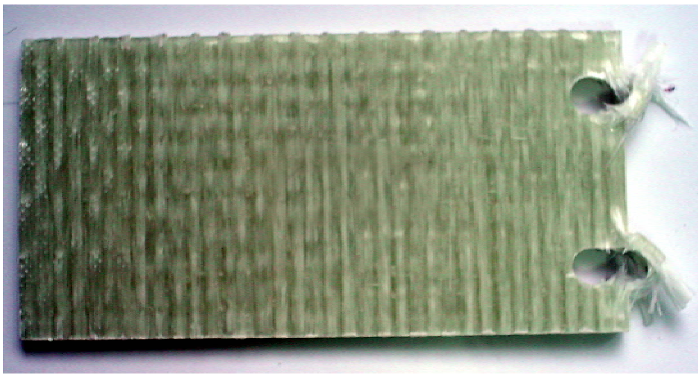
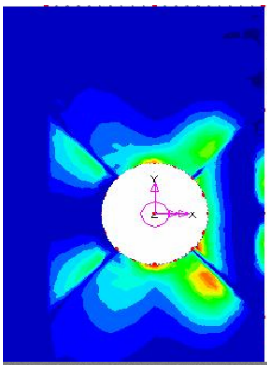

(a)

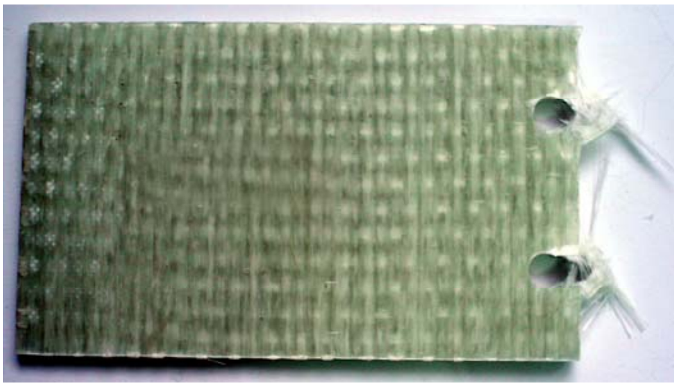
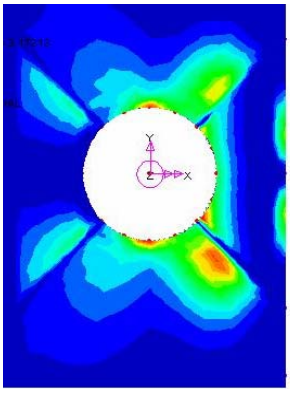

(b)


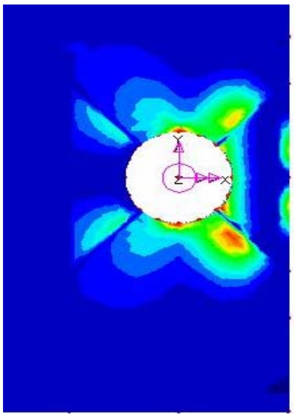

(c)

Figure B.4 Comparison with experimental and Hashin results a) E/D=1 M/D=5 K/D=2, b) E/D=1 M/D=5 K/D=4, c) E/D=1 M/D=5 K/D=3

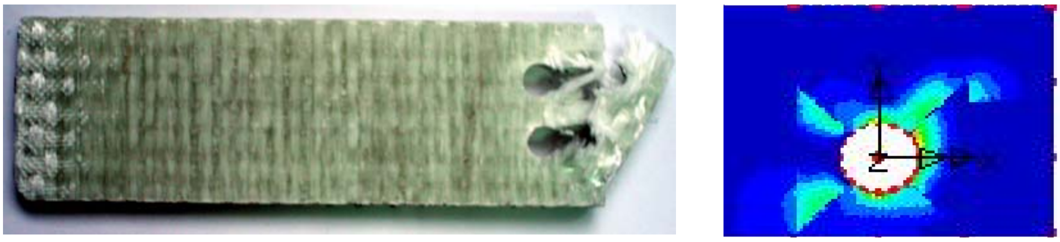

(a)

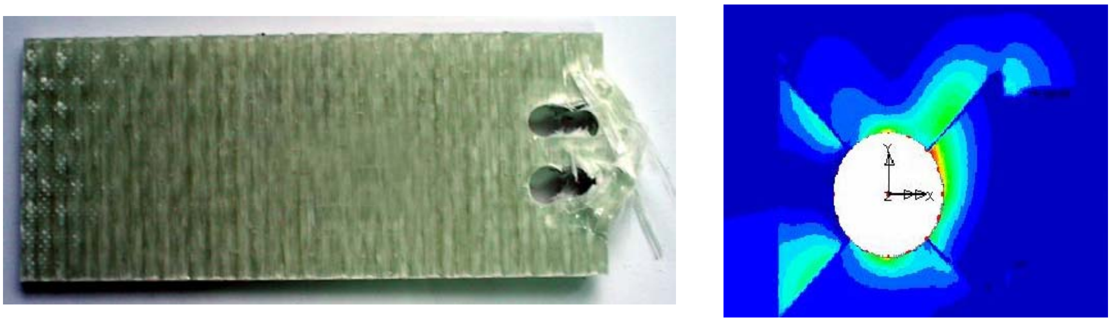

(b)

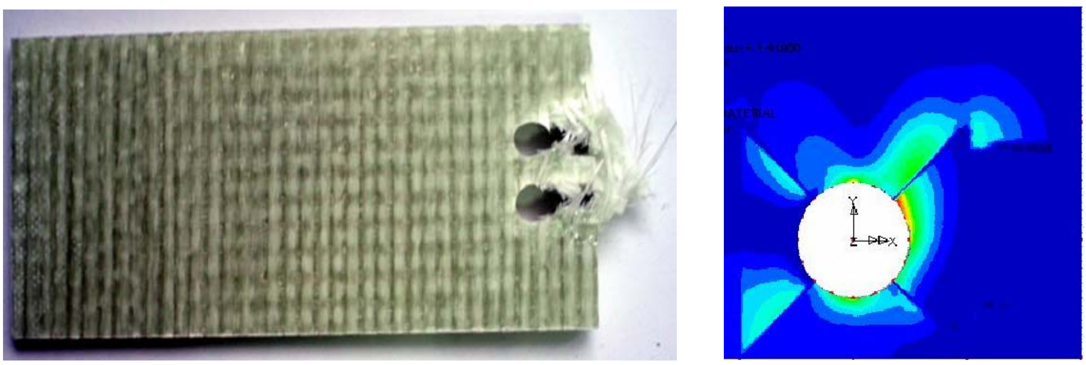

(c)

Figure B.5 Comparison with experimental and Hashin results a) E/D=2 M/D=2 K/D=2, b) E/D=2 M/D=2 K/D=3, c) E/D=2 M/D=2 K/D=4

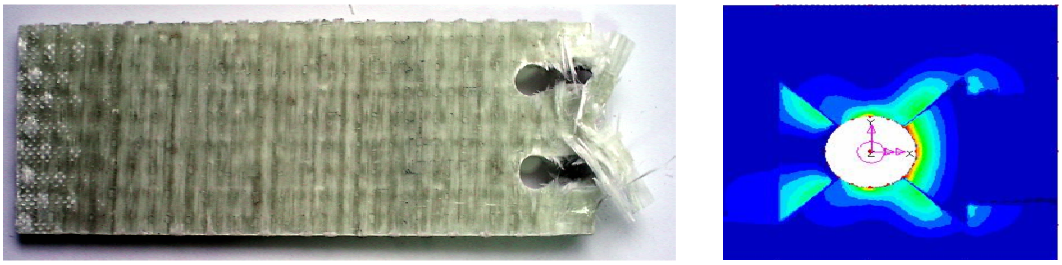

(a)

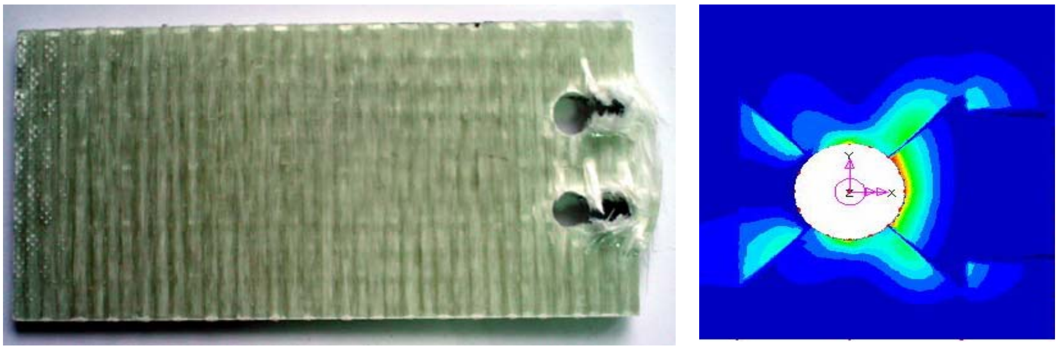

(b)

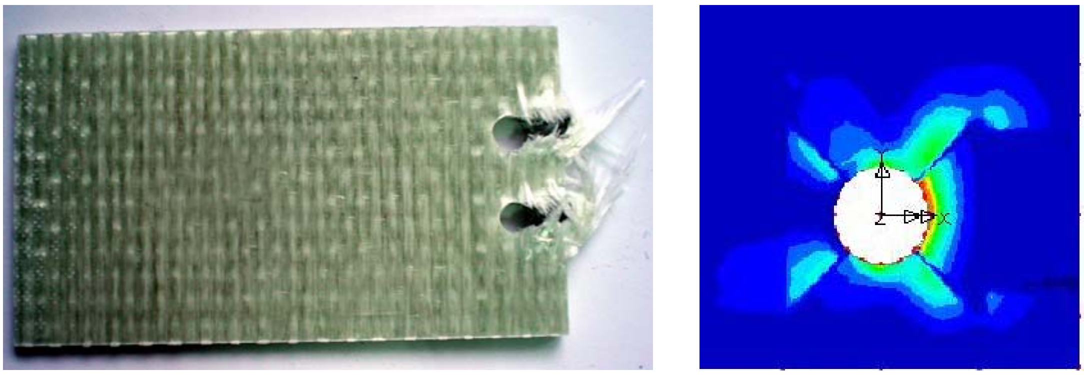

(c)

Figure B.6 Comparison with experimental and Hashin results a) E/D=2 M/D=3 K/D=2, b) E/D=2 M/D=3 K/D=3, c) E/D=2 M/D=3 K/D=4

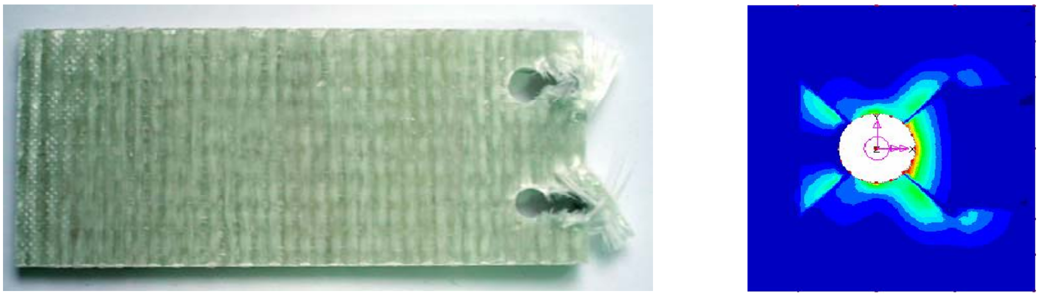

(a)

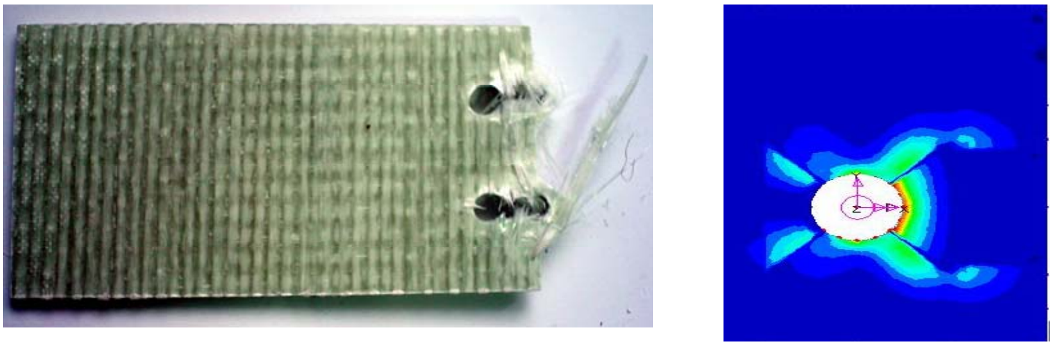

(b)

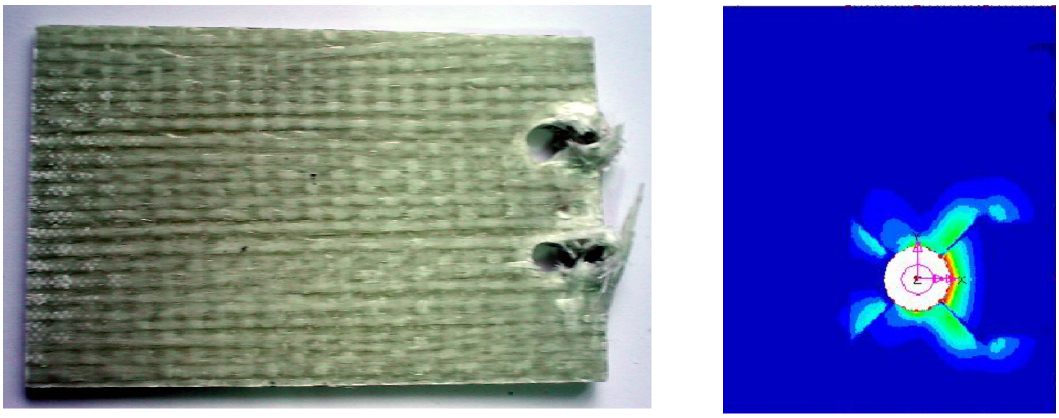

(c)

Figure B.7 Comparison with experimental and Hashin results a) E/D=2 M/D=4 K/D=2, b) E/D=2 M/D=4 K/D=3, c) E/D=2 M/D=4 K/D=4

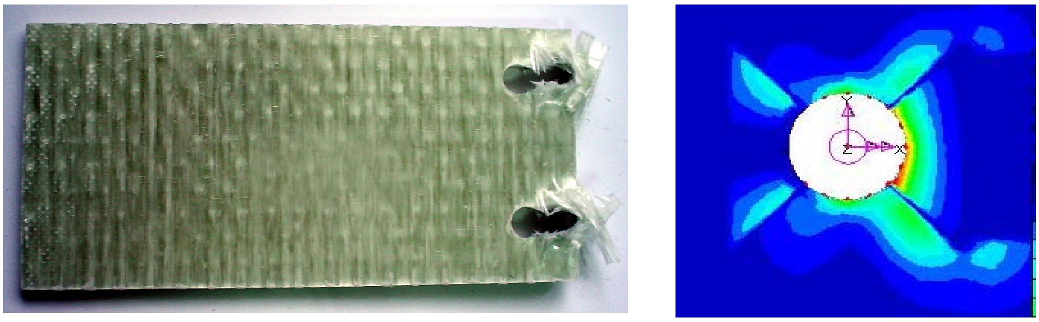

(a)

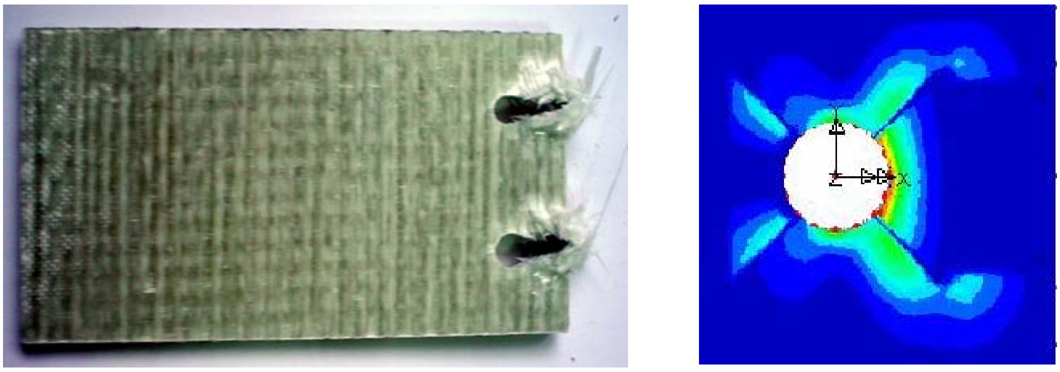

(b)

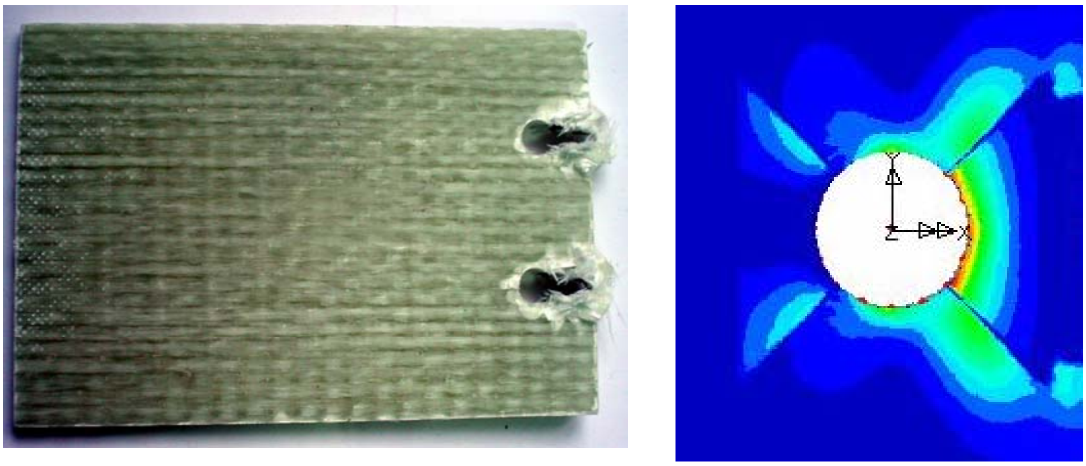

(c)

Figure B.8 Comparison with experimental and Hashin results a) E/D=2 M/D=5 K/D=2, b) E/D=2 M/D=5 K/D=3, c) E/D=2 M/D=5 K/D=4

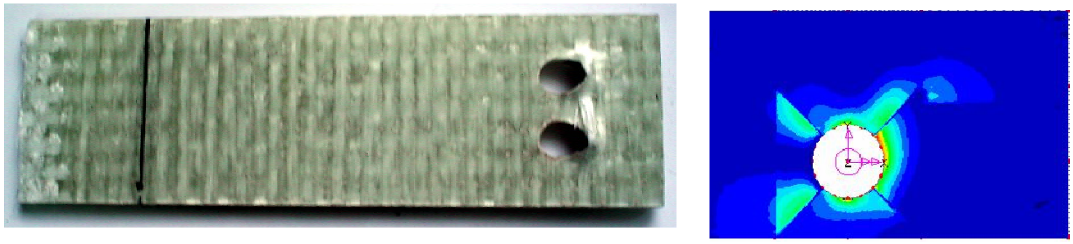

(a)

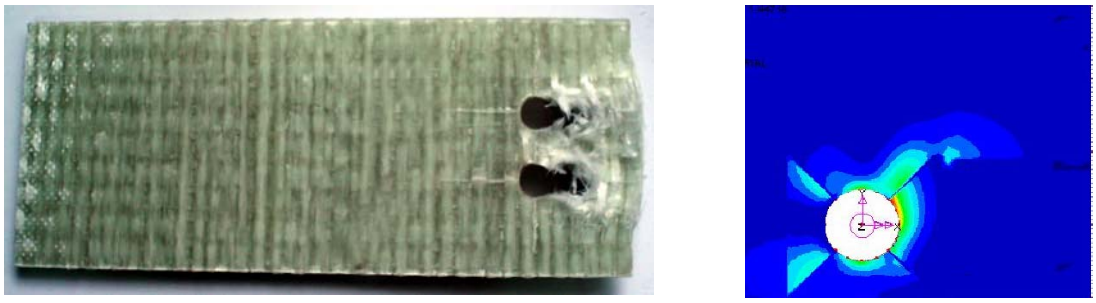

(b)

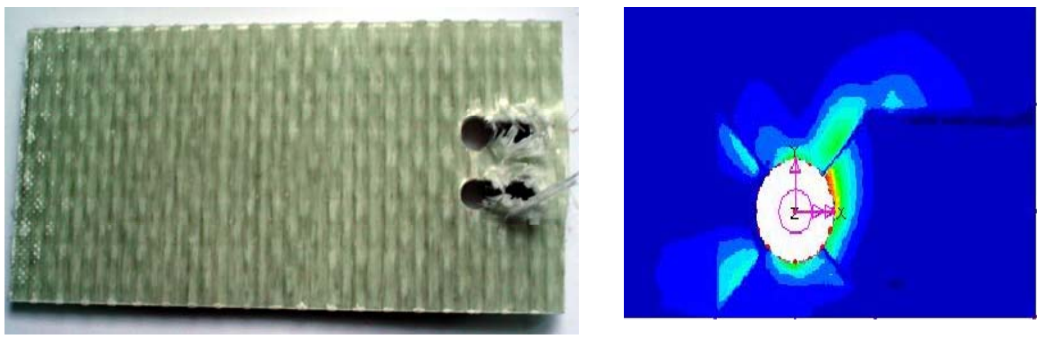

(c)

Figure B.9 Comparison with experimental and Hashin results a) E/D=3 M/D=2 K/D=2, b) E/D=3 M/D=2 K/D=3, c) E/D=3 M/D=2 K/D=4

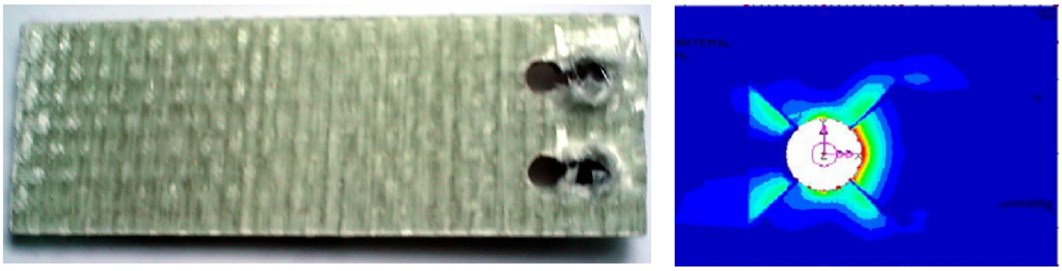

(a)

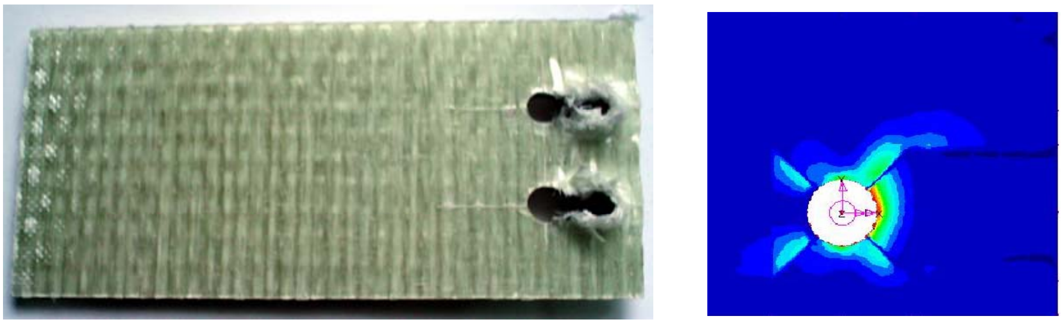

(b)

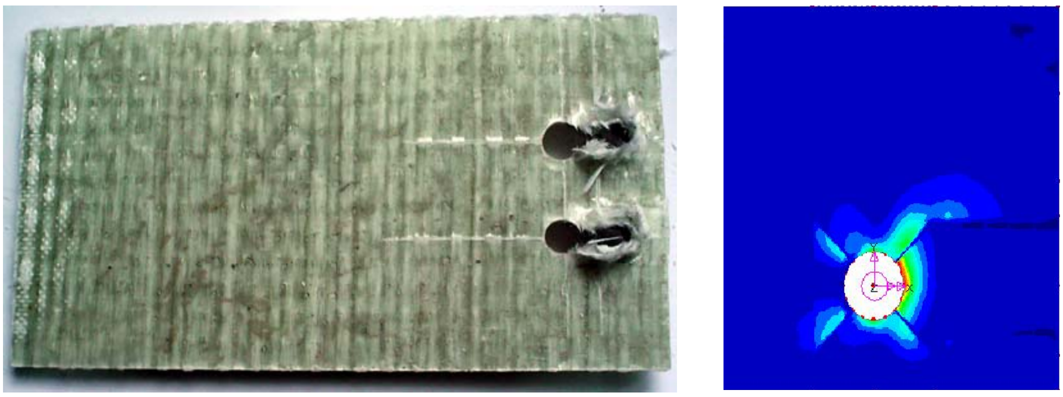

(c)

Figure B.10 Comparison with experimental and Hashin results a) E/D=3 M/D=3 K/D=2, b) E/D=3 M/D=3 K/D=3, c) E/D=3 M/D=3 K/D=4

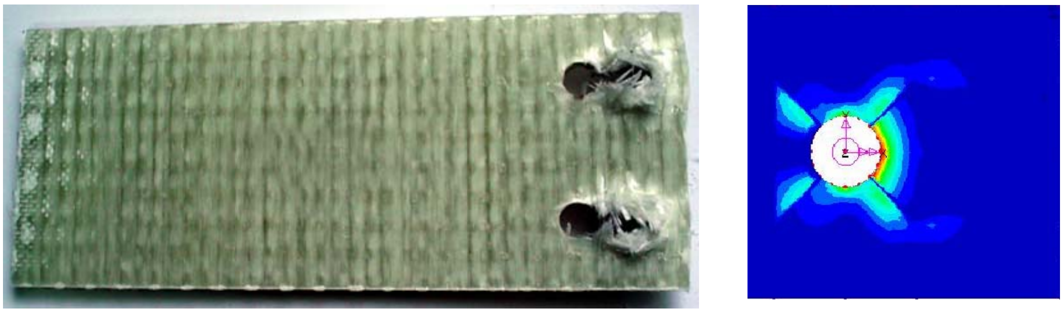

(a)

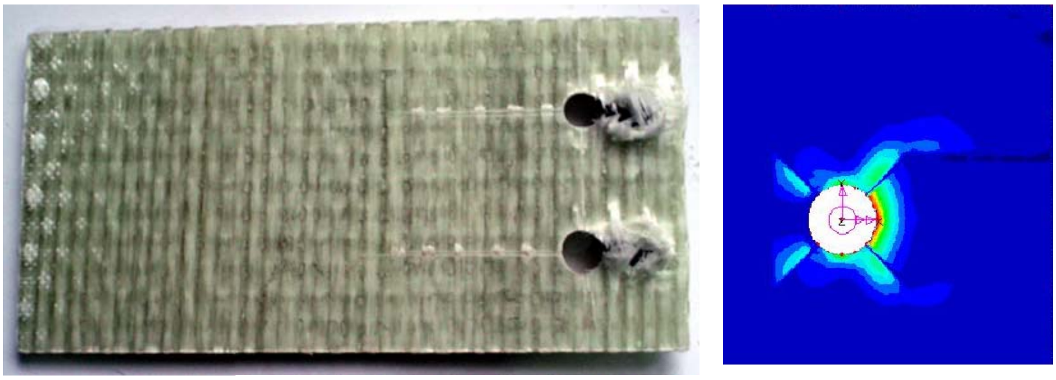

(b)

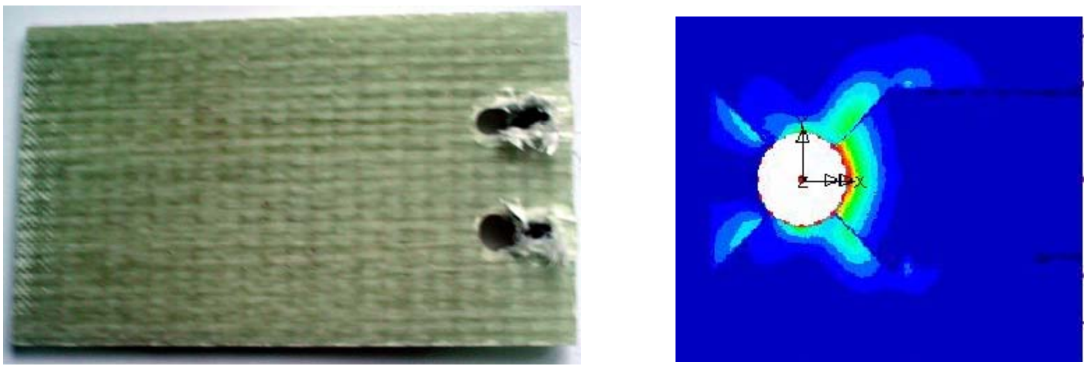

(c)

Figure B.11 Comparison with experimental and Hashin results a) E/D=3 M/D=4 K/D=2, b) E/D=3 M/D=4 K/D=3, c) E/D=3 M/D=4 K/D=4

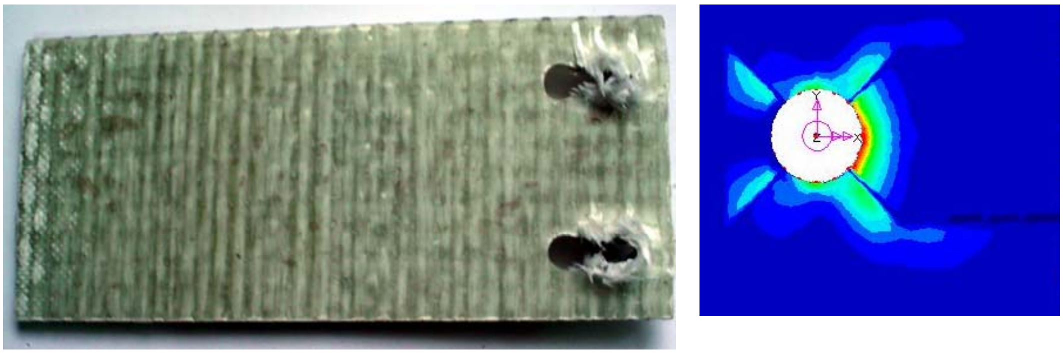

(a)

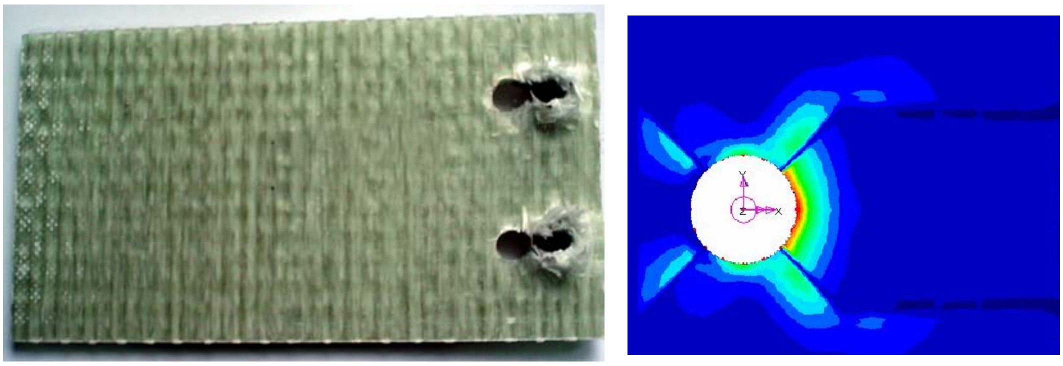

(b)

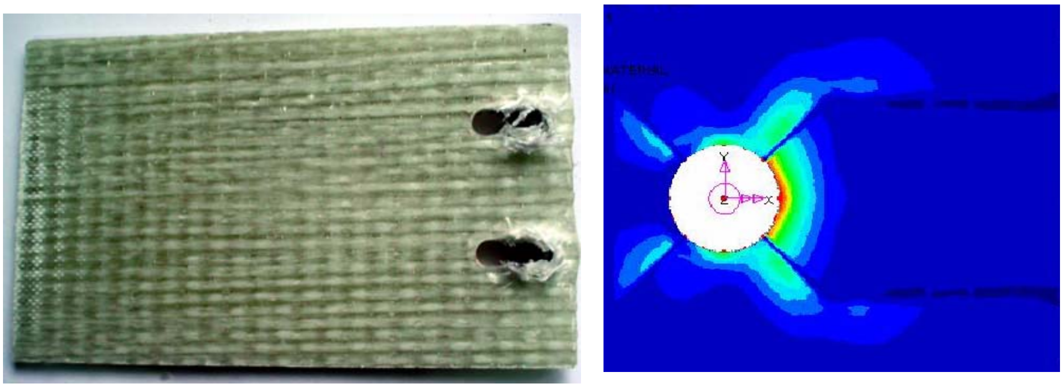

(c)

Figure B.12 Comparison with experimental and Hashin results a) E/D=3 M/D=5 K/D=2, b) E/D=3 M/D=5 K/D=3, c) E/D=3 M/D=5 K/D=4

(a)

(b)

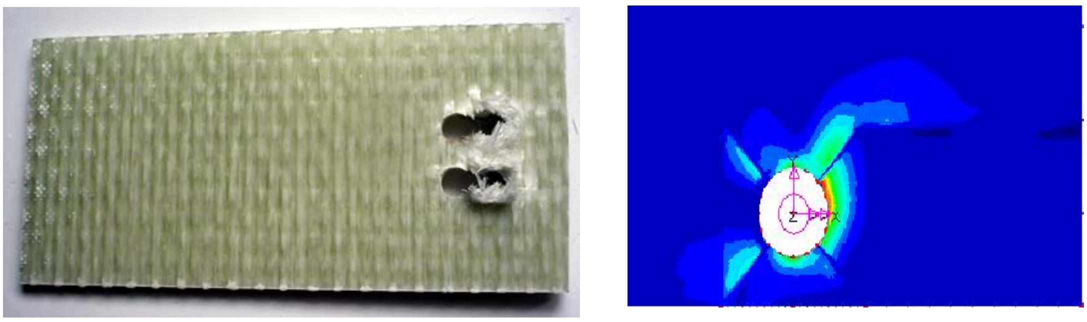

(c)

Figure B.13 Comparison with experimental and Hashin results a) E/D=4 M/D=2 K/D=2, b) E/D=4 M/D=2 K/D=3, c) E/D=4 M/D=2 K/D=4

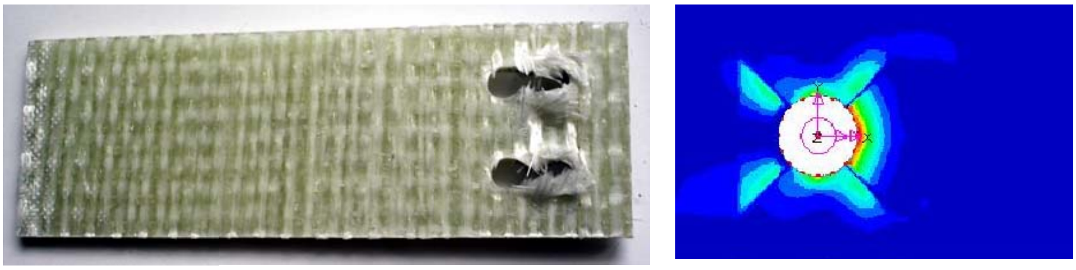

(a)

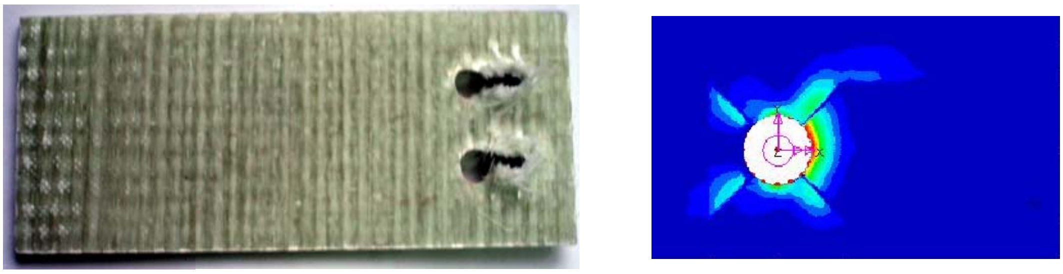

(b)

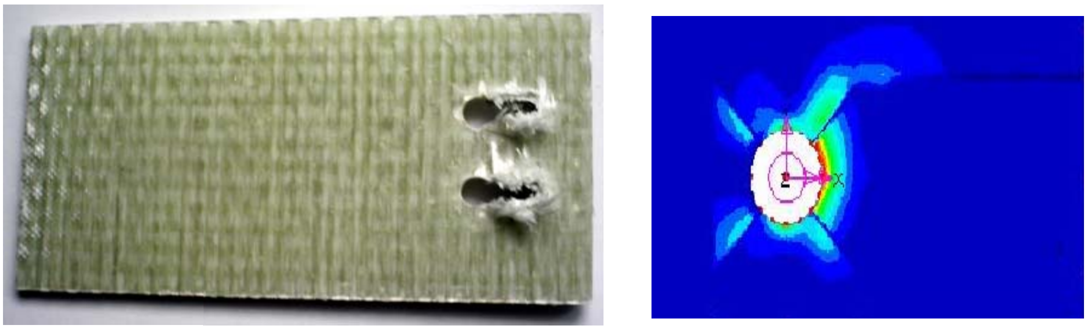

(c)

Figure B.14 Comparison with experimental and Hashin results a) E/D=4 M/D=3 K/D=2, b) E/D=4 M/D=3 K/D=3, c) E/D=4 M/D=3 K/D=4

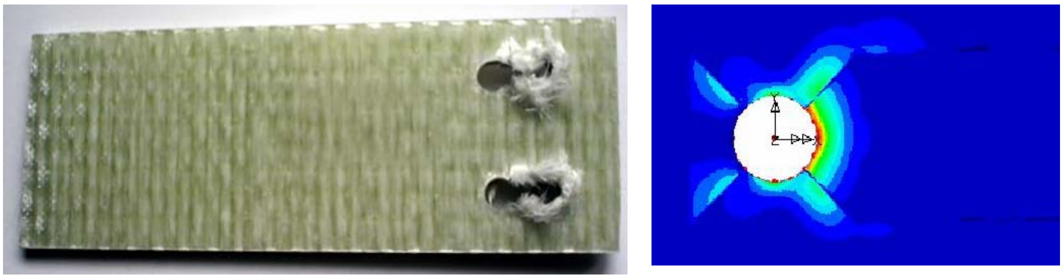

(a)

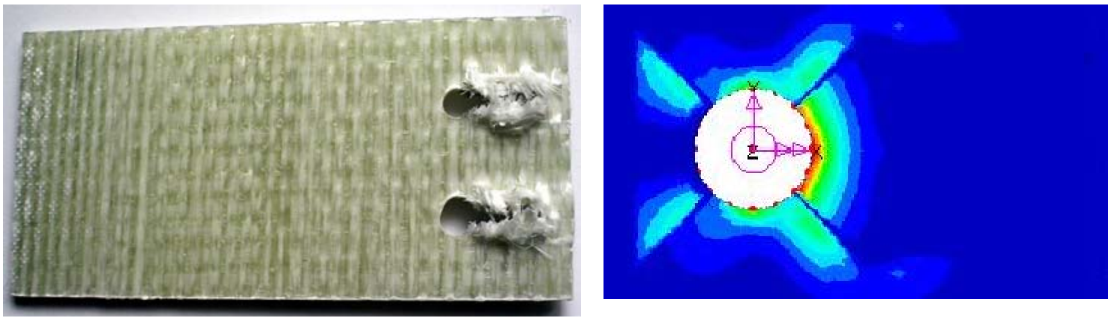

(b)

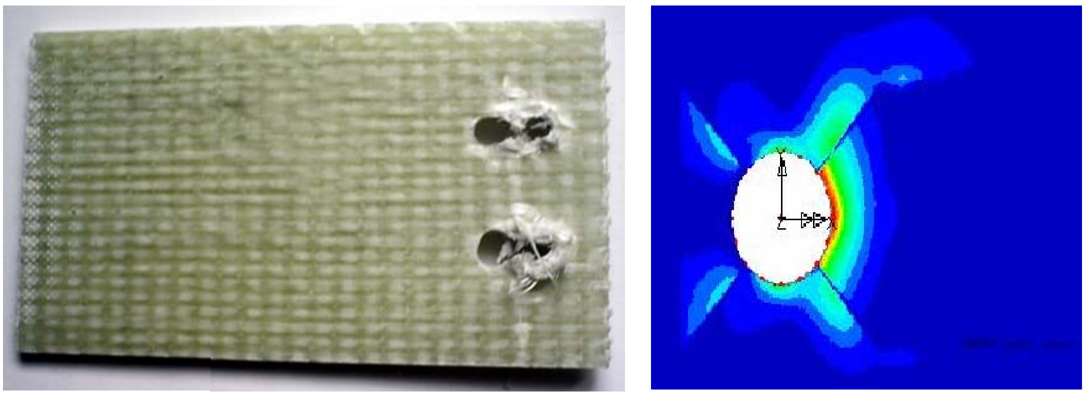

(c)

Figure B.15 Comparison with experimental and Hashin results a) E/D=4 M/D=4 K/D=2, b) E/D=4 M/D=4 K/D=3, c) E/D=4 M/D=4 K/D=4

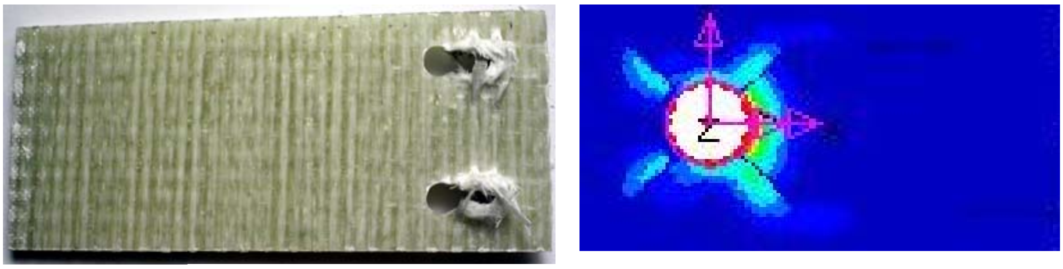

(a)

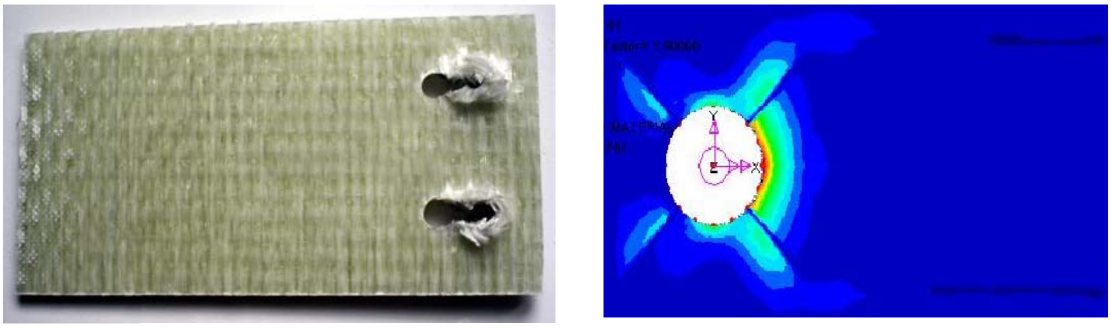

(b)

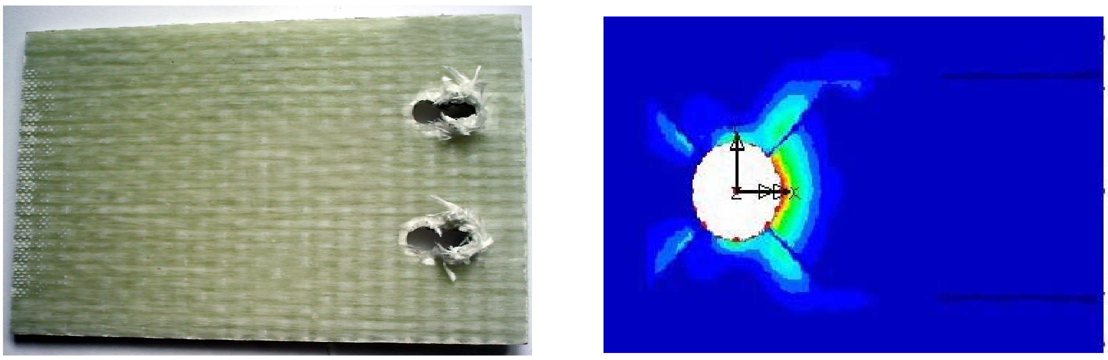

(c)

Figure B.16 Comparison with experimental and Hashin results a) E/D=4 M/D=5 K/D=2, b) E/D=4 M/D=5 K/D=3, c) E/D=4 M/D=5 K/D=4

(a)

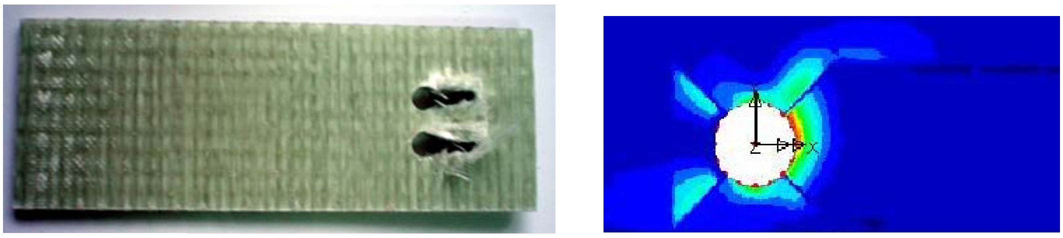

(b)

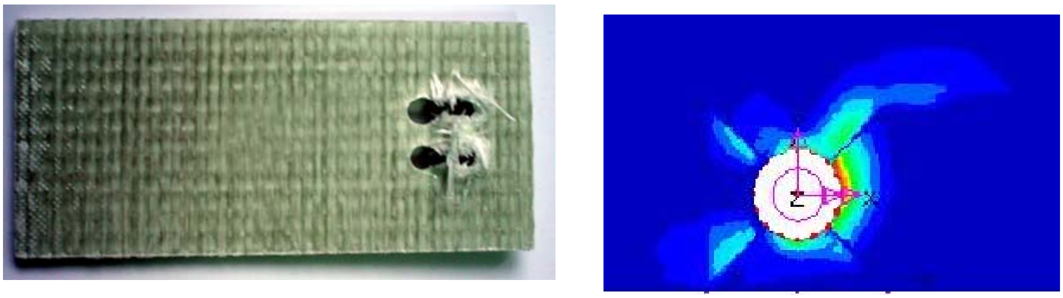

(c)

Figure B.17 Comparison with experimental and Hashin results a) E/D=5 M/D=2 K/D=2, b) E/D=5 M/D=2 K/D=3, c) E/D=5 M/D=2 K/D=4

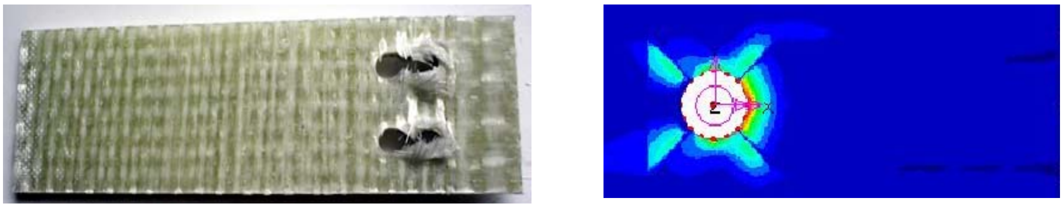

(a)

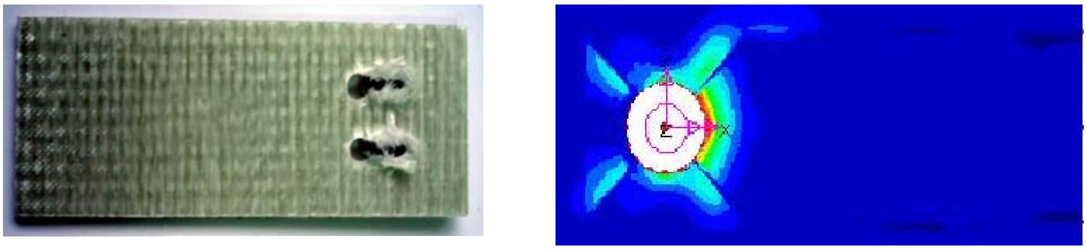

(b)

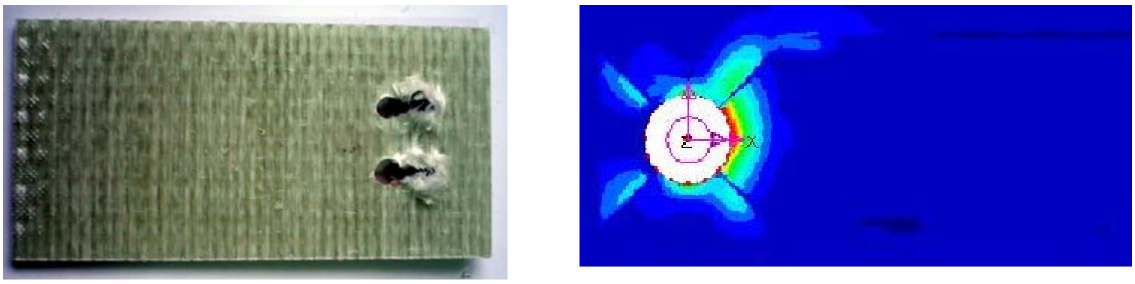

(c)

Figure B.18 Comparison with experimental and Hashin results a) E/D=5 M/D=3 K/D=2, b) E/D=5 M/D=3 K/D=3, c) E/D=5 M/D=3 K/D=4

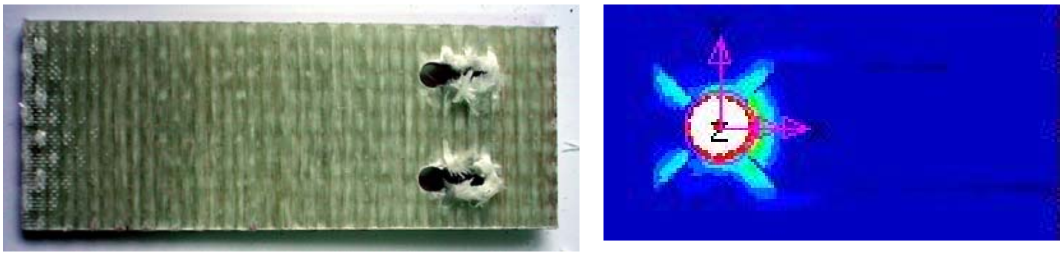

(a)

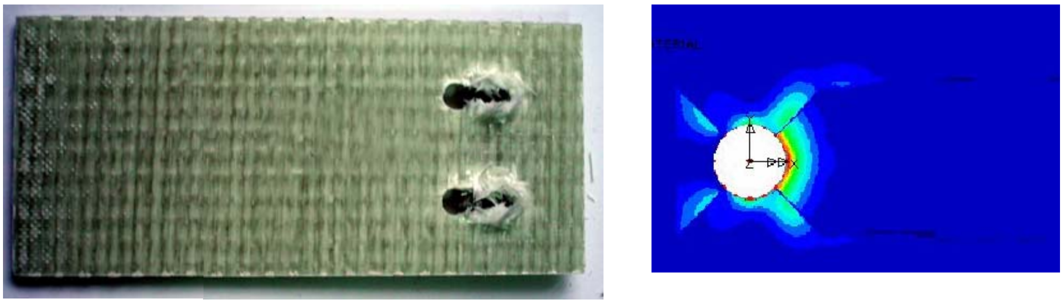

(b)

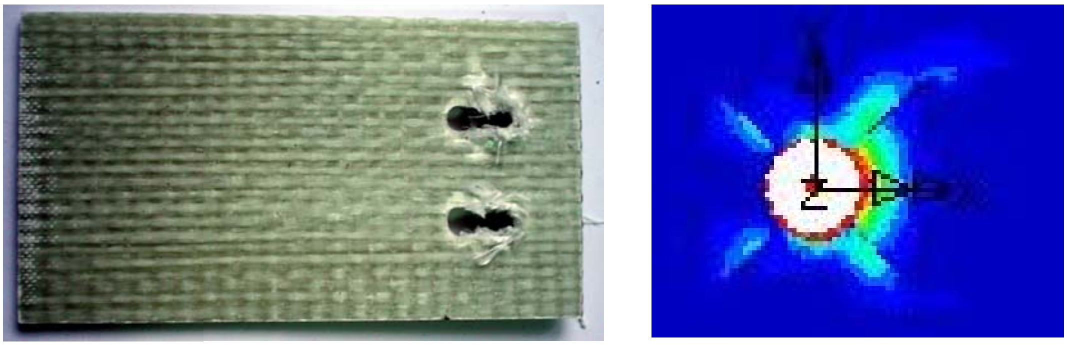

(c)

Figure B.19 Comparison with experimental and Hashin results a) E/D=5 M/D=4 K/D=2, b) E/D=5 M/D=4 K/D=3, c) E/D=5 M/D=4 K/D=4

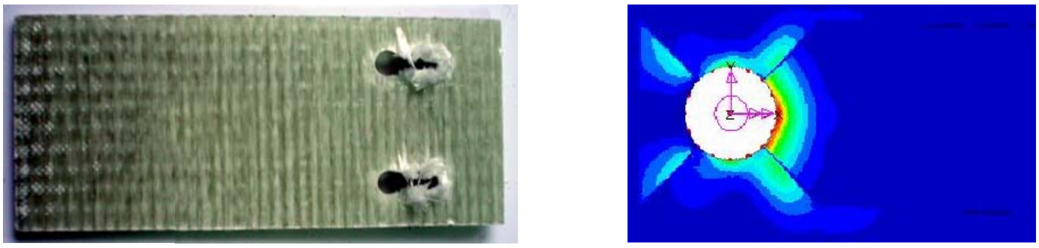

(a)

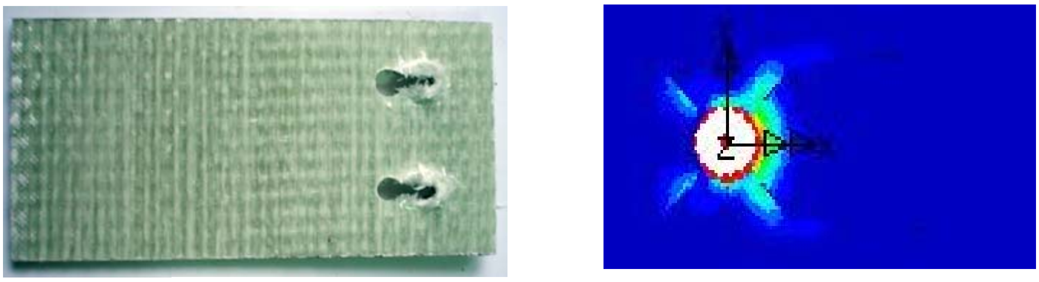

(b)

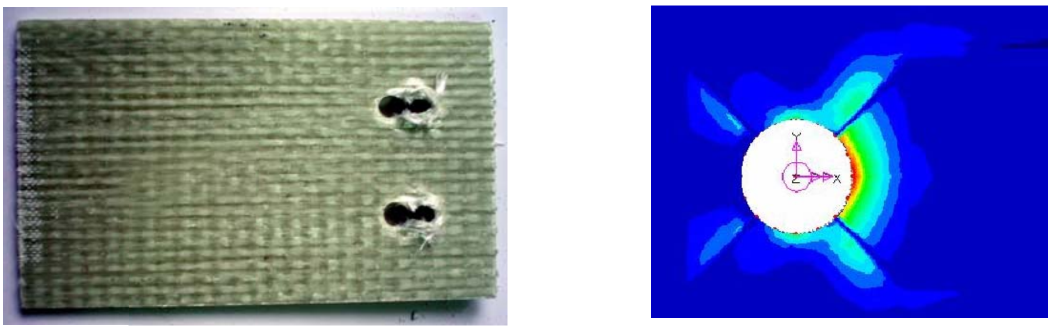

(c)

Figure B.20 Comparison with experimental and Hashin results a) E/D=5 M/D=5 K/D=2, b) E/D=5 M/D=5 K/D=3, c) E/D=5 M/D=5 K/D=4